FOSSIL ENERGY

DOE/BC/14942-9
(OSTI ID: 753525)

ADVANCED RESERVOIR CHARACTERIZATION AND EVALUATION OF CO_2 GRAVITY DRAINAGE IN THE NATURALLY FRACTURED SPRABERRY TREND AREA

Annual Report
September 1, 1998-August 31, 1999

By
Tracy Heckman
David S. Schechter

Date Published: April 2000

Work Performed Under Contract No. DE-FC22-95BC14942

Pioneer Natural Resources
Irving, Texas

National Petroleum Technology Office
U.S. DEPARTMENT OF ENERGY
Tulsa, Oklahoma

DISCLAIMER

This report was prepared as an account of work sponsored by an agency of the United States Government. Neither the United States Government nor any agency thereof, nor any of their employees, makes any warranty, expressed or implied, or assumes any legal liability or responsibility for the accuracy, completeness, or usefulness of any information, apparatus, product, or process disclosed, or represents that its use would not infringe privately owned rights. Reference herein to any specific commercial product, process, or service by trade name, trademark, manufacturer, or otherwise does not necessarily constitute or imply its endorsement, recommendation, or favoring by the United States Government or any agency thereof. The views and opinions of authors expressed herein do not necessarily state or reflect those of the United States Government.

This report has been reproduced directly from the best available copy.

DOE/BC/14942-9
Distribution Category UC-122

Advanced Reservoir Characterization and Evaluation of CO_2 Gravity Drainage in the Naturally Fractured Spraberry Trend Area

By
Tracy Heckman
David S. Schechter

April 2000

Work Performed Under Contract No DE-FC22-95BC14942

Prepared for
U.S. Department of Energy
Assistant Secretary for Fossil Energy

Dan Ferguson, Project Manager
National Petroleum Technology Office
P.O. Box 3628
Tulsa, OK 74101

Prepared by
Pioneer Natural Resources
5205 N. O-Connor Blvd.
Suite 1400
Irving, TX 75039

New Mexico Petroleum Recovery Research Center
New Mexico Institute of Mining and Technology
Socorro, NM 87801

TABLE OF CONTENTS

LIST OF TABLES iv

LIST OF FIGURES v

ABSTRACT ix

ACKNOWLEDGMENTS xi

1. RESERVOIR CHARACTERIZATION 1

  1.1 Natural Fractures in the Spraberry Formation, Midland Basin, TX: The effects of Mechanical Stratigraphy on Fracture Variability and Reservoir Behavior 1

    1.1.1 Abstract 1

    1.1.2 Introduction 1

      1.1.2.1 Background 1

      1.1.2.2 Spraberry Project 3

    1.1.3 Natural Fracture Descriptions 4

    1.1.4 Possible Origins for Three Fracture Sets 5

      1.1.4.1 Option 1 -Three Separate Fracturing Events 5

      1.1.4.2 Option 2 - Conjugate Fractures with Related Extension Fractures 6

      1.1.4.3 Mechanical Properties 6

    1.1.5 Discussion 8

      1.1.5.1 Fracture Spacing 8

      1.1.5.2 Shear 9

      1.1.5.3 Mineralization 9

      1.1.5.4 Stress 10

      1.1.5.5 Microfracturing and Cathodoluminescent 10

    1.1.6 Implications for Regional Geology 10

    1.1.7 Implications for Reservoirs 11

    1.1.8 Summary 14

    1.1.9 References Cited 15

2. INVESTIGATION OF CRUDE OIL/BRINE/ROCK INTERACTION 31

  2.1 Study of Waterflooding Process in Naturally Fractured Reservoirs from Static and Dynamic Imbibition Experiments 31

    2.1.1 Abstract 31

    2.1.2 Static imbibition experiments 31

    2.1.3 Static imbibition modeling 32

    2.1.4 Dynamic imbibition experiments 34

    2.1.5 Dynamic imbibition modeling 35

    2.1.6 Fracture capillary number 36

2.1.7 Results and Discussion 38
2.1.8 Conclusions 41
2.1.9 Nomenclature 42
2.1.0 References 42
3. RESERVOIR PERFORMANCE 57
3.1 Well testing Analysis of the E.T. O'Daniel Wells 57
3.1.1 Introduction 57
3.1.2 Buildup Test 57
3.1.3 Step Rate Testing (SRT) 58
3.1.4 Conclusions 60
3.1.5 References 60
4. EXPERIMENTAL INVESTIGATIONS ON CO_2 GRAVITY DRAINAGE IN A FRACTURED SYSTEM .67
4.1 Laboratory Experiments of CO_2 Gravity Drainage 67
4.1.1 Introduction 67
4.1.2 Laboratory Experiment 68
4.1.2.1 Materials used in the experiment 68
4.1.2.2 Core preparation 68
4.1.2.3 Procedure and experimental results 69
4.1.3 Analysis and Discussion 70
4.1.4 Conclusions 72
4.1.5 References 72

LIST OF TABLES

Table 1.1 Fracture data summary 21
Table 2.1 Core and fluid properties 44
Table 2.2 Core and fluid properties for Berea core 44
Table 2.3 Core and fluid properties for Spraberry core 45
Table 2.4 Rock properties of Spraberry and Berea cores 45
Table 2.5 Critical injection rates for wells in O'Daniel Pilot Area 45
Table 3.1 Fracture propagation 61
Table 4.1 Physical properties of the core samples used in previous experiments and partial results obtained 73
Table 4.2 Physical properties of the core sample used in this experiment. 73
Table 4.3 GC results of the Spraberry dead oil used in the experiment. 74
Table 4.4 Experimental results during different stages. 75

Table 4.5 GC results of different group components of oil samples obtained from CO_2 gravity drainage/injection 75
Table 4.6 Properties of oil samples obtained from CO_2 gravity drainage/injection 75
Table 4.7 Mole fraction of oil samples obtained from CO_2 gravity drainage/injection 76
Table 4.8 Weight percent of oil samples obtained from CO_2 gravity drainage/injection 77

LIST OF FIGURES

Fig. 1.1 Location map, showing the Spraberry trend of West Texas 22
Fig. 1.2 Stratigraphic column/Gamma-Ray profile through the Spraberry formation in the O'Daniel unit, Midland basin, West Texas. IU and 5U intervals are the main producing reservoir units of the Spraberry trend. The horizontal cores were taken from the thinner sandstones near the tops of the 1U and 5U intervals 23
Fig. 1.3 Rose diagrams of fracture strikes in horizontal cores from the O'Daniel #28 well. a) Fractures from the lower cored unit associated with the 5U interval; b) Fractures from the upper cored unit associated with the 1U interval, c) Superimposed rose diagrams of fracture strikes from the upper and lower units 24
Fig. 1.4 Schematic planview of the locations of natural fractures in horizontal core from the upper Spraberry unit, O'Daniel #28 well. (Note: the bedding planes that define lithologic changes are portrayed in side view.) 25
Fig. 1.5 Schematic planview of the locations of natural fractures in horizontal core from the lower Spraberry unit, O'Daniel #28 well. (Note: the bedding planes that define lithologic changes are portrayed in side view.) 26
Fig. 1.6 Spacing histograms of the three cored Spraberry natural fracture sets. (Shading patterns are keyed to the shading of the rose diagrams in Fig. 3) 27
Fig. 1.7 Ideal geometry of a conjugate fracture pair with an extension fracture set that bisects the acute conjugate angle 28
Fig. 1.8 Comparison of the yield strengths for different confining stresses for samples of the upper (lU) and lower (5U) Spraberry siltstone-sandstone units. The lower unit is significantly weaker, causing conjugate fractures to form in this interval whereas extension fractures formed concurrently in the stronger, upper unit 29
Fig. 1.9 Structure contour map on top of the Spraberry formation in the O'Daniel unit area, Midland basin, West Texas. Dashed line is the azimuth of the two horizontal side tracks of the O'Daniel #28 well 30
Fig. 2.1 Physical process of laboratory spontaneous imbibition 46
Fig. 2.2 Concept of dynamic imbibition process 46
Fig. 2.3 Experimental setup of dynamic imbibition 47

Fig. 2.4 Relative permeability curves 47
Fig. 2.5 Schematic representation of matrix and fracture where the viscous and capillary forces are effective... 48
Fig. 2.6 Imbibition capillary pressure obtained from matching spontaneous imbibition data 48
Fig. 2.7 Matching between spontaneous-imbibition experiments with numerical solution using 0.2 S_{or}........ 49
Fig. 2.8 Matching between experimental data and the numerical solution (Berea core - cumulative water production, injection rate = 4.0 cc/hr) 49
Fig. 2.9 Matching between experimental data and the numerical solution (Berea core - cumulative oil production, injection rate = 4.0 cc/hr) 50
Fig. 2.10 Matching between experimental data and the numerical solution (Spraberry core - cumulative water production, injection rate = 1.0 cc/hr) 50
Fig. 2.11 Matching between experimental data and the numerical solution (Spraberry core - cumulative oil production, injection rate = 1.0 cc/hr) 51
Fig. 2.12 Capillary pressure obtained as a result of matching experimental data (Berea and Spraberry 51
Fig. 2.13 Reproducibility of the dynamic imbibition flooding results in Berea Sandstones 52
Fig. 2.14 Oil recovery from fractured Berea cores during water injection using different injection rates 52
Fig. 2.15 Water cut during the dynamic imbibition experiments for fractured Berea cores 53
Fig. 2.16 Oil recovery from fractured and unfractured Spraberry cores during water injection using different injection rates 53
Fig. 2.17 Water cut during the dynamic imbibition experiments for fractured and unfractured Spraberry cores ...54
Fig. 2.18 Injection rate vs. oil cut (TOP/TFP) 54
Fig. 2.19 E.T. O' Daniel pilot area 55
Fig. 3.1 Step rate test (SRT) design for O'Daniel injection Well 46 61
Fig. 3.2 Plot of injection pressure versus cumulative time O'Daniel Well 46 62
Fig. 3.3 Radial Odeh & Jones plot for Well 46 62
Fig. 3.4 Pressure vs. cumulative injection during SRT O'Daniel Well 46 with unit slope line to determine effects of wellbore storage on rates 63
Fig. 3.5 Odeh & Jones linear time plot for O'Daniel Well 46 63
Fig. 3.6 Step rate test history of O'Daniel Well 47 64
Fig. 3.7 Pressure/time history plot of O'Daniel Well 47 64
Fig. 3.8 Cumulative injection plot during SRT on O'Daniel Well 47 65
Fig. 3.9 Odeh & Jones multirate radial plot for O'Daniel Well 47 65
Fig. 3.10 Odeh & Jones multirate linear time plot for O'Daniel 47 66
Fig. 4.1 Oil recovery curves obtained from the five experiments with different permeabilities and initial water saturations 78
Fig. 4.2 Effect of permeability on oil recovery of CO_2 injection 78
Fig. 4.3 Effect of initial water saturation on oil recovery of CO_2 injection 79
Fig. 4.4 Set-up for water and CO_2 gravity drainage experiment 79

Fig. 4.5 Oil and water producing history during the experiment 80
Fig. 4.6 Oil recovery curve for the whole experiment 80
Fig. 4.7 Oil and water saturation history and oil recovery curve 81
Fig. 4.8 Oil recovery and volume of CO_2 used during CO_2 drainage 81
Fig. 4.9 Mole fraction of oil samples from CO_2 gravity drainage 82
Fig. 4.10 Weight percent of components of oil samples from CO_2 drainage 82
Fig. 4.11 Mole fraction of component groups of oil samples during CO_2 drainage 83
Fig. 4.12 Weight percent of component group of oil samples during CO_2 drainage 83
Fig. 4.13 Average molecular weight and density of oil samples from CO_2 drainage 84
Fig. 4.14 Oil recovery curves vs. rock permeability of the six experiments 84

ABSTRACT

The overall goal of this project is to assess the economic feasibility of CO_2 flooding the naturally fractured Spraberry Trend Area in West Texas. This objective is being accomplished by conducting research in four areas: 1) extensive characterization of the reservoirs, 2) experimental studies of crude oil/brine/rock (COBR) interactions in the reservoirs, 3) reservoir performance analysis, and, 4) experimental investigations on CO_2 gravity drainage in Spraberry whole cores. This report provides results of the fourth year of the five-year project for each of the four areas including a status report of field activities leading up to injection of CO_2.

In the first area, we have completed the reservoir characterization, which includes matrix description, pay zone detection (from core-log integration), fracture characterization, a detailed analysis of petrography and diagenesis of the varying rock types, the classification of rock types, and developing relationships between depositional features, petrophysical parameters and reservoir quality. All of this information is found in previous Annual Technical Reports. We have extended fracture characterization found in the 3rd Annual Report. This report provides a detailed analysis of the effect of mechanical stratigraphy on fracture variability and reservoir behavior.

In the second area, we have completed static and dynamic imbibition experiments and modeled the experiments. The results of this study were used to determine the critical injection rate during waterflooding in naturally fractured reservoirs. An equation to determine the critical injection rate was developed to scale-up laboratory results to field dimensions. We found that optimization of injection rate is important prior to conducting waterflooding in naturally fractured reservoirs. As the flow rate increases, contact time between matrix and fluid in fracture decreases, thereby reducing the effectiveness of capillary imbibition. Imbibition transfer is more effective for low injection rates due to lower viscous forces and longer contact time with the matrix. Increasing injection rate beyond the critical injection rate causes faster water breakthrough, which results in significantly higher watercut.

In the third area, buildup and step-rate tests have been analyzed to further characterize the reservoir and define the proper reservoir management strategy. The buildup tests were taken at E.T. O'Daniel Wells 38, 39, and 40. The analysis shows that the calculated permeability is in the range of 0.01-0.04 md. The pressures determined from these tests are low and below the MMP necessary for CO_2 flood. The step rate injection test to obtain formation parting pressures were conducted in the new well injection wells E.T O'Daniel 46 and 47. The parting pressure is conservatively estimated to be 2215 psia. The analysis also indicates that hydraulic fractures may propagate during the test.

In the fourth area, we have completed the water imbibition followed by CO_2 gravity

drainage experiments in Berea whole cores at reservoir conditions and reported in Section 4. The experiment models the actual field experience of first waterflooding and then CO_2 recovery gravity drainage. The experiment was initially designed to use a Berea core and a Spraberry reservoir core. As the experiment on Spraberry core has not been completed at the time of this writing, only the results from the experiment of the Berea core are presented in this report. The results of this experiment demonstrate that CO_2 gravity drainage could significantly increase the oil recovery after waterflooding in naturally fractured Spraberry Trend Area. Water imbibition followed by CO_2 injection may be more efficient than only injecting CO_2. The efficiency of the CO_2 injection decreases as permeability decreases and initial water saturation increases. Cyclic CO_2 injection could enhance oil recovery during CO_2 gravity drainage process. Temperature does not have significant effect on CO_2 gravity drainage process because CO_2 has more pronounced effect on increasing the mobility of oil and decreasing the interfacial tension (IFT).

ACKNOWLEDGMENTS

This work was financially supported by the United States Department of Energy's National Petroleum Technology Office and the following consortium of companies; Marathon Oil Co., Mobil Research and Development Corp., Mobil E&P USA, Pioneer Natural Resources (formerly Parker and Parsley Petroleum Co.), Petroglyph Operating Co., Texaco E&P Technology Dept., The Wiser Oil Co. and Union Pacific Resources. This support is gratefully acknowledged. Geographix Inc. donated software used in reservoir characterization. GeoQuest donated ECLIPSE software used in reservoir simulation. I greatly appreciate diligent efforts from the following individuals who contributed to this project. John Lorenz from Sandia National Laboratory, Jenny L. Cherney from New Mexico Tech and Chris L. Whigham from Pioneer Natural Resources, performed the fracture analysis of the horizontal core reported in Section 1. Erwinsyah Putra and Yan Fidra completed a report on imbibition by experimental work performed at reservoir conditions, mathematical modeling and computer simulations. Their work is reflected throughout Section 2. John Rogers and Erwinsyah Putra conducted step rate injection test analysis reported in Section 3. Hujun Li performed imbibition and gravity drainage experiments in a Berea whole core. His work is reported in Section 4.

Other acknowledgments go to Richard Baker of Epic Consulting Ltd., Steve Melzer and Loren Stiles of UTPB-CEED, Randy Miller of Reservoirs Inc. and Lincoln Elkins. Chris Whigham and Paul McDonald continue to guide this project. Finally, thanks go to Liz Bustamante for proofreading this document.

1. RESERVOIR CHARACTERIZATION

1.1 NATURAL FRACTURES IN THE SPRABERRY FORMATION, MIDLAND BASIN, TX: THE EFFECTS OF MECHANICAL STRATIGRAPHY ON FRACTURE VARIABILITY AND RESERVOIR BEHAVIOR

1.1.1 Abstract

Horizontal cores taken from two of the deep-marine, sandstone-siltstone reservoirs in the Spraberry Formation (Midland basin, West Texas) have documented two entirely different but related systems of vertical natural fractures. Each fracture system is capable of producing the long recognized, generally northeast-trending, strong permeability anisotropy in the Spraberry reservoirs. However, the two fracture systems offer potentially different degrees of permeability anisotropy, and different potentials for fluid deliverability. One fracture set consists of evenly spaced, well mineralized, northeast-striking fractures. The other fracture set, occurring in a similar lithology only 145 feet deeper in the section, consists of a poorly mineralized conjugate fracture pair, striking north-northeast and east-northeast. The geometry of these fracture sets suggests that the maximum compressive stress at the time of fracturing was in the horizontal plane. Subtle differences in the clay and quartz-overgrowth contents of the two layers produced important differences in the mechanical properties: although similar in appearance, the lower strata have a measured mechanical yield strength that is only half of that of the upper layer. This caused the two layers to fracture differently under the same regional stress, with conjugate fractures forming in the weaker layer and extension fractures forming in the stronger layer. Such differences in the mechanical properties, caused by minor variations in the diagenetic and depositional histories of the strata, are probably widespread within the formation and may cause significant variations in the fracture system both across the basin and vertically within the formation.

1.1.2 INTRODUCTION

1.1.2.1 Background

Large reserves of oil were discovered in the Spraberry Formation in the Midland basin of West Texas in 1949. The area of Spraberry production (Fig. 1.1) comprises one of the largest areal reservoirs in the world: it encompassed over 400,000 acres as early as 1953 (Elkins, 1953), and currently covers approximately 16,000,000 acres. Spraberry reservoirs occur at depths of approximately 7000-8000 ft, and consist of nearly 1000 ft of interbedded, fine-grained sandstones, coarse siltstones, and organic-rich shales. The main Spraberry reservoir units in the E.T. O'Daniel Unit described here are two 10-15 ft thick sandstones, designated the 1U and 5U reservoirs, within the sandier parts of the formation (Fig. 1.2).

The Spraberry strata were deposited in a deep-marine environment during the Leonardian stage of the Permian period. The formation is typically interpreted as the deposits of turbidity currents (e.g., Tyler and Gholsten, 1988; Guevara, 1988). The lateral continuity of small-scale bedding, sedimentary structures including sub-millimeter scale depositional-event laminae, and a high degree of size sorting suggest that some of the Spraberry and related systems have resulted from eolian processes and dust-storm activity (Lorenz and Brooks, 1990; Kocurek and Kirkland, 1998).

Poor recovery efficiency has hampered the exploitation of the Spraberry resource. The play has had a cumulative production of 740 million barrels of oil to date, but oil recovery percentages and the daily production rates of individual wells are low. While daily production across the entire play currently averages 62,000 barrels of oil (and 25,000 cubic feet of gas), which is an average of only 7 BO/D from each of the 8,900 producing wells (Whigham, 1998). The estimated ultimate recovery of oil from the play is only 10-15% of the 6-10 billion barrels of oil originally in place. Spraberry reservoirs are underpressured, averaging only 800-900 psi. Porosities range from 6-15%, and restored-state matrix permeabilities are typically significantly less than 1 millidarcy.

All areas of the Spraberry Trend have indications of extensive natural fracturing despite their location in a stable, cratonic setting with minimal faulting and folding. Fracturing and a generally northeasterly-trending, fracture-controlled permeability anisotropy were recognized to be the dominant controls on reservoir plumbing early in the life of the field. However, the data necessary for three-dimensional characterization of this important fracture system, and for prediction of its variability and effects on the reservoir plumbing system, were lacking. The presence of fracturing was corroborated by early workers with limited amounts of core, including one deviated core (Wilkinson, 1953), although many of the fractures logged in those vertical cores would now be classified as coring-induced fractures. These induced fractures are parallel to many of the natural fractures and thus the proper inferences were made, albeit for the wrong reasons. Given the natural fracture spacing demonstrated by the horizontal cores as discussed below and the low probability of intersecting vertical natural fractures with vertical cores (e.g., Lorenz, 1992), only one in five to ten four-inch diameter cores would be expected to intersect a natural fracture in any given Spraberry reservoir.

Much of the early recognition of the importance of fracturing was based on the results of well tests and notations of rapid interference or communication between adjacent wells (Elkins, 1953; Elkins and Skov, 1960, Schechter et al., 1996a,b.) However, these tests often give erratic results, and do not lead to a uniform picture of the fracture characteristics and their effects across the field. Horizontal permeability anisotropy due to fracturing was calculated to average 13:1 but locally ranged up to 1000:1 (Elkins and Skov, 1960). The early data indicated a generally northeast trend to this maximum horizontal reservoir permeability that has been assumed to be the average fracture strike, although the maximum-permeability axes observed locally sites ranges from N 36° E to N 76° E.

Early tracer tests, pulse tests, and pressure-buildup and decline tests (Elkins and Skov, 1963; summarized by Putra, 1998) also suggested that the conductivity of the Spraberry fracture system is sensitive to changes in the in situ stress. Decreased formation pressures during production may cause a partial or complete closing of fracture apertures, accounting in part for the observed rapid declines in production rates in fractured reservoirs. Likewise, increasing the local pressures during injection has caused a significant increase in local reservoir conductivity (see Lorenz, 1999). A sensitivity of the fractures to changes in stress has been confirmed by recent testing (Schechter et al., 1996a.) It is discussed further below.

1.1.2.2 Spraberry Project

A proposal to conduct experiments designed to improve recovery from Spraberry reservoirs was funded by the National Petroleum Technology Office of the U.S. Department of Energy in 1995. This was a cost-sharing proposal submitted to DOE's Class Reservoir program by 1) the Petroleum Recovery Research Center of the New Mexico Institute of Mining and Technology, and 2) Pioneer Natural Resources (then Parker and Parsley, Inc.). The goal of the project has been to assess the economic feasibility of CO_2 flooding in Spraberry reservoirs.

One of the initial tasks of the project was to make a detailed characterization the natural fractures and the in situ stresses in the Spraberry reservoirs through the use of oriented horizontal cores. Samples of the matrix rock would also be taken from these cores, to be tested in the laboratory for suitability for CO_2 flooding as the primary objective of the project (Schechter et al., 1996a). The horizontal cores are the first known from the Spraberry reservoirs in the Midland basin. This paper reports on the characterization of the natural fractures, analyzes the fractures in the context of the geologic variables that produced them, and briefly reports on their effects on the Spraberry reservoirs.

Nineteen horizontal core runs, recovering a total of 395 ft of core, were cut in 1996 from two horizontal sidetracks from the existing E.T. O'Daniel #28 well (McDonald et al., 1997). The principal reservoirs within the 1U and 5U intervals are ten-foot thick sandstone to siltstone units, which are separated vertically from each other at this site by 145 ft of interbedded sandstones, siltstones, and shales (Fig. 1.2). Although the two ten-foot thick units were targeted for coring, post-drilling analysis suggests that most of the cores were cut at near-horizontal angles across thinner, three- to four-ft thick sandy siltstones immediately above the two main-pay reservoirs. Several of the cores missed the reservoir units and were cut in the immediately over- and underlying shale beds, allowing for a comparison of fracture distributions with lithology. The cores were carefully pieced together immediately after recovery, and analyzed for natural fractures before being slabbed, plugged, or sampled (techniques described by Lorenz and Hill, 1992).

1.1.3 NATURAL FRACTURE DESCRIPTIONS

An excellent data set characterizing the local subsurface Spraberry fracture system was obtained from the horizontal cores. Preliminary reports of the natural fracture data have been given in Lorenz (1997a, 1997b) and Malmanger et al. (1997), but the final data set and its in-depth analysis are presented here. The most surprising aspect of the data is the significant difference that exists, despite stratigraphic proximity and lithologic similarity, between the fracture populations of the two cored intervals (Table 1).

The upper cored interval contains forty-six mineralized, northeast-striking fractures (Set 1 fractures, having an average strike of 43^0; Fig. 1.3). In contrast, the lower sandstone contains two poorly mineralized natural fracture sets, the strikes of neither set corresponding to that of Set 1 (Fig. 1.3). The twenty-eight fractures of Set 2 strike generally north-northeast (average strike 32^0), and twenty-nine fractures of Set 3 strike east-northeast (average 70^0 degrees).

Set 1 fractures have a low variability in strike (Fig. 1.3), and occur only in the sandstone and siltstone reservoir facies. These fractures are regularly and closely spaced; corrected spacing normal to fracture strike ranges from just under one ft to 5.8 ft and averages 3.2 ft (Fig. 1.4, 1.5). The fractures are partially to almost wholly mineralized with barite except for the four fractures nearest the base of the sandstone. The fractures of Sets 2 and 3 have irregular spacings (Fig. 1.6): spacings of fractures within Set 2 range from fractions of an inch to 4.5 ft (average 1.6 ft), whereas spacings of Set 3 fractures range from fractions of an inch up to 13 ft (average 3.8 ft). Analyzed together, Set 2 and Set 3 fractures in the lower core have a combined average spacing along a northeast trend (oblique to both fracture strikes) of about 2 ft. Although poorly mineralized, the surfaces of fracture sets 2 and 3 do not resemble the common surfaces of fresh, broken rock in the core. Moreover, minute euhedral crystals of quartz, dolomite, and barite are visible on the fracture surfaces under the microscope (Cather, 1997; Cather and Lorenz, 1998), proving that they are in fact natural.

Fractures of Set 2 occur only within the very fine-grained sandstones to coarse siltstones of the lower reservoir, and Set 1 fractures occur only within this facies in the upper reservoir. Set 3 fractures are more widespread, however. They occur predominantly in the sandstone-siltstone facies of the lower reservoir but are also present within higher, finer-grained zone of the upper sandstone. They are also widely spaced (about 10 ft) but present within the black shales that immediately overlie both upper and lower reservoirs. In contrast, no natural fractures are present within the eighty feet of core inadvertently taken from the black shales immediately below these two reservoirs.

The north-northeast trending fractures of Set 2 are distinct from fractures of the other two sets in several important ways. First, the average spacing of the Set 2 fractures is about half that of the two other fracture sets. Second, these fractures commonly have an irregular, stepped, surface morphology with an en echelon character. This stepping character suggests that these fractures formed by the coalescence of smaller extension fractures within an incipient, right-lateral, Riedel-type shear zone (Petit, 1987; Lorenz, 1997c,d). In contrast, fracture surfaces from the other two sets are typically planar, suggesting an origin in extension.

Although the data reported here from the horizontal Spraberry cores have documented an unexpected variability in the Spraberry natural-fracture system, they probably have not defined the total range of that variability. Moreover, these data should not be extrapolated uniformly as a natural-fracture template to the Spraberry strata in all other parts of the basin. Rather, the stress conditions and mechanical properties that produced the observed variability in fractures should be considered, as detailed below, when predicting local Spraberry fracture characteristics.

1.1.4 POSSIBLE ORIGINS FOR THREE FRACTURE SETS

The presence of significantly different fracture populations in the two cored Spraberry reservoirs in the E.T. O'Daniel #28 well, within this relatively non-structural province of the Midland basin (average dips less than 2^0), begs explanation. Hole geometries suggest that both of the cored sandstones are between three and four ft thick, thus differences in bed thickness should not have caused significantly different fracture characteristics. The two most likely scenarios by which three such fracture sets may form are: Three fracture sets may result from three separate, sequential fracturing events, or Three fracture sets may form contemporaneously as parts of an integrated fracture system.

Although the distinctive characteristics of the three natural fracture sets initially favored the first option, the second option is the simplest and, by Occam's razor, the most likely. It is supported by the most plausible interpretations of the data, as discussed below. However, the first sequence cannot be entirely discounted without further comment.

1.1.4.1 Option 1 – Three Separate Fracturing Events

Each of the fracture sets has its own characteristic patterns of spacing (Fig. 1.6), distribution of fracture strikes (Fig. 1.3), fracture distribution with respect to lithology (Figs. 1.4, 1.5), and mineralization. Such variability initially suggested that each set formed in response to a different stress event and was mineralized during separate diagenetic events. The presence of better-developed mineralization in the northeast-striking fractures of Set 1 might even suggest a relative age relationship, i.e., that it formed and was mineralized prior to the formation of either of the other two unmineralized sets, accounting for their lack of mineralization.

However, reconstructions of the tectonic history of the basin (e.g., Ewing, 1991; Winfree, 1994, 1995) suggest that there have been very few post-depositional tectonic events likely to have produced stresses capable of fracturing the Spraberry strata. The only significant post-Permian tectonic events to affect the area have been the Laramide orogeny (Late Cretaceous to Eocene), followed by or possibly contemporaneous with gentle uplift and tilting of the strata and broad folding over basement faults.

Thus it is difficult to conceive of three or even of two separate, significant, structural-deformation events to account for three separate fracturing events. In fact, an even more convolute sequence would be required by the measurements showing that the maximum horizontal compressive stress now trends parallel to the fractures of Set 1 (Holcomb, 1997). This observation mandates that if the Set 1 fractures in fact represent a separate and oldest event, then an improbable, fourth, and final tectonic event is necessary to bring the maximum stress back again into coincidental alignment with these hypothetically oldest fractures. This would seem to be an overly contrived sequence of four stress events for this structurally simple province, and it is not supported by the tectonic history of the basin.

1.1.4.2 Option 2 – Conjugate Fractures with Related Extension Fractures

The preferred interpretation of the three fracture sets is suggested by their relative orientations. The geometry of the fractures is close to that of an ideal conjugate fracture pair (Sets 2 and 3) with an associated extension-fracture set (Set 1), the strike of the latter bisecting the acute conjugate angle (Fig. 1.7). The stepped surfaces of the fractures of Set 2 show the proper indications of incipient right-lateral shear and therefore support this interpretation, although in a perfect case complementary left-lateral shear indications would be found on the associated fractures of Set 3.

The formation of extension fractures in one bed contemporaneously with conjugate fractures in the other would require that there were significant differences in either the local effective stresses or in the mechanical properties of the two beds at the time of fracturing. The lithologic similarity and stratigraphic proximity of the two beds argue conclusively against significant local differences in stress magnitudes, in the stress differential, or in the formation pore pressures, thus local stress differences are not considered further here as a potential cause for the observed fracture variability. Rather, laboratory measurements suggest that a difference in the mechanical properties of the beds was the controlling factor.

1.1.4.3 Mechanical Properties

Strata of the two sandstone-siltstone reservoir units are similar in appearance and have similar, low, average Poisson's ratios (0.11). The elastic moduli of these strata are also nearly equal (about 2.4×10^4 MPa) (Cherney, 1998). However, the mechanical yield strength of the upper unit as measured by triaxial tests is, on average, nearly twice that of the lower unit (262.5 MPa and 150.2 MPa respectively; Fig. 1.8).

This important mechanical difference may result from subtle differences in the clay and quartz contents of the two units. Petrographic examinations (Reservoirs Inc, 1997; Saleta, 1998) show that the average total clay content of the lower unit is 10% whereas it is only about half that (6%) in the stronger, upper unit. Moreover, the type of clay apparently varies between the units: the lower unit has more common diffuse clay laminae and "an unusually high amount of detrital clay" (Reservoirs Inc, 1997). Probably because of this difference in clay content and distribution, euhedral quartz overgrowths on the component sand grains are better developed in the strong upper unit where they comprise an average of 7% of the rock volume, compared to only 3% of the rock volume in the lower unit.

Low clay contents and better cementation by quartz overgrowths would both tend to strengthen a rock mechanically. Theoretical considerations (e.g., Griggs and Handin, 1960; Lorenz, 1997c) and empirical observations of other formations (e.g., Lorenz, 1997d) suggest that weaker rock may fail in conjugate shear under the same stress conditions that create extension fractures in stronger rock. Assuming that the rock properties at the time of fracturing were similar to those measured presently, this offers a plausible basis for the presence of different fracture sets in the two units since the rock of the lower unit has only half the strength of the upper unit. The assumption of similar properties since fracturing is tenable given that the rocks were deeply buried and lithified at the time of fracturing, and considering the present depth of burial and the 200 million year hiatus between deposition and the inferred time of fracturing.

The measured yield strengths of the Spraberry samples are high, and fracturing such rock would require higher stresses than are generated in most tectonic settings. However, the strengths of these rocks would have been significantly less if formation pressures were high during fracturing, allowing fracturing under reduced differential stress conditions (see Lorenz et al., 1991). Despite the significantly underpressured nature of the current Spraberry reservoir system, it is very likely that the reservoir was overpressured at some point during its geologic history. Spraberry shales have relatively high Total Organic Carbon contents (up to 5%; Dutton, 1980), and most of the formation has passed through the oil window. The maturation of kerogen to oil and of oil to gas produces significant volume increases that may result in significantly increased formation pore pressures (e.g., Barker, 1990; Meissner, 1980, 1981). Thus the most likely time of fracturing of the Spraberry Formation was during the coincidence of high pore pressures and regional tectonic activity, when it passed through the oil window during Laramide time (Winfree, 1995).

Mechanical property variations may also explain the observed absence of fractures in strata underlying the reservoirs. The upper zones of the shale beds underlying the reservoirs are the most clay rich and therefore likely to be the most ductile zones in the shales, and devoid of fractures. In contrast, the widely spaced fractures in the lower zones of shale beds immediately overlying the reservoirs are likely to have a certain silt content. The distribution and nature of the shale mechanical properties is still under study.

1.1.5 DISCUSSION

Some fracture characteristics that initially seemed to support the scenario requiring three sequential fracture events can be reinterpreted, with deeper insight, to support the conjugates-with-bisector model.

1.1.5.1 Fracture Spacing

The three cored Spraberry fracture sets have three unique spacing distributions (Fig. 1.6). This initially suggested that each set formed as a separate system under a different stress condition. However, such differences in spacing distribution can also be attributed to different modes of formation (i.e., extension vs. shear), to the common differential development of the sets of a shear-fracture pair, and to the variable numbers of fractures of each type required to accommodate equivalent amounts of strain.

The reported spacing distributions of most fracture sets (e.g., Lorenz and Laubach, 1994; Hanks et al., 1997; Lorenz and Hill, 1994) are log-normal, i.e., with numerous close spacings and significantly fewer wide spacings. This common log-normal pattern contrasts strongly with the regular, nearly Gaussian (normal) distribution of the spacings of Set 1 fractures, and, to a lesser extent, with the modified log-normal patterns of the Set 2 and Set 3 fracture spacings.

A Gaussian distribution of extension fracture spacings has been suggested to indicate that a fracture set is exceptionally well developed or "saturated" (Wu et al., 1994; Wu and Pollard, 1995). The fractures of such a population are typically long relative to their spacing. The production and interference characteristics of the Spraberry reservoirs are consistent with a well-developed and inter-connected system of long fractures, and therefore the Set 1 fractures are inferred to be saturated.

We are unaware of published distributions of shear-fracture spacings for comparison, although Wu (personal communication, 7/97) suggests that they might be expected to follow the same pattern of development (i.e., log-normal spacings early in fracture development history, becoming Gaussian with continued development and maturation.) If so, then the log-normal spacing distributions of fracture sets 2 and 3 suggest fracture sets that are less mature than fracture set 1. However, combined, the two less-mature fracture sets of the conjugate pair appear to have accommodated an amount of strain equivalent to that accommodated by the single, well developed set of Set 1 extension fractures. The average aperture of the Set 1 extension fractures and the average offset of the Set 2 and 3 conjugate fractures are estimated to be 0.5 mm, and the average spacing of Set 2 and Set 3 fractures (combined) is about two feet. Back-of-the-envelope calculations considering the geometries of these fractures suggest that both the extension and the conjugate fracture systems accommodated about 0.05% horizontal extension in the southeast-northwest direction. This supports an interpretation of the concurrent formation of different fracture types having different characteristics under the same stress system.

1.1.5.2 Shear

The shear offset across the fractures of many conjugate systems is minimal and therefore difficult to discern. However, the subtle, consistent, Riedel-type shear steps on Set 2 fracture surfaces are convincing evidence that incipient shear did in fact occur on these fractures.

The absence of obvious shear indicators on the complementary Set 3 fractures is problematic but not insurmountable. One member of a fracture pair is better developed than the other in many conjugate systems, although the reasons for this are usually obscure. We infer that local structures may have played an important role in the differential fracture development observed in the Spraberry reservoirs. Winfree (1994, 1995) has suggested that many of the flexures within the strata of the Permian basin formed contemporaneously with fracturing of the Spraberry in Laramide time. Extension across the east-west axis of the small nose at the O'Daniel site (Fig. 1.9) during folding would have superimposed a small amount of north-south extension on the developing fracture systems, leading to a hybrid shear-extension fracturing in the Set 3 fracture orientation. Moreover, the smaller average angle between the sheared Set 2 fractures and the inferred northeast-trending maximum horizontal compressive stress (compared to the angle between Set 3 fractures and the compressive stress) means that Set 2 fractures would have been more readily sheared than Set 3 fractures.

1.1.5.3 Mineralization

The differences in fracture mineralization that initially suggested sequential fracture development may, rather, be the result of differences in either the fluid flow capacities of the two fracture systems or to the differences in apertures of the three sets. Interconnected conjugate fractures should have had better conductivity and interconnectedness within the reservoirs, allowing for easy mineralization and/or its dissolution. A system of poorly-connected, sub-parallel extension fractures, on the other hand, may have become a relatively closed system early on during mineralization, minimizing subsequent fluid flow. Shear fractures also accommodate strain via slip on an incline with no aperture required, whereas extension fractures accommodate strain via the opening of void-space apertures along the fracture planes. Therefore, shear fractures, especially incipient shears, would typically have less aperture within which to deposit large volumes of mineralization such as are found in Set 1extension-fractures.

1.1.5.4 Stress

Detailed circumferential velocity-anisotropy measurements on the core indicate a northeast-trending present-day, in situ, maximum horizontal stress (Holcomb, 1997). This trend is parallel to the Set 1 fracture strikes and bisects the acute angle between Sets 2 and 3, as would be expected for stresses capable of concurrently forming both the Set 1 extension fractures and the Set 2-3 conjugate fractures (Fig. 1.7). This stress orientation provides strong support for an origin of the three fracture sets as an integrated system.

1.1.5.5 Microfracturing and cathodoluminescence

Microfractures visible only under the microscope and illuminated by cathodoluminescence (CL) have been suggested to be predictors for larger-scale fracture trends (Laubach, 1997). Three samples of sandstones from the upper zone were analyzed for microfracturing using CL techniques. The results (BEG, 1997) do not predict the three fracture sets described above.

One CL sample, located midway between two mineralized fractures spaced 5.5 ft apart and having strikes of 40^0 and 45^0, is reported to have a vector mean microfracture strike measured by cathodoluminescence of 25^0 degrees.
Two CL analyses from the second sample, located immediately adjacent to a fracture with a 45^0 strike, have reported vector mean microfracture strikes of 19^0 and 347^0.
Three CL analyses of the third sample, located exactly midway between two fractures with 80^0 and 40^0 strikes and spaced 4.4 ft apart, have reported vector mean microfracture strikes of 25^0, 42^0, and 32^0.

Most of the fractures from the interval sampled for cathodoluminescence are extension fractures, with an average strike of 43^0. However, the reported average of 25^0 +_10^0 for all analyzed cathodoluminescence microfractures would appear to be best aligned with the average 32^0 strike of the Set 2 shear fractures in the other sandstone. Cathodoluminecence results do not reflect the average 70^0 fracture set (Set 3) that is also common in the other zone or the 80^0 extension fracture present 2.2 feet from the third sample. There is little or no field evidence (from vertical cores, from horizontal cores, or from well tests,) for the 347^0 fracture trend inferred from cathodoluminescence, and this fracture trend does not affect the Spraberry reservoirs if it is present.

1.1.6 IMPLICATIONS FOR REGIONAL GEOLOGY

Northeastward-directed Laramide compressive stresses have been suggested to be the source of much if not all of the post-Permian structural deformation in this basin (e.g., Hills, 1970; Price and Henry, 1985; Calhoun and Webster, 1983; Erdlac, 1993, Winfree, 1994, 1995). The closest of the Laramide thrust systems is only 300-350 km distant, located south of the El Paso region (Drewes, 1991). Its trend is northwest-southeast, consistent with a northeast-southwest directed compressive stress in the forelands as inferred from the geometries of the Spraberry fractures, and as measured in situ today.

Interestingly, the interpretation of fracture sets 2 and 3 as a system of conjugate fractures with a northeast-striking bisector mandates the unconventional interpretation that, at the time of fracturing, the vertical, overburden stress was not the maximum compressive stress. Rather, a conjugate fracture pair with this geometry (i.e., with a vertically oriented axis of fracture-plane intersection), records a stress system oriented such that the maximum compressive stress was northeast-southwest in the horizontal plane, the minimum stress was southeast-northwest, and the intermediate stress was vertical.

The interpretation that the vertical, overburden stress in the Permian basin was only the intermediate stress at the time of fracturing suggests that the horizontal stress magnitudes, and by implication the stress anisotropies, were large during Laramide tectonic events. A configuration where the maximum stress is horizontal rather than vertical is not a commonly recognized condition in basins distant from obvious sources of significant horizontal stress. However, Craddock and van der Pluijm (1989) have suggested that significant differential stresses can be derived from a thrust system and imparted to strata up to a thousand kilometers beyond a thrust front by measuring calcite twin lamellae in strata in front of the Appalachian-Ouachita thrust-belt. Conjugate shear fractures with similar geometries and which thus indicate similar stress orientations have been documented elsewhere (e.g., in the Tertiary strata of the Piceance basin of Colorado; Lorenz, 1997d).

Although the present-day stresses are still aligned with this trend, the stress magnitudes are low. Differential velocity (P and S waves) and strain measurements made on samples from the horizontal and nearby vertical cores (Holcomb, 1997) suggest that there is presently only a 1-3% difference in the velocity anisotropy in these rocks, implying that the horizontal stress magnitudes in Spraberry reservoirs are similarly low. Measurements of stress in other formations of the basin (Nolen-Hoeksmema et al., 1992; Avasthi et al., 1991) are generally consistent with the northeast-trending maximum stress orientation measured at the O'Daniel site, although they suggest that a somewhat larger stress differential exists in other parts of the basin. These authors also report that the in situ stresses may locally be reoriented over structures. If the above stress/fracture model is valid, then the present day stress field is a weaker, relaxed remnant of the fracturing stresses. Reduction of pore pressures over geologic time would have contributed to this diminution of the total stress magnitudes.

Similar relaxed stresses have been documented elsewhere. One example is the Mesaverde strata in the Piceance basin of Colorado. A low-magnitude, remnant, stress anisotropy has been measured within the lenticular sandstones in this formation. The remnant status of that stress is proven by measurements of stresses in the enclosing shales showing that they have completely relaxed to the overburden stress state, and are thus not transmitting an active stress to the sandstones to produce the measured anisotropy (Lorenz and Finley, 1991.)

1.1.7 IMPLICATIONS FOR RESERVOIRS

The natural fracture system in the Spraberry reservoirs creates a permeability anisotropy of up to 1000:1 despite the absence of a strong stress anisotropy. The permeability anisotropy is typically but not universally aligned along a northeast-southwest trend. This much has been known for some time. However, data from the horizontal, E.T. O'Daniel #28 cores highlight an unsettling variability in fracture characteristics, a variability that may be present within reservoirs despite seemingly homogeneous lithologies and an absence of major structure. Well tests and tracer tests in Spraberry reservoirs commonly give erratic results when measuring the magnitude and orientation of the horizontal permeability anisotropy in the formation, indicating that horizontal permeability ratios and their orientations are variable with location. As discussed below, this study suggests that both observations may be a function of subtle differences in lithology, which in turn control mechanical properties such that different types of fracture systems formed. Anisotropy ratios and orientations also change with time, as the in situ stresses are altered by production or injection and cause different fracture sets to open or close. Finally, variability in the production potential of different zones may be related to the different interconnectivity and conductivity of the different fracture systems. Such non-uniformity is explained by low horizontal stress differentials in combination with multiple fracture orientations.

The ratio of maximum to minimum horizontal permeability should be higher in zones that contain only the northeast-southwest (Set 1) fracture type. Reservoirs with weaker strata and the resulting conjugate fractures should have a less pronounced permeability anisotropy. Production potential from a conjugate fracture system should be greater, both because of the better fracture interconnection and because of the insignificant mineralization. Moreover, the sensitivity to changes in the in situ stresses during production should be different for the two fracture systems: increases in confining stress should close the apertures of extension fractures, but should initiate slip on shear fractures (see Lorenz, 1997c). Unfortunately, the lateral leg of the E.T. O'Daniel #28 well through the lower horizon containing conjugate fractures was lost before a comparison could be made between the production capabilities of the two fracture systems.

The horizontal permeability ratios and the trends of maximum permeability are also variable in this system. Extension fractures will provide little enhancement over matrix permeability in the transverse direction and will thus produce large anisotropy ratios. Conjugate fractures create drainage areas with less ellipticity. One leg of a conjugate fracture pair may be better developed or may be preferentially held open by the in situ stresses, creating unexpected deviations to the maximum permeability trend. Although the maximum permeability orientation within the Spraberry Trend is often close to N45^{0}E, many operators have noted preferential east-west movement of fluids. The Humble pulse test from the 1960's in the Midkiff Unit (see Putra, 1998) illustrates this variability. A test in one section of the Midkiff Unit confirmed the known northeast-southwest directional permeability, but a pulse test conducted in less than one mile away yielded a faster pulse transmissibility in the east-west direction.

Anisotropy orientations and ratios in the Spraberry may change as a function of changes in stress. Hydraulic fractures tend to follow natural fractures below a threshold injection pressure, but are less constrained above this threshold because the low stress anisotropy is easily overcome by local injection pressures. Similarly, injections of tracers at relatively low pressures are capable of opening up communication pathways that are not aligned with the primary northeast-southwest trend. Humble's pulse test in the Midkiff Unit can also be used to illustrate this: water was injected into a pilot pattern during this test over a period of six months, and communication was established between wells along the northeast-southwest trend early in the test. No communication was apparent initially between the injection wells and production wells aligned perpendicular to this trend. Once injection water was recovered from wells along the off-trend direction, however, the volume of water recovered from these wells gradually increased as injection proceeded. A secondary, stress-sensitive fracture network was probably opened and exploited by the increased reservoir pressures created by continued water injection, decreasing the horizontal permeability anisotropy of the system. This "breathing" effect that is dependent on reservoir pressure is probably a large part of the reason for the wide variability in measured permeability anisotropy ratios and directions throughout the field.

Further evidence of stress-sensitive fractures was observed in 1993 during an 80-acre water-injection pilot in Upper Spraberry reservoirs, also in the Midkiff Unit (Schechter et al., 1996a). Production wells at this site, again oriented along the trend of the northeast-southwest fracture trend from an injection well, were monitored after initiation of water injection. No injected water was observed in the nearest offset well for nearly 300 days. However, a radioactive tracer injected once communication between the wells had been established reached the same production well within 24 hours. This change in conductivity of the reservoir system is a clear indication that permeability of the fracture system had increased as the local pressure increased.

The stresses and related resistance of the Spraberry Formation to fracturing are so low that mud weights and/or the piston action of tripping a core barrel into the hole are commonly sufficient to cause inadvertent hydraulic fracturing of the formation below the bit. This results in Spraberry cores that are intensely petal-fractured or that are split along one or more parallel planes along the core axis. Many such coring-induced fractures merely extend the existing plane of a natural fracture, obscuring the distinction between natural and induced fractures. This below-the-bit, inadvertent hydraulic fracturing is undoubtedly common but undocumented in uncored holes as well. So-called “vacuum fracs” are also a typical stimulation practice in the field: the formation is broken down and stimulated by a hydraulic fracture created merely by the weight of a column of fluid in a wellbore.

1.1.8 SUMMARY

Horizontal cores taken from two different levels of the Spraberry Formation show that significantly different systems of natural fractures are present in the two otherwise similar, closely adjacent sandstone-siltstone reservoirs. One fracture set consists of evenly spaced, mineralized, vertical, northeast-striking fractures. The other fracture set, occurring in strata only 145 feet deeper, consists of a poorly mineralized, vertical, conjugate pair, the members of which strike north-northeast and east-northeast. Both fracture systems formed during the same Laramide tectonic event, when the regional compressive stress was directed northeast-southwest and pore pressures in the formation were probably high. The conjugate geometry indicates that the maximum compressive stress was in the horizontal plane at the time of fracturing. Differences in the petrographic makeup of the two layers, primarily their clay content and the volume of quartz overgrowths, caused subtle but important differences in the mechanical properties, specifically the yield strengths, of the rocks. Conjugate fractures formed in the weaker strata at the same time that extension fractures formed in the stronger layer. This variability may be predictable to the extent that the subtleties in local diagenetic and depositional histories can be accurately reconstructed and integrated with subtle structural variations. The minimal differential between the present-day in situ horizontal stresses, as well as the low in situ stress magnitudes, provide poor constraints on the azimuths of injections into the formation, and off-trend fracture permeability may be opened up at higher injection pressures.

Fracture characteristics may vary significantly between different Spraberry reservoir units: an understanding of the basis for this variability should lead to a rationale for designing and positioning development wells. The observed system of extension fractures in the upper zone with conjugate fractures in the lower Spraberry reservoir unit should *not* be extrapolated universally to the 1U and 5U Spraberry reservoirs across the Midland basin. Predictions of fracture characteristics will be most successful where subtle changes in depositional environments and the related petrologic characteristics can be delineated, and where good control exists on the structural configuration of the basin.

1.1.9 REFERENCES CITED

Avasthi, J.M., R.C. Nolen-Hoeksema, and A.W.M. Rabaa, 1991, In-situ stress evaluation in the McElroy field, West Texas: *SPEFE*, v. 6, p. 301-309.

Bureau of Economic Geology, 1988, Reservoir Characterization Research Laboratory, Sixth Quarterly Report, 58 p.

Bureau of Economic Geology, 1997, Determination of natural fracture orientation using scanned CL; Natural fracture analysis project progress report NM-004, March 14, 1997; 7 p., 2 figs.

Barker, Colin, 1990, Calculated volume and pressure changes during the thermal cracking of oil to gas in reservoirs: *AAPG Bull.*, v. 74, p. 1254-1261.

Calhoun, G.C., and R.E. Webster, 1983, Surface and subsurface expression of the Devils River Uplift, Kinney and Val Verde counties, Texas, *in* Kettenbrink, E.C., Jr. (ed.), Structure and stratigraphy of the Val Verde basin-Devils River Uplift, Texas: West Texas Geological Society Publication 83-77, p. 101-118.

Cather, Martha, 1997, Spraberry fracture diagenesis: The microscopic view of fractures; Third Naturally Fractured Reservoir Symposium, Petroleum Recovery Research Center, New Mexico Institute of Mining and Technology, Socorro, NM, October 28, 1997, (unpaginated).

Cather, Martha, and J.C. Lorenz, Characterization of natural fractures in Spraberry trend area reservoirs, Permian basin, West Texas (abstract); AAPG annual convention, Salt Lake City, 17-28 May, 1998 (unpaginated).

Cherney, J.L., 1998, Investigation of anisotropy from Spraberry horizontal cores: Fourth Annual Naturally Fractured Reservoir Symposium, Petroleum Recovery Research Center, New Mexico Institute of Mining and Technology, Socorro, NM, October 27, 1998 (unpaginated).

Craddock, J.P., and B.A. van der Pluijm, 1989, Late Paleozoic deformation of the cratonic carbonate cover of eastern North America: Geology, v. 17, p. 416-419.

Drewes, Harald, 1991, Description and development of the Cordilleran Orogenic Belt in the southwestern United States and northern Mexico; US Geological Survey Professional Paper 1512, 87 p.

Dutton, S.P., 1980, Petroleum source rock potential and thermal maturity, Palo Duro basin, Texas: Bureau of Economic Geology Geological Circular 80-10, 32p.

Elkins, L. F., 1953, Reservoir performance and well spacing, Spraberry trend area field of West Texas*: Trans., AIME*, v. 198, p. 177-196.

Elkins, L.F., and A.M. Skov, 1960, Determination of fracture orientation from pressure interference: *Trans., AIME*, v. 219, p. 301-304.

Elkins, L.F., and A.M. Skov, 1963, Cyclic water flooding in the Spraberry utilizes "end effects" to increase oil production rate: *JPT*, v. 15, p. 877-884.

Erdlac, R.J., 1993, Small-scale structures in the Guadalupe Mountains region: Implication for Laramide stress trends in the Permian basin: New Mexico Geological Society Guidebook, 44th Field Conference, Carlsbad region, New Mexico and West Texas: p. 167-174.

Ewing, T.E., 1991, The tectonic framework of Texas; text to accompany the tectonic map of Texas: University of Texas at Austin, Bureau of Economic Geology, 36 p.

Griggs, D., and J. Handin, 1960, Observations on fracture and a hypothesis of earthquakes: Geological Society of America Memoir 79, p. 347-364.

Guevara, E.H., 1988, Geological characterization of Permian submarine fan reservoirs of the Driver waterflood unit, Spraberry Trend, Midland basin, Texas: Bureau of Economic Geology Report of Investigations No. 172, 44 p.

Hanks, C.L., Lorenz, J.C., Teufel, L.W., and Krumhardt, A.P., 1997, Lithologic and structural controls on natural fracture distribution and behavior within the Lisburne Group, northeastern Brooks Range and North Slope subsurface, Alaska*: AAPG Bull.*, v. 81, p. 1700-1720.

Hills, J.M., 1970, Late Paleozoic structural directions in southern Permian basin, West Texas and southeastern New Mexico: *AAPG Bull.*, v. 54, p. 1809-1827.

Holcomb, D.J., 1997, In situ stress from Core (E.T. O'Daniel #28): Third Naturally Fractured Reservoir Symposium, October 28, 1997, New Mexico Petroleum

Recovery Research Center, New Mexico Institute of Mining and Technology, Socorro, NM, (unpaginated).

Kocurek, G., and B.L. Kirkland, 1998, Getting to the source: Aeolian influx to the Permian Delaware basin region: Sedimentary Geology, v. 117, p. 143-149.

Laubach, S.E., 1997, A method to detect natural fracture strike in sandstones: *AAPG Bull.*, v. 81, p.

Lorenz, J.C., and L.L. Brooks, 1990, Suspension- and current-deposit reservoirs in the Delaware basin: Trends and cycles in siltstones of the Permian Bone Spring Limestone (abstract), *AAPG Bull.*, v. 74, p. 708.

Lorenz, J.C., and R.E. Hill, 1992, Measurement and analysis of fractures in core; *in*, Geologic studies relevant to horizontal drilling: Examples from western North America, Schmoker, J.W., E.B. Coalson, and C.A. Brown (eds.): Rocky Mountain Association of Geologists, p. 47-59.

Lorenz, J.C., and R.E. Hill, 1994, Subsurface fracture spacing: Comparison of inferences from slant/horizontal and vertical cores: *SPEFE*, v. 9, p. 66-72.

Lorenz, J.C., N.R. Warpinski, and L.W. Teufel, 1991, Regional fractures I: A mechanism for the formation of regional fractures at depth in flat-lying reservoirs *AAPG Bull.*, v. 75, p. 1714-1737.

Lorenz, J.C., and S.J. Finley, 1991, Regional Fractures II: Fracturing of Mesaverde reservoirs in the Piceance basin, Colorado: *AAPG Bull*, v. 75, p. 1738-1757.

Lorenz, J.C., and S.E. Laubach, 1994, Description and interpretation of natural fracture patterns in sandstones of the Frontier Formation along the Hogsback, southwestern Wyoming: Gas Research Institute Topical Report GRI-94/0020, 89p.

Lorenz, J.C., 1992, Well-bore geometries for optimum fracture characterization and drainage: West Texas Geological Society Bulletin, v. 32, p. 5-8.

Lorenz, J.C., 1997a, Horizontal core fracture description: Spraberry Symposium, Sponsored by Parker and Parsley Development Company and the U.S. Department of Energy, held at the University of Texas Permian Basin Center for Energy and Economic Diversification, Midland, TX, January 30, 1997, section K.

Lorenz, J.C., 1997b, Non-congruent natural fracture sets in adjacent beds at depth: Data from horizontal cores from the Spraberry Formation, Midland basin, TX (expanded abstract): *AAPG*, Hedberg Research Conference on Reservoir Scale Deformation - Characterization and Prediction: June 22-28, 1997, Bryce , UT.

Lorenz, 1997c, Conjugate fracture zones: Potential "sweet spot" reservoirs within regional parallel-fracture systems: SPE 38749 presented at SPE Annual Technical Conference and Exhibition, San Antonio, TX, 5-8 October, 1997, p. 481-484.

Lorenz, J.C., 1997d, Conjugate fracture pairs in the Molina Member of the Wasatch Formation, Piceance basin, Colorado: Implications for fracture origins and hydrocarbon production/exploration, *in*, Natural Fracture Systems in the Southern Rockies, Close, J.C., and T. A. Casey (eds.): Four Corners Geological Society, p. 97-104.

Lorenz, J.C., 1999, Stress-Sensitive Reservoirs: *JPT*, v. 51, p. 61-63.

Lorenz, J.C., S.J. Finley, and N.R. Warpinski, 1990, Significance of coring-induced fractures in Mesaverde core, northwestern Colorado: *AAPG Bull.*, v. 74, p. 1017-1029.

Malmanger, E.M., J.C. Lorenz, and L.W. Teufel, 1997, Fractures in horizontal core from the Spraberry Formation, Midland basin; Interpreted and modeled using data from analog outcrop fractures in the Brushy Canyon Formation (abstract), American *AAPG Bull.*, v. 81, p. 1228-1229.

McDonald, Paul, J.C. Lorenz, Charlie Sizemore,, D.S. Schechter, and Tom Sheffield, 1997, Fracture characterization based on oriented horizontal core from the Spraberry Trend reservoir: a case study: SPE 38664 presented at Annual Technical Conference and Exhibition, San Antonio, Texas, 5-8 October, 1997, p. 231-239.

Meissner, F.F. 1980, Examples of abnormal fluid pressure produced by hydrocarbon generation (abstract); *AAPG Bull.*, v. 64, p. 749.

Meissner, F.F. 1981, Abnormal pressures produced by hydrocarbon generation and maturation and their relation to processes of migration and accumulation (abstract); American Association of Petroleum Geologists Bulletin, v. 65, p. 2467.

Nolen-Hoeksema, R.C., J.M. Avasthi, W.C. Pape, and A.W.M. El Rabaa, 1992, Waterflood improvement in the Permian basin: Impact of in-situ stress evaluations: SPE 24873 presented at Annual Technical Conference and Exhibition, Washington, D.C., 4-7 October, 1992, p. 81-92.

Petit, J.P., 1987, Criteria for the sense of movement on fault surfaces in brittle rocks: Journal of Structural Geology, v. 9, p. 597-608.

Price, J.G., and C.D. Henry, 1985, Summary of Tertiary stress orientations and tectonic history of trans-Pecos Texas, *in*, Dickerson, T.W., and W.R. Muehlberger (eds.),Structure and tectonics of Trans-Pecos Texas; West Texas Geological Society Field Conference, p. 149-151.

Putra, Erwinsyah, 1998, Reservoir simulation issues in the Spraberry trend area: Fourth Annual Naturally Fractured Reservoir Symposium, Petroleum Recovery Research Center, New Mexico Institute of Mining and Technology, Socorro, NM, October 27, 1998 (unpaginated).

Reservoirs Inc, 1997, Volume 2, Geological and petrophysical analysis of the upper Spraberry Formation in Midland County, Texas: E.T. O'Daniel No. 28 horizontal cores: Report RSH 3588, May, 1997.

Saleta, C.J., 1998, Geological and petrophysical analysis of reservoir cores: Fourth Annual Naturally Fractured Reservoir Symposium, Petroleum Recovery Research Center, New Mexico Institute of Mining and Technology, Socorro, NM, October 27, 1998 (unpaginated).

Schechter, D.S., Paul McDonald, Tom Sheffield, and R.O. Baker, 1996a, Reservoir characterization and CO_2 pilot design in the naturally fractured Spraberry trend area: SPE 36469 presented Permian Basin Oil and Gas Recovery Conference, Midland, TX, 27-29 March, 1996, p. 819-833.

Schechter, D.S., Paul McDonald, Tom Sheffield, and R.O. Baker, 1996b, Integration of laboratory and field data for development of a CO_2 pilot in the naturally fractured Spraberry trend; SPE 36657 presented at Annual Technical Conference and Exhibition, Denver, CO, 6-9 October, 1996, p. 939-944.

Tyler, N., and J.C. Gholston, 1988, Heterogeneous deep-sea fan reservoir, Shackelford and Preston waterflood units, Spraberry trend, West Texas: Report of Investigation No. 171, Bureau of Economic Geology, The University of Texas, Austin. 38 p.

Whigham, C.L., 1998, Overview of the CO_2 pilot in the Spraberry trend area: Fourth Annual Naturally Fractured Reservoir Symposium, Petroleum Recovery Research Center, New Mexico Institute of Mining and Technology, Socorro, NM, October 27, 1998 (unpaginated).

Wilkinson, W.M., 1953, Fracturing in Spraberry reservoir, West Texas: *AAPG Bull.*, v. 37, p. 250-265.

Winfree, K.E., 1994, Post-Permian folding and fracturing of the Spraberry and San Andres formations within the Midland basin region of West Texas, *in*, Laroche, T.M., and J.J. Viveiros, (eds.), Structures and tectonics of the Big Bend and southern Permian basin, Texas: West Texas Geological Society field trip guidebook, publication 94-95, p. 189-212.

Winfree, K.E., 1995, Post-Permian folding and fracturing of the Spraberry and San Andres formations within the Midland basin region of West Texas: West Texas Geological Society Bulletin, v. 35, no. 3, p. 5-20.

Wu, H., E.J.M. Willemse, and D.D. Pollard, 1994, Prediction of fracture density and drainage distance in layered rock masses using borehole data: Rock Mechanics in Petroleum Engineering, Society of Petroleum Engineers/International Society of Rock Mechanics International Conference, Eurock '94, 29-31 August 1994, Proceedings, p. 487-494.

Wu, H., and D.D. Pollard, 1995, An experimental study of the relationship between joint spacing and layer thickness: Journal of Structural Geology, v. 17, p. 887-905.

TABLE 1.1: FRACTURE DATA SUMMARY

	SET 1	SET 2	SET 3
SPACING (ft)*			
Range	0.8-5.8	0.05-4.5	0.04-13.0
Average	3.2	1.6	3.8
Shape	normal, regular	log-normal, narrow range	skewed; log-normal
ORIENTATION (degrees)			
Total Range	35-55	20-50	50-85
Typical Range	40-45	20-50	60-80
Average Strike	43	32	70
FRACTURE TYPE	extension	shear	(shear?)
MINERALIZATION	barite, most fracs w/ high percentage surface coverage	minimal	minimal
DISTRIBUTION	upper reservoir	lower reservoir	upper reservoir, plus shales that overlie upper and lower reservoirs
NUMBER OF FRACS	35	24	28

*Fracture spacing normal to the average fracture strike of that set, corrected from observed spacing in core

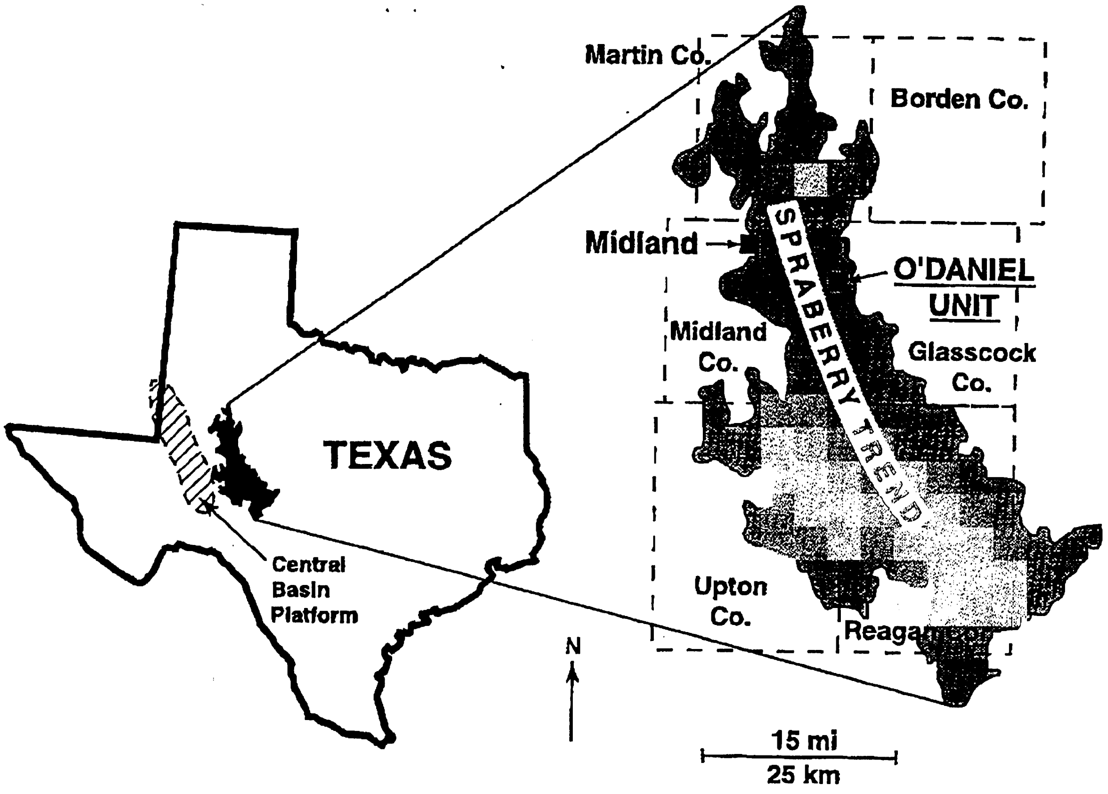
Martin Co.
Borden Co.
Midland
O'DANIEL UNIT
SPRABERRY TREND
Midland Co.
Glasscock Co.
Upton Co.
Reagan Co.
TEXAS
Central Basin Platform
N
15 mi
25 km

Fig.1.1—Location map, showing the Spraberry trend of West Texas.

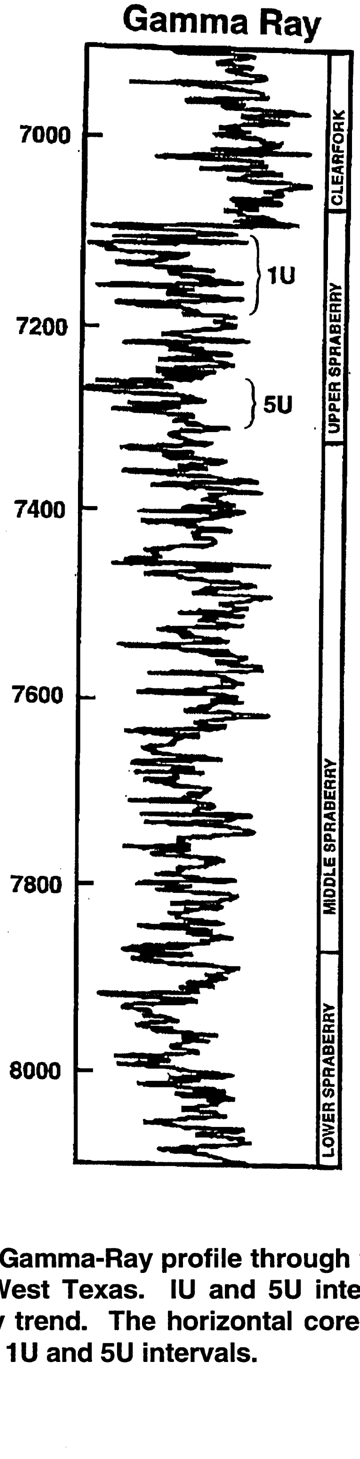

Fig. 1.2— Stratigraphic column/Gamma-Ray profile through the Spraberry formation in the O'Daniel unit, Midland basin, West Texas. IU and 5U intervals are the main producing reservoir units of the Spraberry trend. The horizontal cores were taken from the thinner sandstones near the tops of the 1U and 5U intervals.

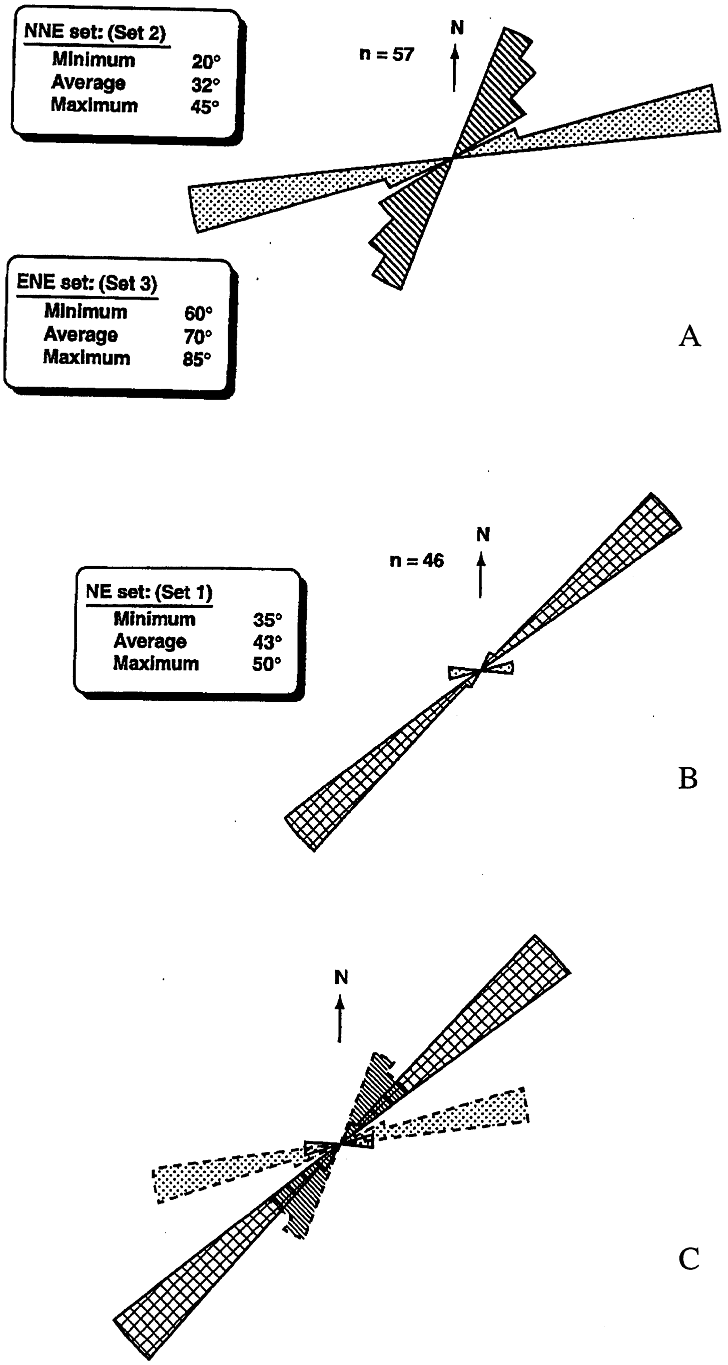

Fig. 1.3—Rose diagrams of fracture strikes in horizontal cores from the O'Daniel #28 well. a) Fractures from the lower cored unit associated with the 5U interval; b) Fractures from the upper cored unit associated with the 1U interval, c) Superimposed rose diagrams of fracture strikes from the upper and lower units.

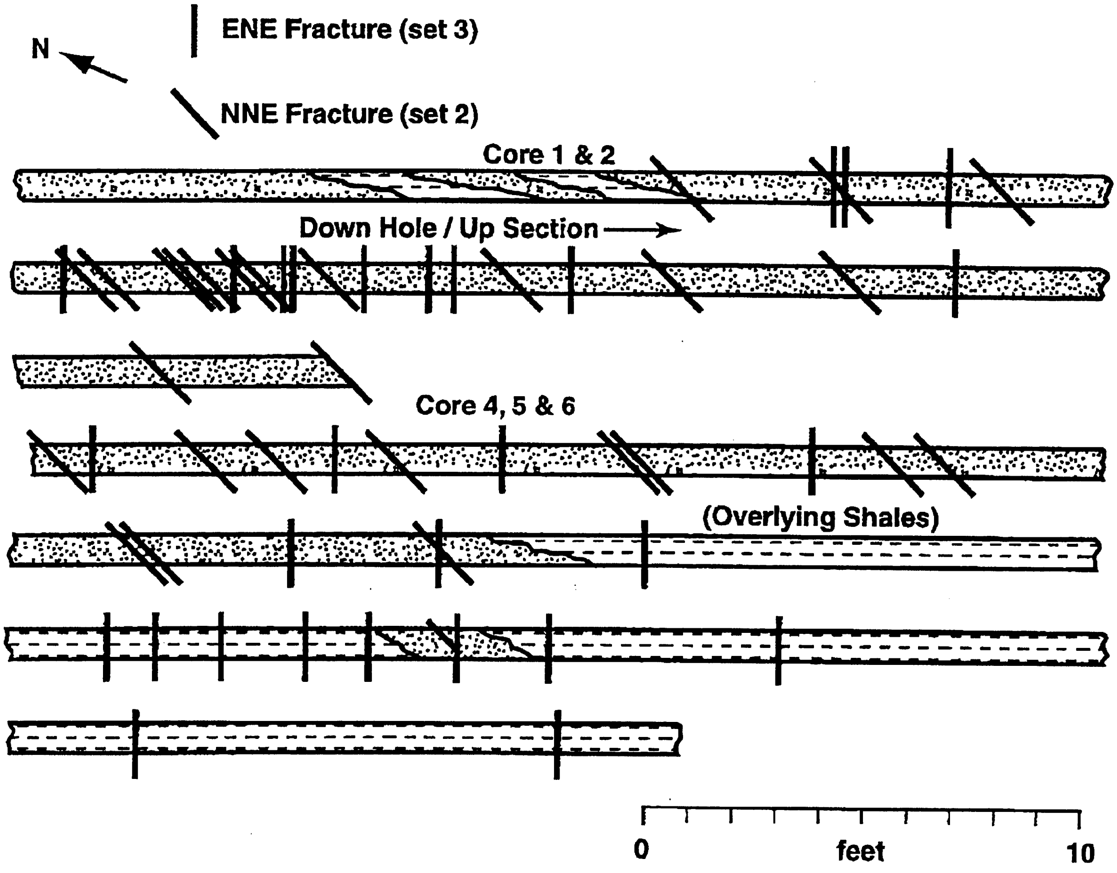
N
ENE Fracture (set 3)
NNE Fracture (set 2)
Core 1 & 2
Down Hole / Up Section
Core 4, 5 & 6
(Overlying Shales)
0
feet
10

Fig. 1.4—Schematic planview of the locations of natural fractures in horizontal core from the upper Spraberry unit, O'Daniel #28 well. (Note: the bedding planes that define lithologic changes are portrayed in side view.)

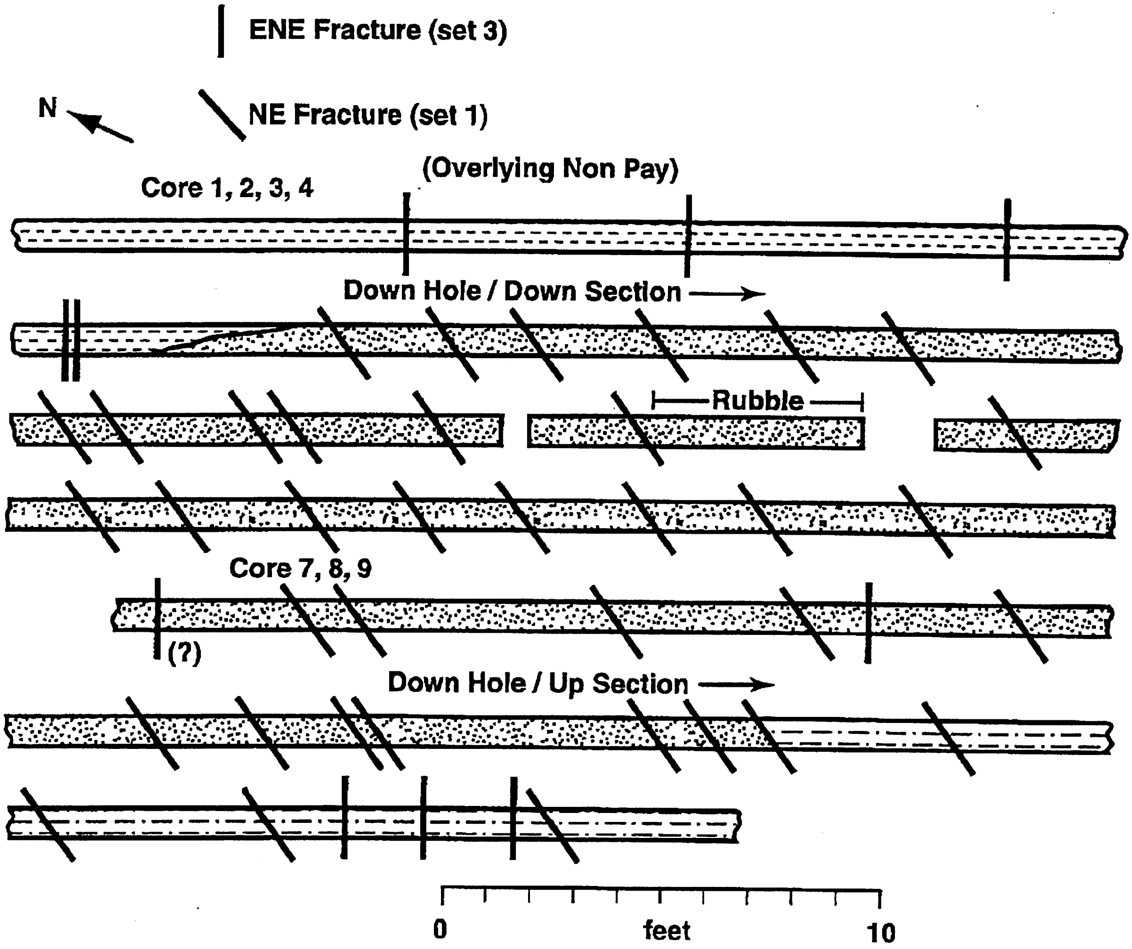
ENE Fracture (set 3)
N
NE Fracture (set 1)
(Overlying Non Pay)
Core 1, 2, 3, 4
Down Hole / Down Section
Rubble
Core 7, 8, 9
(?)
Down Hole / Up Section
0
feet
10

Fig. 1.5—Schematic planview of the locations of natural fractures in horizontal core from the lower Spraberry unit, O'Daniel #28 well. (Note: the bedding planes that define lithologic changes are portrayed in side view.)

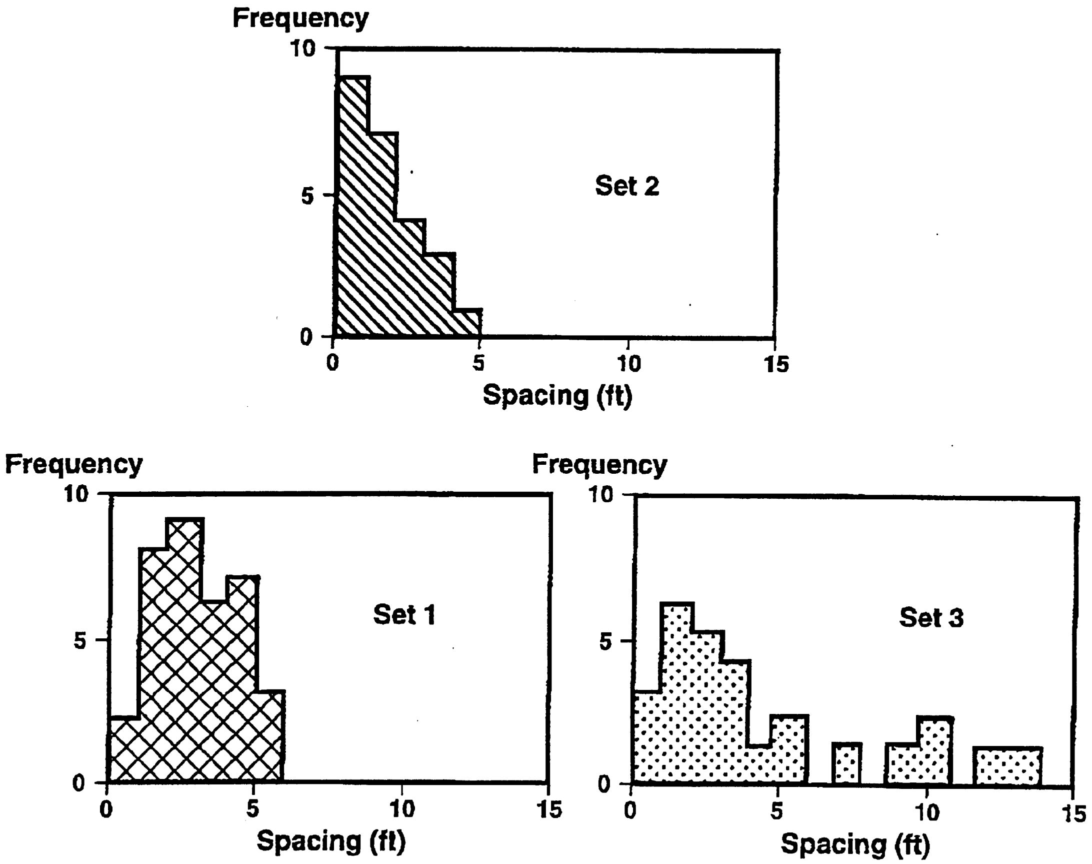

Fig. 1.6—Spacing histograms of the three cored Spraberry natural fracture sets. (Shading patterns are keyed to the shading of the rose diagrams in Fig. 1.3)

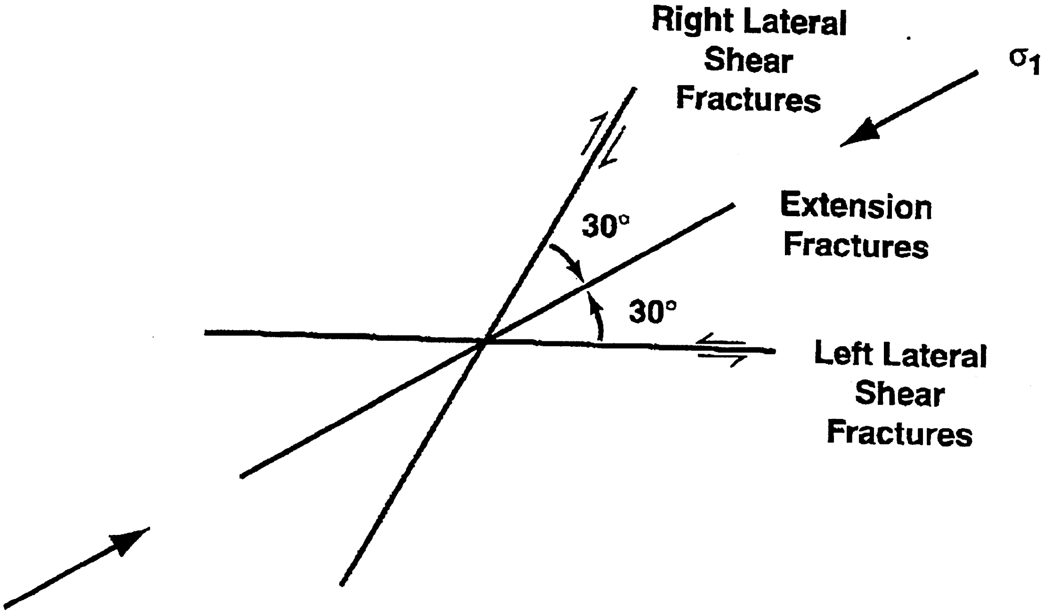
Right Lateral Shear Fractures
σ1
Extension Fractures
30°
30°
Left Lateral Shear Fractures

Fig. 1.7—Ideal geometry of a conjugate fracture pair with an extension fracture set that bisects the acute conjugate angle.

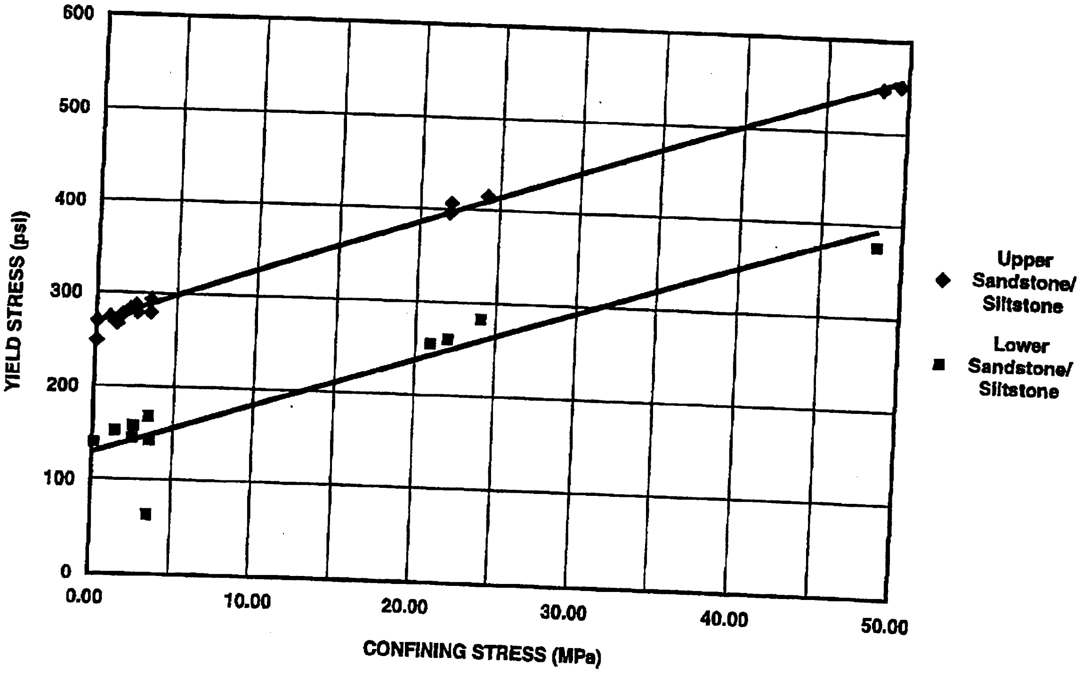

Fig. 1.8—Comparison of the yield strengths for different confining stresses for samples of the upper (1U) and lower (5U) Spraberry siltstone-sandstone units. The lower unit is significantly weaker, causing conjugate fractures to form in this interval whereas extension fractures formed concurrently in the stronger, upper unit.

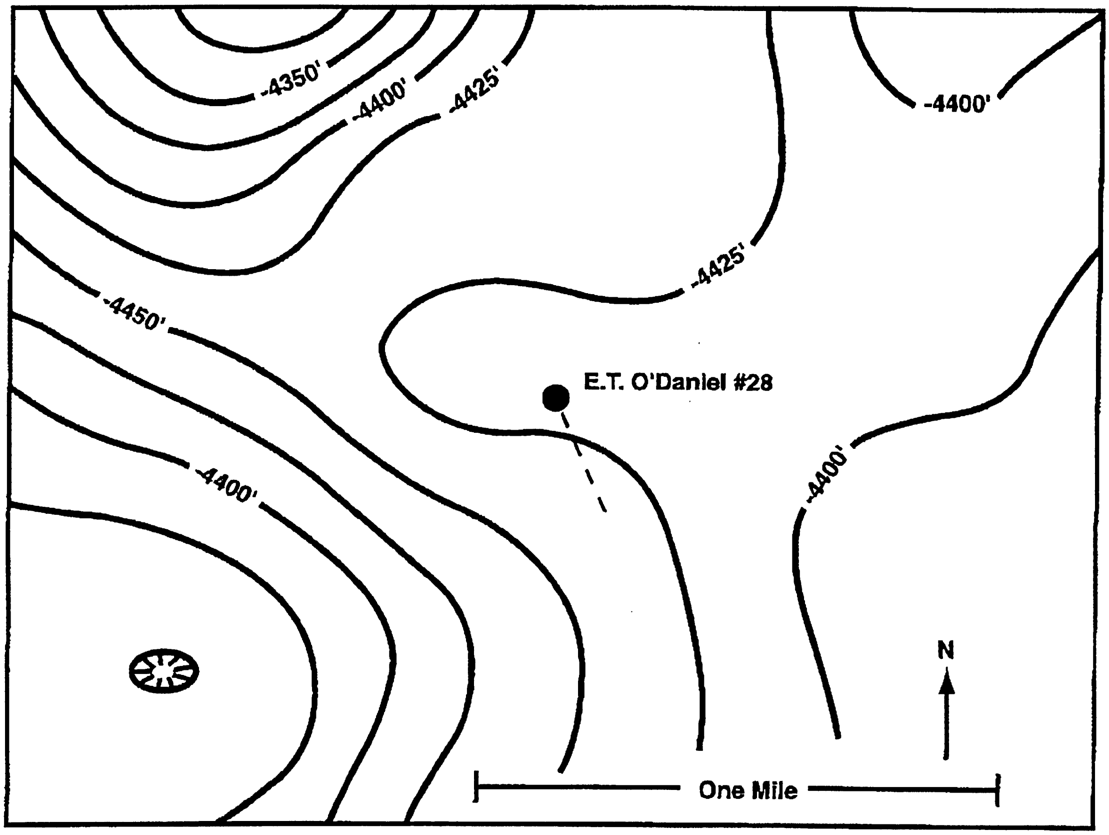
-4350'
-4400'
-4425'
-4400'
-4425'
-4450'
E.T. O'Daniel #28
-4400'
-4400'
N
One Mile

Fig. 1.9—Structure contour map on top of the Spraberry formation in the O'Daniel unit area, Midland basin, West Texas. Dashed line is the azimuth of the two horizontal side tracks of the O'Daniel #28 well.

2. INVESTIGATION OF CRUDE OIL/BRINE/ROCK INTERACTION

2.1 STUDY OF WATERFLOODING PROCESS IN NATURALLY FRACTURED RESERVOIRS FROM STATIC AND DYNAMIC IMBIBITION EXPERIMENTS

2.1.1 Abstract

Imbibition plays an important role in oil recovery from the naturally fractured Spraberry Trend Area. Therefore, understanding matrix-fracture transfer and the key parameters associated with the imbibition process are important. We examined these issues by performing static and dynamic imbibition experiments. Oil recoveries from both experiments were matched and the imbibition processes were investigated by developing a numerical finite difference scheme and utilizing a commercial simulator.
Static imbibition experiments, followed by waterflooding, were performed at reservoir conditions to investigate rock wettability. A two-phase and 2-D, fully finite-difference implicit scheme was developed to solve non-linear diffusion in the static imbibition equation. The numerical results that matched satisfactorily with the spontaneous imbibition data were applied to investigate the effect of key variables on the imbibition rate. We found that the measurement of Amott wettability index and the capillary pressure result suggested that the Spraberry rock matrix is weakly water-wet.

Dynamic imbibition experiments were performed using artificially fractured Berea and Spraberry cores at reservoir conditions to illustrate the actual process of waterflooding in naturally fractured reservoirs. A commercial numerical simulator was used to match these experiments to generate matrix capillary pressures. A comparison between capillary pressures obtained from both experiments has been made. The results of this study were also used to determine the critical injection rate. The critical injection rate from core dimensions was up-scaled to field dimensions using a dimensionless equation. Knowledge of the critical injection rate is useful in solving the problem of early breakthrough, one of the hazards of water injection in naturally fractured reservoirs.

The results of these two studies, static and dynamic imbibitions, provide useful guidelines for reservoir simulation field development in naturally fractured reservoirs.

2.1.2 Static imbibition experiments

Imbibition plays an important role in the recovery of oil from the naturally fractured Spraberry area. Imbibition describes the rate of mass transfer between the rock and the fractures. Therefore, understanding the imbibition process and the key parameters that control the imbibition process are crucial. Several studies have been conducted to simulate spontaneous imbibition in a core plug. These studies were concerned primarily with capillary pressure as the only driving force in the spontaneous imbibition process.[1-5]

In order to understand the physical process of imbibition, the spontaneous imbibition experiments were performed using the imbibition apparatus schematically shown in **Fig. 2.1**. As can be seen from the figure, the apparatus is basically a simple glass container equipped with a graduated glass cap. To perform an imbibition test, a core sample was immersed in the glass container filled with preheated brine solution. The container was then covered with the graduated cap. After fully filling the cap with brine solution, the container was then stored in an air bath that had been set at a constant temperature of 138°F.

Synthetic Spraberry brine and Spraberry dead oil were used in the experiments. The brine contains NaCl and $CaCl_2.H_2O$ mixed with distilled water. Viscosity was determined using a Cannon-Fenske routine viscometer and density was determined using a digital density meter. The interfacial tensions (IFTs) of the oil/brine systems were measured using a pendant drop instrument and a de Nouy Ring. The viscosity, density and IFT of the synthetic brine and Spraberry dead oil measured at elevated temperature were tabulated in **Table – 2.1**.

Due to capillary imbibition action, oil was displaced from the core sample by the imbibing brine. The displaced oil accumulated in the graduated cap by gravity segregation. During the experiment, the volume of produced oil was recorded against time. Before taking the oil volume reading, the glass container was gently shaken to expel oil drops adhering to the core surface and the lower part of the cap, so that all of the produced oil accumulated in the graduated portion of the glass cap. At an early stage of the test the oil volume was recorded every half-hour while toward the end of the test the oil volume reading was made every 24 hours. Excluding the core preparation, one series of tests was usually completed within 21 days. After spontaneous imbibition in brine was completed, the core sample was subjected to forced displacement by water using a pressure ranging from 120 to 200 psi depending on the wetting condition. The injections were performed under reservoir conditions. Once the imbibition test was stopped, the core was flushed by preheated brine right away. The amount of oil produced was used to determine the wettability index for water (I_w).

2.1.3 Static imbibition modeling

We realize that spontaneous imbibition experiments usually takes a long time, especially when we need to vary some parameters to investigate their effects on the imbibition rate. Sometimes may be very difficult to determine capillary pressure and to illustrate water saturation profiles at different times and locations. Therefore, numerical modeling is needed to simulate this process.

In order to describe the spontaneous imbibition process, mathematical formulation for that process was derived. In deriving the governing equation, some assumptions are used; gravity terms are negligible, capillary pressure is the only driving force where total velocity is zero, and fluid and rock are incompressible. By using the simultaneous flow of two-phase formulation the governing equation for describing the spontaneous imbibition process can be obtained as follows (Chen *et al.,* 1995)[5]:

$$\nabla \cdot D(S_w)\frac{\partial S_w}{\partial x} = -\phi \frac{\partial S_w}{\partial t} \qquad (1)$$

where the non-linear capillary diffusion coefficient is defined as

$$D(S_w) = \frac{k}{\mu_o} k_{ro} f_w \frac{\partial p_c}{\partial S_w} \qquad (2)$$

where water fractional flow is defined as

$$f_w = \left(1 + \frac{k_{ro}}{\mu_o}\frac{\mu_w}{k_{rw}}\right)^{-1} \qquad (3)$$

Because of the non-linear capillary diffusion coefficient, Eq. 1 was solved by numerical methods.

In order to solve it numerically, Eq. 1 was discretized in 2D finite-difference form. The left-hand side was discretized by applying the Taylor series using central difference and the right-hand side using backward difference. Note that the relative permeabilities and capillary pressure are functions of water saturation, thus, Eq. 1 must be solved iteratively. Once the new saturations are solved using the initial guess, these new water saturations are compared with the old water saturations until acceptable convergence has been reached.

The core plug is totally immersed in the water and therefore, boundary conditions are set to be 1-S_{or}. This implies that instantaneous imbibition occurs at the matrix-fracture interface. Initial conditions are required to begin the time step sequence. In this study, initial conditions are specified equal to initial water saturation.

In order to match the recovery from the imbibition experiments, only capillary pressure was altered and other parameters were kept constant. The following relative permeability correlations from Honarpour *et al* (1986)[6] were used as inputs:

$$k_{ro} = k_{ro}^o (1 - S_w{}^*)^3 \qquad (4)$$

$$k_{rw} = k_{rw}^o (S_w{}^*)^3 \qquad (5)$$

For the base case, the maximum oil relative permeability (k_{ro}^o) was set to 1.0 and the maximum water relative permeability (k_{rw}^o) was set to 0.3. In these relationships, the S_w* is expressed as $S_w{}^* = \frac{(S_w - S_{wi})}{(1 - S_{or} - S_{wi})}$. The residual oil saturation (S_{or}) was set to 0.5437 and irreducible water saturation (S_{wi}) was set to 0.37. Those average values of S_{or} and S_{wi} values are obtained from **Table 2.1**.

2.1.4 Dynamic imbibition experiments

The capillary force is the only force to recover oil during static imbibition tests. However, there are two processes involved during producing oil by waterflooding in naturally fractured reservoirs, spontaneous imbibition (capillary force) and displacement processes (viscous force). During spontaneous imbibition, water imbibes into the matrix and oil is expelled from the matrix to the fracture (counter current mechanism). The oil that reaches the fracture is displaced by injected water to the production end of the fracture, as shown in **Fig. 2.2**. Several laboratory and numerical studies have been conducted regarding this subject.[7-11]

In order to understand the imbibition process in an artificially fractured core, a coreflood experiment at low water injection rate was performed at reservoir temperature. A low-permeability Berea core sample was cut in cylindrical shape, 3 in. long and 1.5 in. diameter. The fracture pattern on the core sample was generated along the long axis using a hydraulic cutter. The cut sections were put back together without polishing the cut surfaces and without spacers. Synthetic Spraberry brine and Spraberry crude oil were used as wetting and non-wetting phases. The properties of rock and fluids for both cores used in this experiment are shown on **Tables 2.2 and 2.3**.

In general, the experimental process was started by saturating the core sample with 100% Spraberry oil. This process was followed by brine imbibition flooding as the wetting phase. The experimental procedure is described in detail as follows:

- Dimension of core sample was measured and then weighed.
- Core sample was inserted into a Hassler-type core holder using a confining pressure of 500 psi to saturate the core by oil. About 2-5 PV of Spraberry crude oil were passed through the core sample using the constant pressure of 30 psi supplied by a nitrogen tank. Then, the volume of oil produced was measured to determine the oil rate. By using Darcy's law, the absolute matrix permeability to oil was then calculated.
- After permeability measurement, oil-saturated core was taken from the core holder and covered with aluminum foil to prevent air penetration into the core sample. Then, it was cut in half using a hydraulic cutter to generate fracture horizontally along the axis of the core. The oil-saturated artificially fractured core was then weighed to determine core pore volume and porosity.
- The core was inserted back into the Hassler-type core holder. The effective permeability of the fractured core was determined by injecting oil into fractured core in the core holder. The fracture permeability (Guo and Svec, 1998)[12] was calculated based on the following equation by assuming the fracture porosity of 1%:

$$k_e = k_m + \phi_f k_f \qquad (6)$$

where k_e(mD), k_m(mD) k_f(mD)and ϕ_f(fraction) are the effective reservoir permeability, matrix permeability, fracture permeability and fracture porosity, respectively.

- The fracture width, w_f(cm), was calculated based on the correlation developed by Seright *et al* (1996)[13]:

$$w_f = 0.000131\sqrt{k_f} \qquad (7)$$

- The oil-saturated artificially fractured core was taken again from the core holder to clean oil from the core surface. Then, the core was inserted back into the core holder to start the experiment. The face of the matrix was sealed off by wrapping plastic and aluminum foil, in order to allow brine injection flow only through the fracture. This set-up was stored in an air bath with constant temperature of 138°F, as shown in **Fig. 2.3**.
- During the experiment, the oil-saturated core sample was flooded by injecting synthetic Spraberry brine into the fracture with constant brine injection rate of 4.0 cc/hour. The oil and brine produced were collected against time at the producing end of the fractured core for about 48 hours, until zero oil production-rate was achieved.

2.1.5 Dynamic imbibition modeling

Single porosity simulation was used instead of dual porosity simulation, because single porosity is more representative for modeling a single fracture from the artificially fractured core. However, this single porosity simulation has to be able to duplicate the behavior of dual porosity simulation, which has different properties for matrix and fracture media. Thus, the properties of a fracture should be added in the single porosity simulator, such as porosity, permeability, relative permeability, and capillary pressure.

The rectangular grid block was used to overcome the difficulty of modeling the cylindrical core shape. The pore volume of the rectangular shape was set to be the same as the cylindrical core pore volume. Three layers were used in the model with the fracture layer between the matrix layers. In addition, 10 x 10 grid blocks were used in x and y direction. The fracture layer was injected at one end with low constant water injection rate of 4.0 cc/hour (Berea core). Oil and water were produced at the opposite end of the fracture layer. The rest of the boundary blocks had a specified no-flow boundary condition.

Relative permeability for the matrix layer was calculated from the following relationships (Kazemi and Merrill, 1977).[14]

$$k_{rw} = S_w{}^3 \qquad (8)$$

$$k_{ro} = (S_o - S_{or})^3 \qquad (9)$$

while relative permeability for the fracture layer was assumed to be a straight line for both k_{rw} and k_{ro}.

Similar procedures were carried out with the Spraberry core, except for using a more refined grid block in the vertical direction and Spraberry relative permeability curves (**Fig. 2.4**). The refined grid block was used to avoid numerical instability because the grid blocks representing the fracture are very small and the matrix permeability is very low (0.1 md) compared to that of Berea core (28.09 md). As with the Berea core, relative permeability was fixed and the main adjusted parameter was the matrix capillary pressure. Zero capillary pressure was used as the base case in fracture layer for both Berea and Spraberry cores.

The initial condition from the reservoir simulator is obtained from the hydrostatic equilibrium calculation. For instance, initial water saturation is determined by capillary pressure, which is based on the difference between oil pressure and water pressure. Thus, it is difficult to use the equilibrium option to represent initial conditions for the laboratory experiment. Instead of using the equilibrium option, initial water saturation and pressure were input directly, since those initials were known from laboratory experiments.

2.1.6 Fracture capillary number

Naturally fractured reservoirs are characterized by two distinct media, a low permeability matrix and a high permeability fracture system. This distinction in permeability may result in rapid water breakthrough during water injection, depending on the wettability of the matrix.

Fluid displacement in a fracture network occurs due to the fracture system's higher conductivity compared to that of the matrix when an exchange of fluids occurs between matrix and fracture system. The fluid transfer process is controlled by the flow of water under naturally imposed pressure gradients (viscous force) and the spontaneous movement of water into the matrix under capillary forces (imbibition). During spontaneous imbibition, water imbibes into the matrix and oil is expelled from the matrix to the fracture (countercurrent mechanism). The oil that reaches the fracture is displaced by injected water to the production end of the fracture, as illustrated in **Fig. 2.1**.

High water injection rate is one of the causes of low productivity in the Spraberry Trend Area, west Texas. Water breakthrough occurred in most producing wells without any flush production of oil after waterflooding was initiated.[15] Elkin and Skov[16] proposed to stop water injection temporarily to permit the reservoir to equalize between capillary and viscous forces. Water injection was ceased and within five days oil production increased threefold. In the months following, cyclic pressure pulsing was performed during injections, which increased the recoveries above those observed during continuous water injection.

Several papers were published on dynamic imbibition experiments using fractured cores to illustrate the actual waterflooding mechanism in naturally fractured reservoirs. These papers were concerned primarily with developing mathematical models to match the results of experimental work.[9,10]

Few studies have been conducted to optimize water injection rates at field dimensions scaled up from coreflood experiments. A recent study conducted by Babadagli[11] addressed this subject He concluded that the injection rate should be adjusted depending on the matrix permeability and maximum matrix capillary pressure to obtain the efficient capillary imbibition transfer. Using a similar basic equation as derived by Babadagli[11], we propose the fracture capillary number (FCN) equation to scale up laboratory data to field dimensions. Derivation of our FCN equation is not based on dimensionless analysis, but on the geometry and properties of the matrix and fracture system (**Fig. 2.5**). Therefore, it is not universal, even though it is dimensionless. The dynamic imbibition data from different cores do not superimpose onto one curve as is characteristic of a dimensionless equation. However, the use of this equation provides an estimate of the injection rate necessary to avoid early breakthrough during waterflooding in naturally fractured reservoirs.

The parameters that affect the viscous and capillary forces can be grouped into a fracture capillary number (FCN) equation, which is used to determine the critical injection rate. It is defined as the ratio between the viscous force (parallel to the fracture direction) and the capillary force (perpendicular to the fracture direction). The viscous force is defined as a function of water velocity, water viscosity and fracture volume and is assumed to occur only in the fracture (**Fig. 2.5**). The capillary force that occurs only in the matrix is defined as a function of interfacial tension, contact angle and matrix volume (**Fig. 2.5**). Thus, the fracture capillary number can be written below:

$$N_{f_{VC}} = \frac{Viscous\ Force}{Capillary\ Force} = \frac{v\,\mu_w\,A_f}{\sigma \cos\theta\ A_m} \quad \text{...} (3)$$

where v is the velocity of the injected fluid in the fracture, defined as $\frac{q_{inj}}{A_f}$, where q_{inj} is the volumetric injection rate, and A_f is the fracture cross-sectional area. A_f is the fracture area, where the viscous force occurs, and can be defined as $A_f = w \times dz$. dz is the height of the core, μ_w is the water viscosity, σ is the interfacial tension and θ is the contact angle. σ $cos\theta$ can be substituted with $\frac{P_{c,\max}}{J(S_{wi})}\sqrt{\frac{k_m}{\phi_m}}$, where $P_{c,max}$ is the maximum capillary pressure at S_{wi}, k_m is the matrix permeability, ϕ_m is the matrix porosity, and $J(S_{wi})$ is the J-function at S_{wi}. A_m is the matrix area, where the capillary force occurs that can be defined as $A_m \approx dy \times dz$, where dy is the length of the core in the y-direction.

Rearranging and substituting all those parameters into Eq. 3, it can be rewritten as follows:

$$N_{f_{VC}} = \frac{q_{inj}\mu_w}{\frac{Pc,\max}{J(S_{wi})}\sqrt{\frac{k_m}{\phi_m}}A_m} \quad \text{...} (4)$$

For laboratory units, Eq. 4 can be written as

$$N_{f_{VC}} = \frac{1.27e-5 * q_{inj}(cc/hr)\mu_w(cp)}{\dfrac{Pc,\max(psi)}{J(S_{wi})}\sqrt{\dfrac{k_m(md)}{\phi_m}A_m(cm^2)}} \qquad (5)$$

In the same way, laboratory units can be scaled to field units as written below:

$$N_{f_{VC}} = \frac{9.05e-5 * q_{inj}(STB/Day)\mu_w(cp)}{\dfrac{Pc,\max(psi)}{J(S_{wi})}\sqrt{\dfrac{k_m(md)}{\phi_m}A_m(ft^2)}} \qquad (6)$$

2.1.7 Results and Discussion

The average of residual oil saturations after spontaneous imbibition experiments was still very high. Therefore, the water saturation changes during the simulation are very small, which causes the numerical solution to become unstable and the result cannot be obtained. In order to approach this problem, three lower residual oil saturations of 0.2, 0.3 and 0.4 were used. Once the numerical solution matched with the experimental data, the matrix capillary pressures from different residual oil saturations were obtained. Then, the matrix capillary pressure for 0.54 residual oil saturation was estimated as shown in **Fig. 2.6**. The low-capillary pressure curve obtained indicates that the Spraberry cores are weakly water-wet. The weakly water-wet indication is also found by the measurement of wettability index (average Amott index is 0.3).

Figure 2.7 shows four experimental data and numerical solution matches for recovery against time using residual oil saturation of 0.2. The diffusion coefficient as shown in Eq. 2 is strongly non-linear due to varying capillary pressure and relative permeability curves as functions of water saturation. Therefore, using constant capillary pressure and relative permeability curves to solve the spontaneous imbibition equation, which is always solved by analytical solution, may fail to predict oil recovery by spontaneous imbibition.

Sensitivity studies on imbibition rate for varying capillary pressure, oil and water relative permeability curves, oil and water viscosity, and initial water saturation were conducted using 0.2 S_{or} case. The numerical results using the value from **Table 2.2** show that increasing and decreasing the value of water viscosity and water relative permeability have no effect on the imbibition rate.

In numerical modeling of the dynamic imbibition process, the matrix capillary pressure controlling the imbibition mechanism was the primary parameter adjusted to match the experimental data. Meanwhile, the fracture capillary pressure was set to be zero. The cumulative water production, oil production rate, cumulative oil production, oil recovery and water cut were parameters used to match between the observed experimental data and the numerical model. The best matches between experimental data and numerical solution (only cumulative water production and cumulative oil production are presented) can be seen in the **Figs. 2.8** through **2.11**.

The cumulative water production of Berea core shows that once brine injection was started with a constant rate of 4.0 cc/hr, oil was produced simultaneously. However, the water still was not produced. This indicated that the water was imbibing into the rock and oil was expelled from the matrix to the fracture. After two hours of brine injection, the water breakthrough was occurred because the maximum of matrix capillary pressure was reached. Consequently, water started to produce before being completely imbibed. Water was produced until 100% watercut was reached. Similar behavior was also shown by the performance of cumulative water production of Spraberry core.

The matrix capillary pressures for Berea and Spraberry cores generated, after matching was obtained, are shown in **Fig. 2.12**. Although matrix capillary pressure for Berea core is lower than for Spraberry core, oil recovery for Berea core is higher than for Spraberry core. The higher cumulative oil production is because of capillary imbibition transfer for Berea core is higher than for Spraberry core.

Satisfactory reproducibility of the dynamic imbibition procedure using Berea cores was obtained when two series of dynamic imbibition tests with different cores at the same experimental conditions were performed, as shown in **Fig. 2.13**. Then, different water injection experiments were conducted at different rates (*i.e.*, 1, 2, 4, 8, 16 and 40 cc/hr). The results were plotted on oil recovery curves versus total production for continuous flow in the fracture as shown in **Fig. 2.14**. The oil recovery curves seen in this figure imply that once capillary imbibition is initiated (*i.e.*, the first drop of water penetrates the matrix), imbibition is continuous until the recoverable amount of the oil in the matrix is displaced by capillary imbibition. However, the oil recovery rate of this process is different at each injection rate. As the injection rate is increased, the brine tends to flow in the fracture because of the high fracture-matrix permeability ratio, which results in slower oil recovery because faster injection rate results in shorter residence time for water to contact the matrix. The water cuts at different injection rates were also plotted against time as shown in **Fig. 2.15**. The plot indicates that an increase in the injection rate causes high water cut and results in significantly faster water breakthrough.

An extension of the dynamic imbibition experiment was performed using four low-permeability Spraberry cores. Three cores were designated as fractured cores with dynamic imbibition investigated at different injection rates. The other core was designated as an unfractured core. The experiments were carried out for 70 hours. The results are presented in **Fig. 2.16**. If unfractured core is compared with fractured core at the same injection rate of 0.2 cc/hr, brine displaces oil in a piston-like process in the unfractured core with an ultimate recovery of about 55% IOIP at the production end. The ultimate recovery of the fractured core was lower than that of the unfractured core. Obviously, this is due to a difference in the displacement mechanisms. The experiment using unfractured core is a piston-like displacement, while countercurrent imbibition and viscous displacement were involved in the fractured core.

For fractured cores with different injection rates (*i.e.*, 0.2, 0.5 and 1.0 cc/hr), the results were similar to those of experiments using fractured Berea cores. Faster injection rates resulted in a slower rate of oil recovery, while the ultimate recovery approached the same value as shown in **Fig. 2.16.** However, higher injection rates are associated with faster water breakthrough (**Fig. 2.17**).

According to Babadagli,[11] when the injection rate increases and reaches a certain value, there is no capillary imbibition because the contact time with the matrix was not long enough. Based on this mechanism, the limiting value of injection rate can be defined as a critical injection rate. The critical injection rate is the maximum injection rate at which the capillary imbibition is not effective. At this point the injected fluid does not contact the matrix long enough to initiate capillary imbibition. Thus, water flows only in the fracture, displacing the oil, and no matrix interaction occurs.

To determine the critical injection rate, the ultimate oil recovery at a certain total fluid production at different injection rates for both Berea and Spraberry cores (**Figs. 2.14** and **2.16**) was chosen. The results were then plotted in the form of injection rate against the ratio between total oil produced and total fluid produced (TOP/TFP) called an oil cut, as shown in **Fig. 2.18**. The results show that the oil cut produced from Berea core is higher than that from Spraberry core. At lower (2.0 cc/hr) injection rates used in fractured Berea core, the capillary force (static imbibition mechanism) was the only force in the coreflooding process. Thus, oil recovery took a substantial amount of time. When using the injection rates between 2.0 and 16.0 cc/hr, both capillary pressure and viscous forces were dominant (dynamic imbibition mechanism). This means that when water imbibed into the matrix and released oil from the matrix to the fractures, the oil in the fracture was pushed by the volume of the water injected (viscous forces). However, at a higher injection rate (more than 16 cc/hr), coreflooding was inefficient because the viscous force was the only dominant mechanism. After the maximum capillary pressure was reached, the producing end only produced water. Thus the oil cuts from 16 cc/hr injection rate were about the same as the oil cut using injection rate of 40 cc/hr. However, the field cost of higher injection rate is greater since more water must be processed to achieve the same recovery. The results also suggest that the critical injection rate, which also can defined as the maximum injection rate in which the capillary and viscous forces are still dominant, was determined to be 20 cc/hr for this set of experiments. The critical injection rate is the point where the curves bend. Beyond this point, the curves are essentially constant and steadily approach zero oil cut.

An exponential correlation was used to fit the experimental data. Then, the injection rate beyond experimental points could be approximated. The critical injection rate for Spraberry reservoir rock was found to be approximately 10 cc/hr.

In order to upscale the critical injection experiments to field dimensions, Eq. 5 and Spraberry rock properties (**Table 2.3**) were used. The critical injection rate of 10 cc/hr from Spraberry core was converted to N_{fvc} of 1.0e-7. Using this N_{fvc} number, the critical injection rate for field dimensions can be calculated using a rearranged version of Eq. 6. The upscaling of laboratory data to field dimensions is tabulated in **Table 2.4**, with Berea sandstone used as a comparison. For the Spraberry waterflood case, the waterflood pilot consisted of four injection wells with a center producer for creating a confined 40-acre five-spot pattern, 0.1 md matrix permeability, 10% porosity and 10 ft net pay. The critical injection rate is about 393 bbl/day water. Meanwhile, the critical injection rate for the more permeable rock (Berea sandstone) is about 1013 bbl/day.

This fracture capillary number concept was also applied for the O'Daniel Pilot area assuming the same properties as in the Spraberry core case. This pilot area consists of six water injection wells, four CO_2 injection wells, three oil production wells, and two logging-observation wells. The well location is shown in **Fig. 2.19**. The distance between the center production well (well 39) and the seven water injection wells (well 41, 42, 43, 44, 45, 47, and 48) that are parallel to fracture orientation is tabulated in **Table 2.5** along with the critical injection rate for each well. Meanwhile, the critical injection rate for well 46 can not be determined because its orientation with respect to well 39 is perpendicular to the fracture direction.

2.1.8 Conclusions

1. Low imbibition capillary pressure was generated from the model in order to match the experimental data. Laboratory experiments indicate that the wettability of the core plug was weakly water-wet.
2. An effective capillary pressure curve can be obtained from dynamic imbibition experiments by matching the recovery curves from experimental data and numerical simulation.
3. The matrix capillary pressure indicates that the wettability of Berea core is more water-wet than that of Spraberry core, even though Spraberry has much smaller pore throat sizes. Thus, imbibition capillary pressure is more dominant in Berea core than in Spraberry core.
4. The imbibition transfer is more effective for low injection rates due to lower viscous forces and longer contact time with the matrix.
5. Optimization of the injection rate is important prior to conducting waterflooding in naturally fractured reservoirs. As the flow rate increases, contact time between matrix and fluid in fracture decreases, thereby reducing the effectiveness of capillary imbibition.
6. Increasing injection rate beyond the critical injection rate causes high water cut, which results in significantly faster water breakthrough (the displacement process is inefficient).
7. The critical injection rate depends on the properties of the rock. The critical injection rate for Berea core in lab experiments and 40-acre field dimensions is 20 cc/hr and 1013 STB/D, respectively, and for Spraberry core, the critical injection rate is 10.0 cc/hr and 393 STB/D, respectively.

2.1.9 Nomenclature

A = area, L^2
dy = length of the core in y-direction, L
dz = height of the core, L
D = capillary diffusion coefficient, ML^3T^{-2}
f = fractional flow, dimensionless
$J(S_{wi})$ = J-function at S_{wi}, dimensionless
k = permeability, L^2
k_r = relative permeability, dimensionless
$P_{c,max}$ = maximum capillary pressure, $ML^{-1}T^{-2}$
q_{inj} = volumetric injection rate, L^3T^{-1}
S = saturation, fraction
t = time, T
v = velocity of the injected fluid in the fracture, LT^{-1}
w = fracture width, L
x = spatial coordinate, L

Greek letters

σ = interfacial tension, MT^{-2}
θ = contact angle, degree
ϕ = fracture porosity, fraction
μ = viscosity, $ML^{-1}T^{-1}$

Subscripts

e = effective
f = fracture
i = initial
m = matrix
o = oil
r = residual
w = water

2.1.10 References

1. Baker, R and Wilson, G.: " Numerical Simulation of Laboratory Scale Imbibition Experiment," Internal Report Epic Consultant Services Ltd., (April 1997).
2. Bech, N., Jensen, O.K. and Nielsen, B.: "Modeling of Gravity-Imbibition and Gravity-Drainage Processes," *SPERE* (Feb. 1991) 129-136.
3. Beckner, B. L., Ishimoto, K., Yamaguchi, S., A. Firoozabadi and Azis, K.: "Imbibition-Dominated Matrix-Fracture Fluid Transfer in Dual Porosity Simulators," paper SPE 16981 presented at the 1987 SPE Annual Technical Conference and Exhibition, Dallas, TX., Sept. 27-30.
4. Blair, P.M.: "Calculation of Oil Displacement by Countercurrent water Imbibition," *SPEJ*, Sept. 1964, 195-202; *Trans.,* AIME, **231**.

5. Chen, J., Miller, M.A. and Sepehrnoori, K.: "Theoretical Investigation of Countercurrent Imbibition in Fractured Reservoir Matrix Blocks," paper SPE 29141 presented at the 1995 symposium on reservoir simulation, San Antonio, TX., Feb. 12-15.
6. Honarpour, M., Koederitz, L. and Harvey, A. H.: Relative Permeability of Petroleum Reservoirs, CRC Press, Inc., Boca Raton, FL, (1986).
7. Brownscobe, E.R. and Dyes, A.B.: "Water-Imbibition Displacement-A Possibility for the Spraberry," *Drill. and Prod. Prac.* API (1952), 383-390.
8. Mannon, R.W. and Chilingar, G.V.: "Experiment on Effect of Water Injection Rate on Imbibition Rate in Fractured Reservoirs," paper SPE 4101 presented at the 1972 Annual Fall Meeting of the SPE of AIME, San Antonio, Oct. 8-11.
9. Kleppe, J. and Morse, R.A.: "Oil production from Fractured Reservoirs by Water Displacement," paper SPE 5084 presented at the 1974 SPE Annual Meeting, Houston, Oct. 6-9.
10. Kazemi, H. and Merrill, L.S.: "Numerical Simulation of Water Imbibition in Fractured Cores," paper SPE 6895 presented at the 1977 SPE Annual Technical Conference and Exhibition, Denver, Oct. 9-12.
11. Babadagli, T.: "Injection Rate Controlled Capillary Imbibition Transfer in Fractured Systems," paper SPE 28640 presented at the 1994 SPE Annual Technical Conference and Exhibition, New Orleans, Sept. 25-28.
12. Guo, B. and Svec, R.: "A Preliminary Analysis of Permeabilities in the Teague-Blinebry Reservoir based on Step-Rate Test on Well Lamunyon Federal #62 and Whole Cores from Well Lamunyon Federal #50," PRRC internal report, January 29, 1998.
13. Seright, R., *et al.*: "Gel Placement Technique," unpublished manuscript, PRRC internal report (1996).
14. Kazemi, H., Merrill, L.S., Porterfield, L.K., and Zeman, P.R.: "Numerical Simulation of Water-Oil Flow in Naturally Fractured Reservoirs," *SPEJ* (Dec. 1976), 317-26.
15. Schechter, D. S., McDonald, P., and Sheffield, T.: "Reservoir Characterization and CO_2 Pilot Design in the Naturally Fractured Spraberry Trend Area, " paper SPE 35469 presented at the 1996 SPE Permian Basin Oil and Gas Recovery, Midland, March 27-29.
16. Elkins, L. F.: "Cyclic Water Flooding the Spraberry Utilizes 'End Effect' to Increase Oil Production Rate," *JPT* (August 1963), 877-884.

Table 2.1—Core and fluid properties

Core Properties							Fluid properties at 138°F	
Cores #	Length, (cm)	Diam., (cm)	Perm. to brine, (md)	ϕ, (%)	S_{wi}, (%)	S_{or}, (%)	μ_o, (cp)	5.92
SPR-8H	6.487	3.608	0.17	10.98	34.04	57.03	μ_w, (cp)	0.68
SPR-9H	6.502	3.607	0.33	10.26	41.29	49.90	ρ_o, (gr/cc)	0.850
SPR-10H	5.433	3.607	0.14	10.11	39.96	52.53	ρ_w, (gr/cc)	1.076
SPR-11H	5.842	3.607	0.10	10.71	40.55	51.62	IFT, (dyne/cm)	26.22

Table 2.2—Core and fluid properties for Berea core

Core Properties		Fluid Properties	
D (cm)	3.786	Oil	Spraberry oil
L (cm)	6.8936	Water	Spraberry brine
k_m (md)	28.09	μ_o (cp)	3.52
ϕ_m (%)	17.16	μ_w (cp)	0.68
k_f (md)	3429	S_{wi} (%)	0
ϕ_f (%)	1.0	S_{or} (%)	40
w_f (cm)	0.0076		

Table 2.3—Core and fluid properties for Spraberry core

Core Properties		Fluid Properties	
D (cm)	3.607	Oil	Spraberry oil
L (cm)	5.842	Water	Spraberry brine
k_m (md)	0.5	μ_o (cp)	5.92
ϕ_m (%)	10.84	μ_w (cp)	0.68
k_f (md)	335	S_{wi} (%)	36.6
ϕ_f (%)	1.0	S_{or} (%)	42.51
w_f (cm)	0.0024		

Table 2.4—Rock properties of Spraberry and Berea cores

	Spraberry Core		Berea Core	
Parameter	Lab unit	Field unit	Lab unit	Field unit
μ_w	0.68	0.68	0.68	0.68
A	-	40	-	40
$L_{inj\text{-}prod}$	6.8	933.4	7.1	933.4
H	3.6	10	3.7	10
A_m	24.8	9333.81	25.807	9333.81
K	0.1	0.1	63.41	63.41
ϕ	0.1	0.1	0.166	0.166
P_{cmax}	7	7	1.2	1.2
θ	0	0	25	25
σ	26.2	26.2	26.2	26.2
J	0.27	0.27	0.99	0.99
q_{crit}	10	393.22	20	1013.26
$Nfvc$	1.010^{-7}	-	2.8210^{-7}	-

Table 2.5—Critical injection rates for wells in O'Daniel Pilot Area

Injection Well	Distance to well 39 (ft)	Critical injection rate (STB/D)
w-41	1020	430
w-42	1040	438
w-43	1040	438
w-44	1020	430
w-45	1420	598
w-47	1450	610
w-48	1460	615

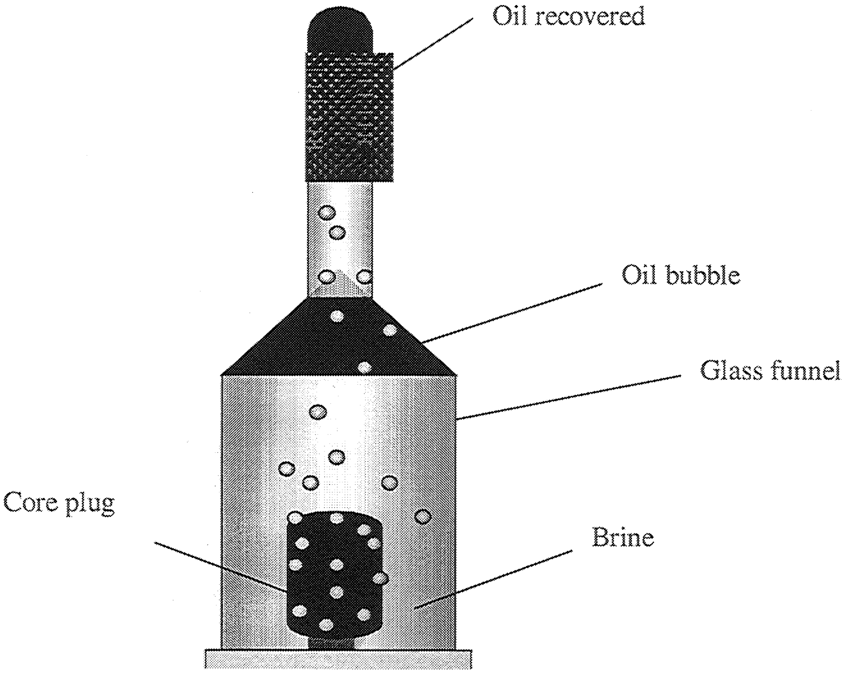
Oil recovered
Oil bubble
Glass funnel
Core plug
Brine

Fig. 2.1—Physical process of laboratory spontaneous imbibition.

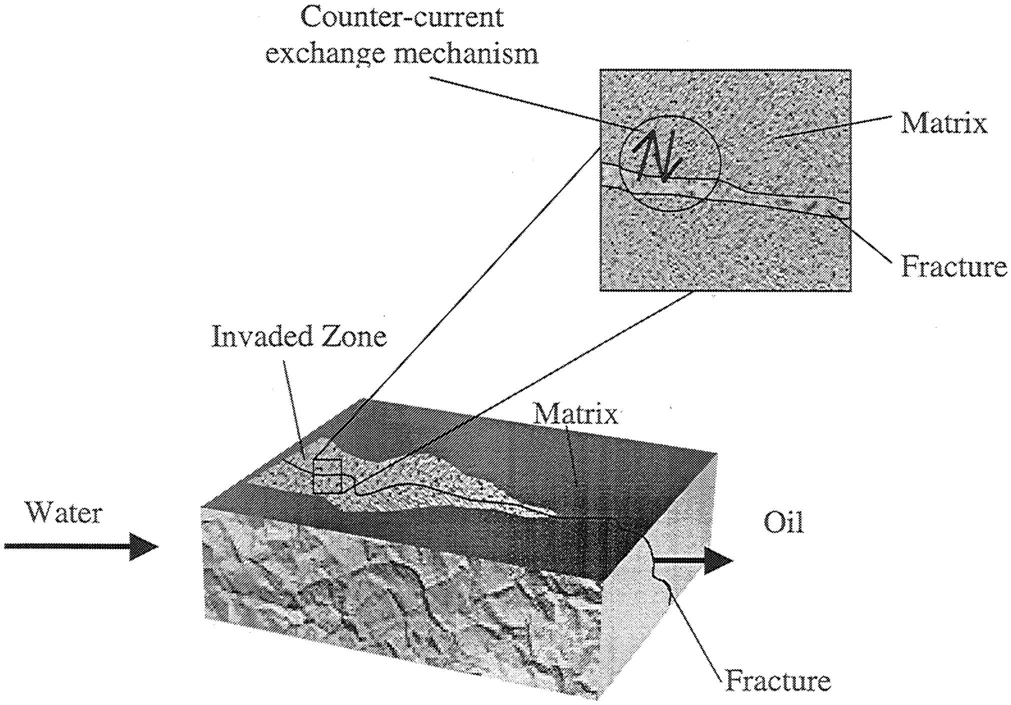
Counter-current
exchange mechanism
Matrix
Fracture
Invaded Zone
Matrix
Water
Oil
Fracture

Fig. 2.2— Concept of dynamic imbibition process.

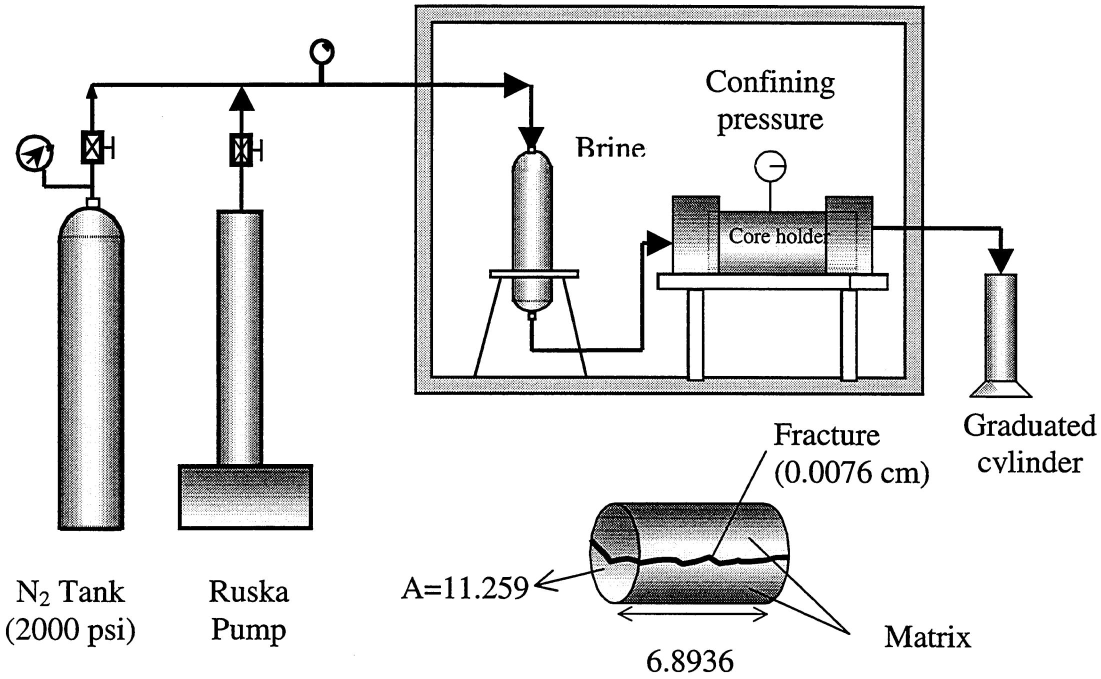
Confining
pressure
Brine
Core holder
N2 Tank
(2000 psi)
Ruska
Pump
Graduated
cvlinder
Fracture
(0.0076 cm)
A=11.259
6.8936
Matrix

Fig. 2.3—Experimental setup of dynamic imbibition.

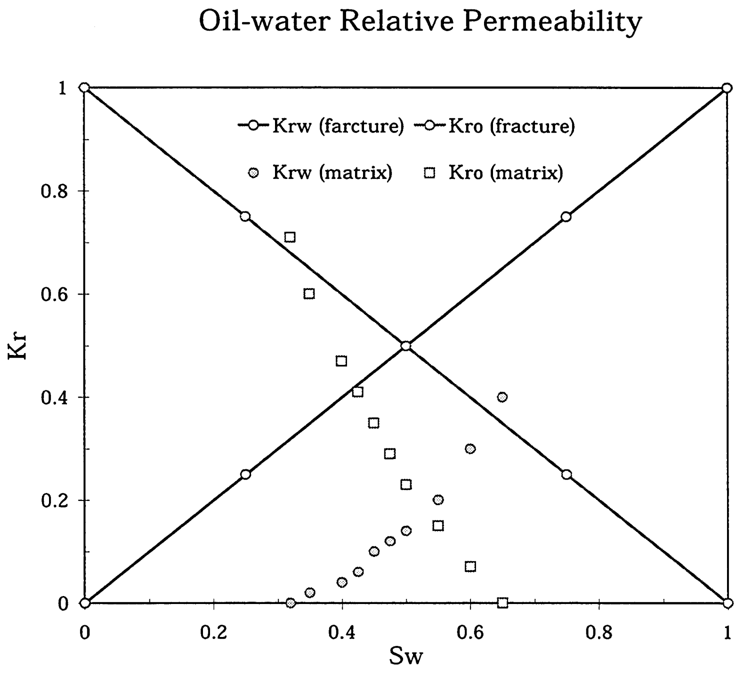

Fig. 2.4—Relative permeability curves.

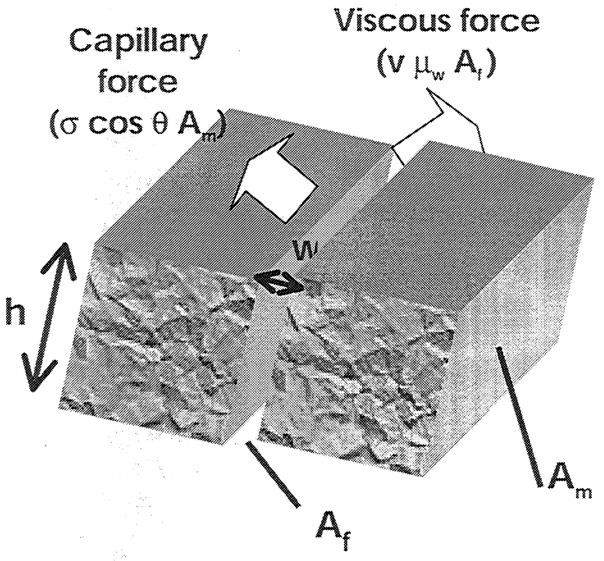
Capillary force
(σ cos θ A_m)
Viscous force
(v μ_w A_f)
w
h
A_m
A_f

Fig. 2.5—Schematic representation of matrix and fracture where the viscous and capillary forces are effective.

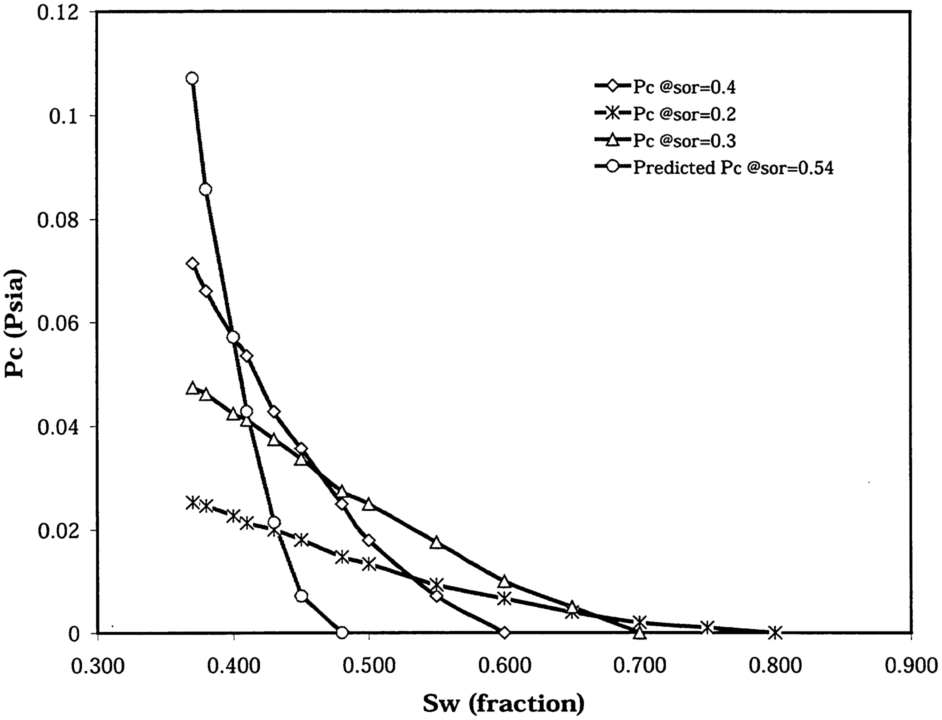

Fig. 2.6 —Imbibition capillary pressure obtained from matching spontaneous imbibition data.

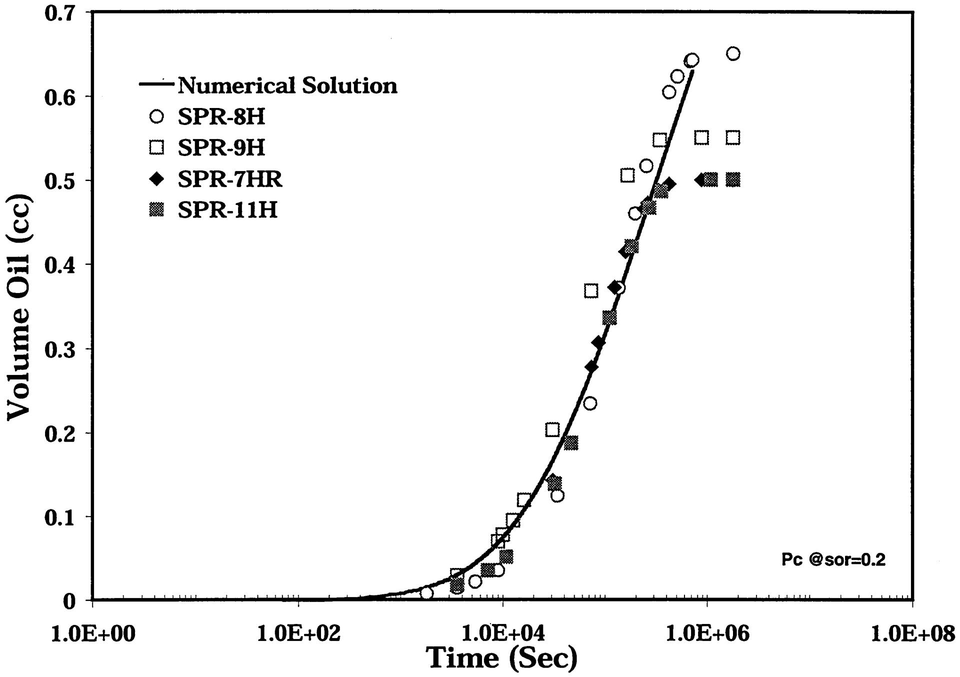

Fig. 2.7—Matching between spontaneous-imbibition experiments with numerical solution using 0.2 S_{or}.

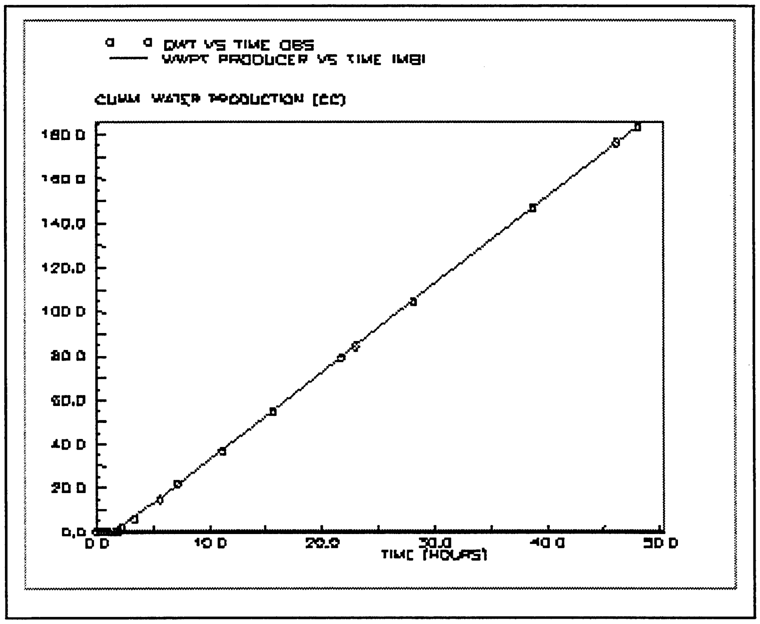

Fig. 2.8—Matching between experimental data and the numerical solution (Berea core - cumulative water production, injection rate = 4.0 cc/hr).

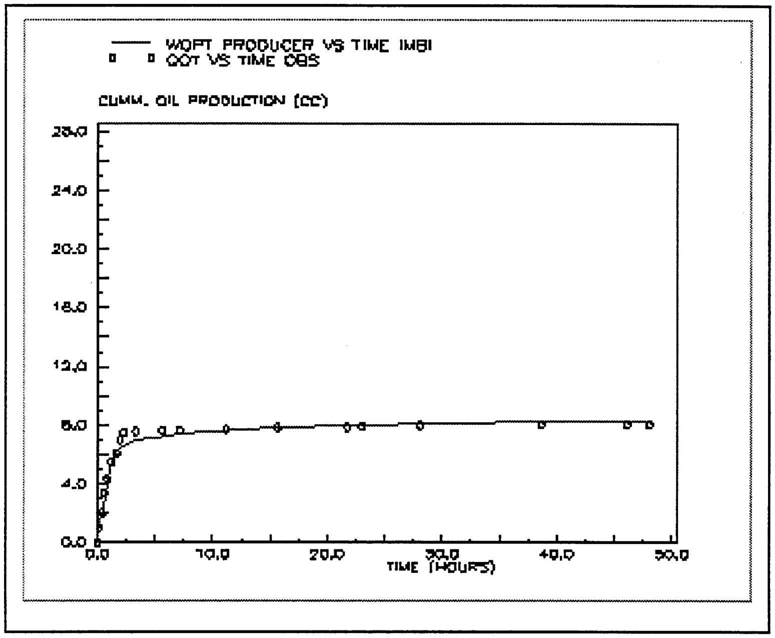

Fig. 2.9—Matching between experimental data and the numerical solution (Berea core - cumulative oil production, injection rate = 4.0 cc/hr).

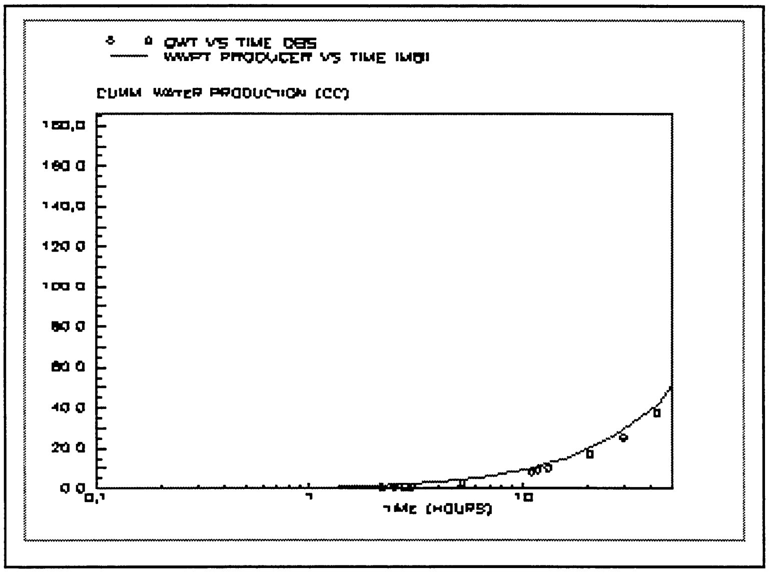

Fig. 2.10—Matching between experimental data and the numerical solution (Spraberry core - cumulative water production, injection rate = 1.0 cc/hr).

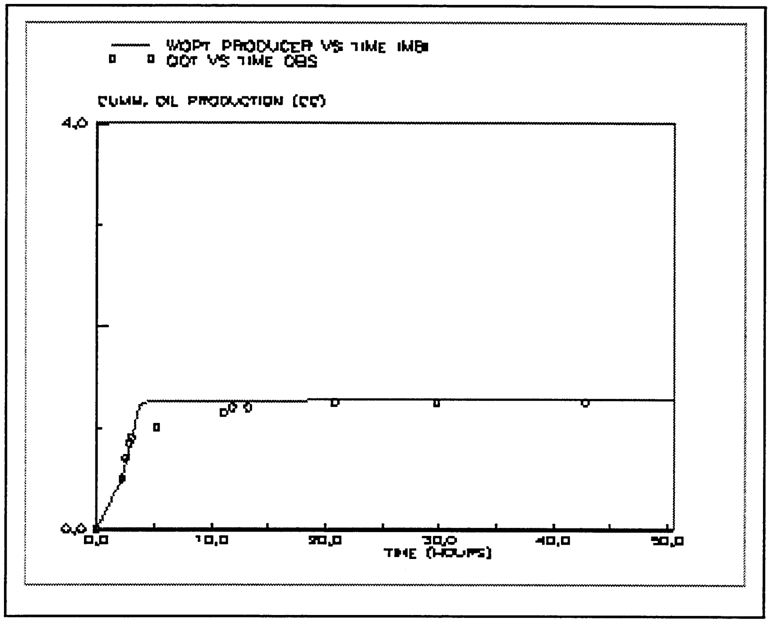

Fig. 2.11—Matching between experimental data and the numerical solution (Spraberry core - cumulative oil production, injection rate = 1.0 cc/hr).

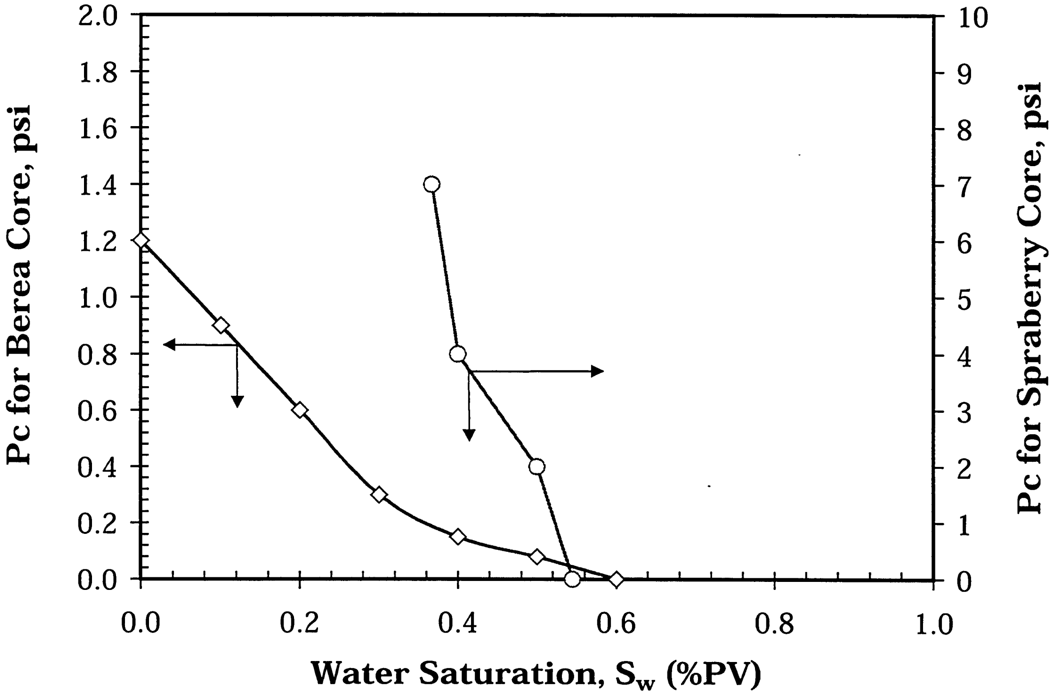

Fig. 2.12—Capillary pressure obtained as a result of matching experimental data (Berea and Spraberry cores).

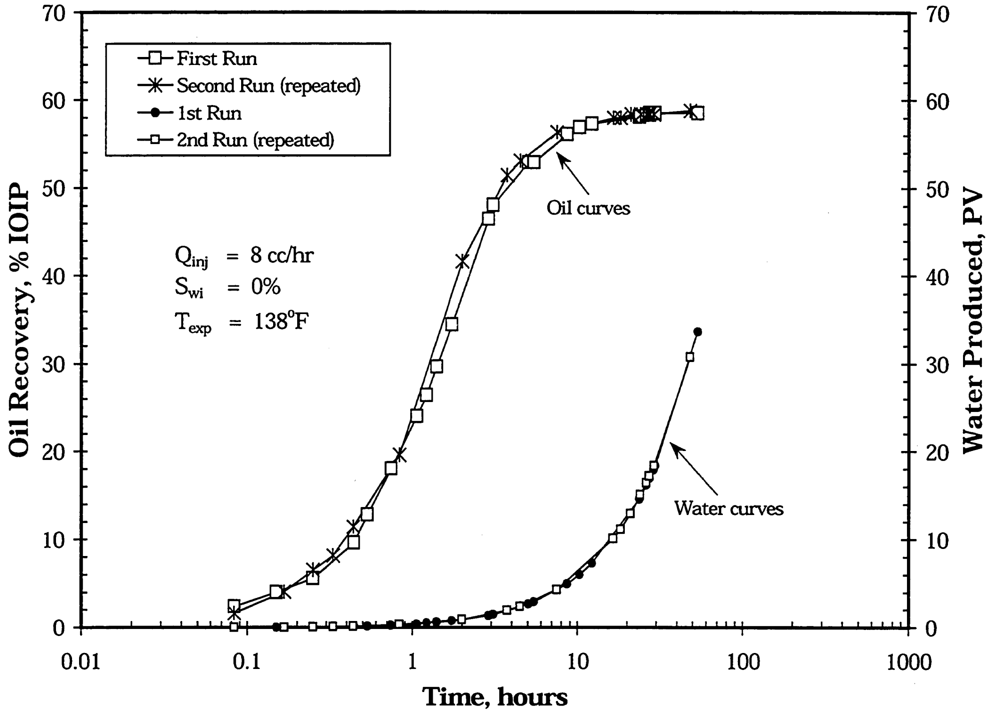

Fig. 2.13—Reproducibility of the dynamic imbibition flooding results in Berea Sandstones.

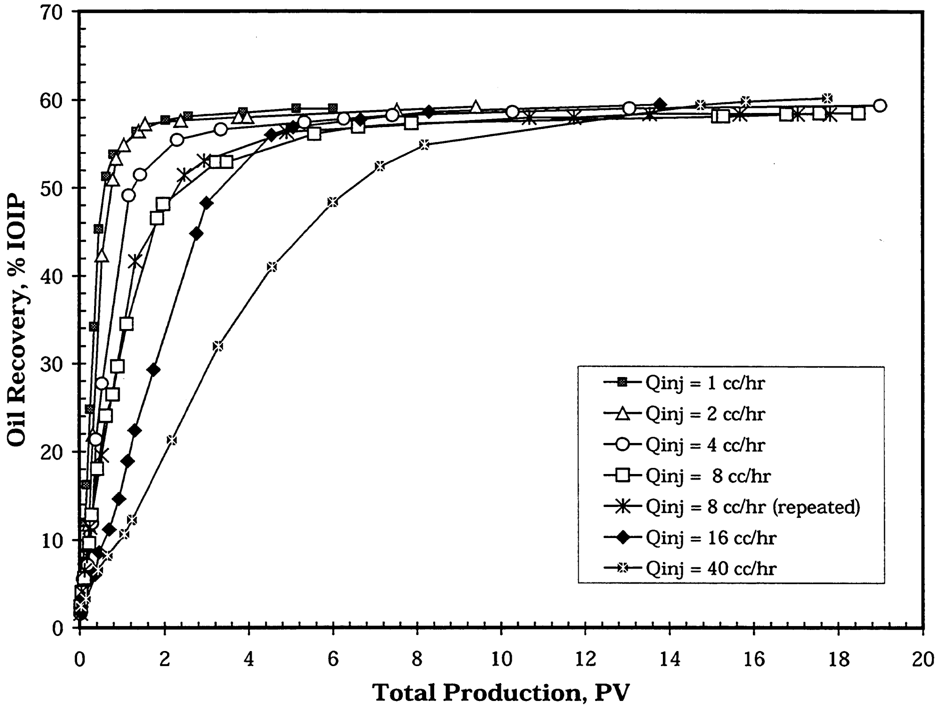

Fig. 2.14—Oil recovery from fractured Berea cores during water injection using different injection rates.

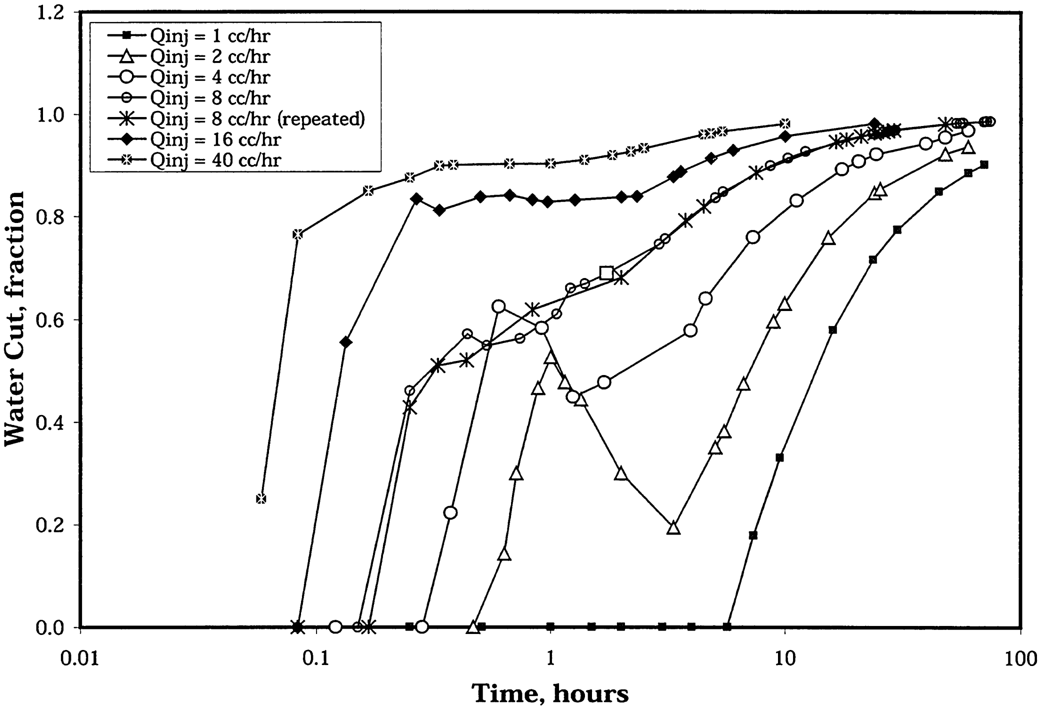

Fig. 2.15—Water cut during the dynamic imbibition experiments for fractured Berea cores.

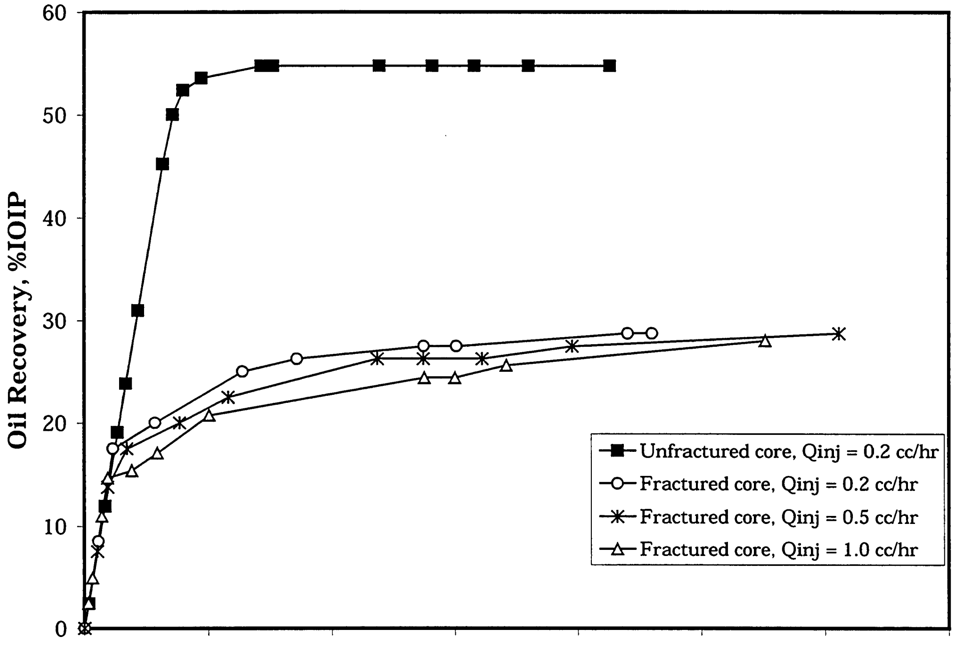

Fig. 2.16—Oil recovery from fractured and unfractured Spraberry cores during water injection using different injection rates.

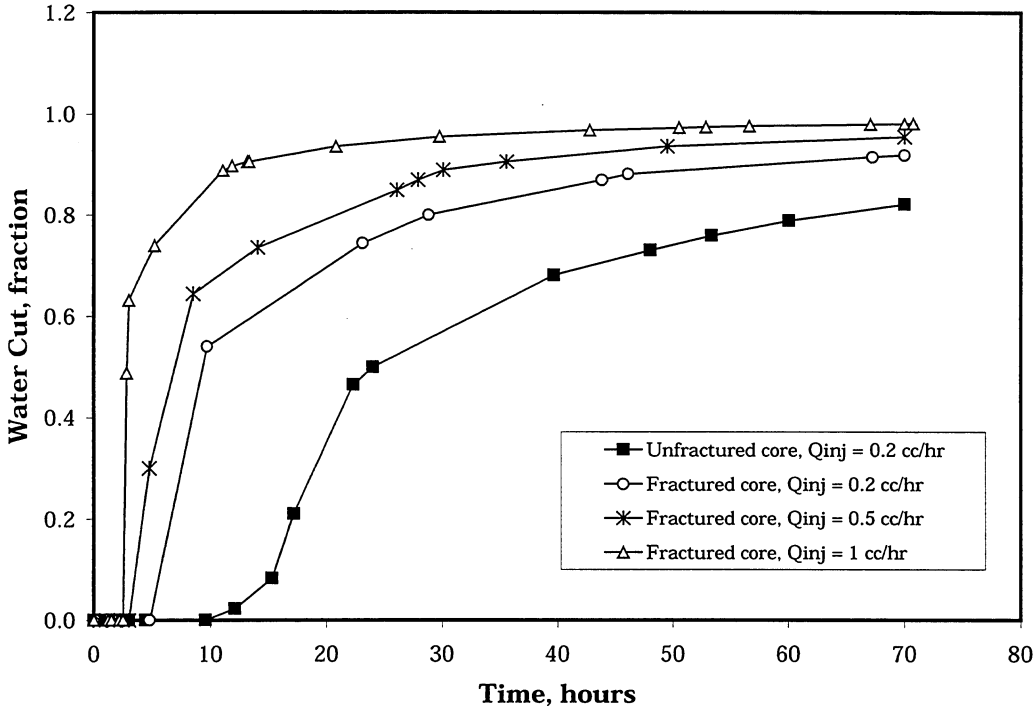

Fig. 2.17—Water cut during the dynamic imbibition experiments for fractured and unfractured Spraberry cores.

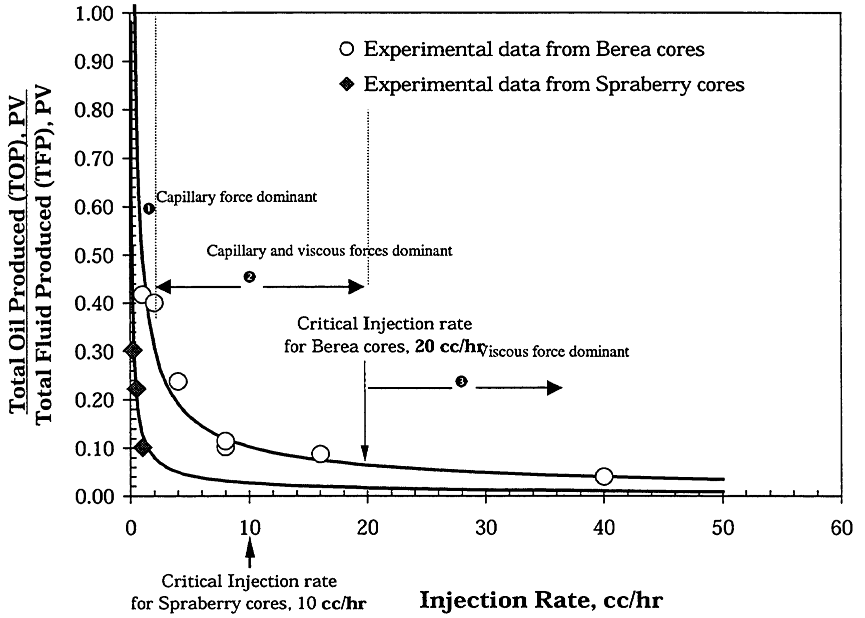

Fig. 2.18—Injection rate vs. oil cut (TOP/TFP).

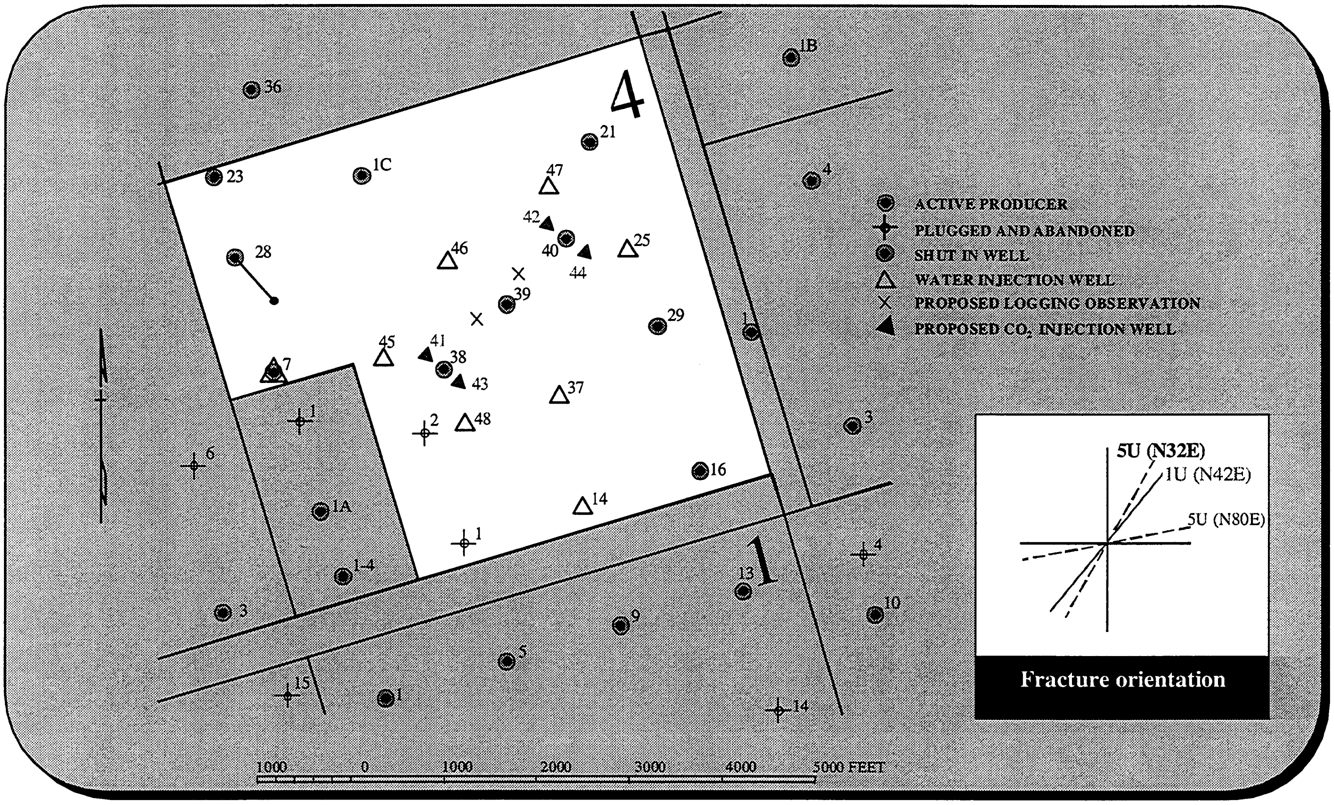
4
1
36
1B
21
23
1C
47
4
42
40
44
25
28
46
39
29
1
41
45
38
7
43
37
1
3
2
48
6
16
14
1A
1
4
1-4
13
10
3
9
5
15
1
14
ACTIVE PRODUCER
PLUGGED AND ABANDONED
SHUT IN WELL
WATER INJECTION WELL
PROPOSED LOGGING OBSERVATION
PROPOSED CO_2 INJECTION WELL
5U (N32E)
1U (N42E)
5U (N80E)
Fracture orientation
1000
0
1000
2000
3000
4000
5000 FEET

Fig. 2.19—E.T. O' Daniel pilot area.

3. RESERVOIR PERFORMANCE

3.1 WELL TESTING ANALYSIS OF THE E.T. O'DANIEL WELLS

3.1.1 Introduction

The production equipment facilities are complete and currently in use. All six proposed water injection wells and three producers for the 10-acre field demonstration pilot have been drilled and completed. The four CO_2 injection wells will be completed in 1999 along with the two logging observation wells.

The first water injection well completed was the O'Daniel No. 47. Water injection into this well initiated the beginning of the pulse test March 10, 1999. The pulse test consists of injecting water in a single well and monitoring the pressure response in the three producing wells. During the pulse test, only one well will be injecting. Projected length of the pulse test is four to six months but depends on observing breakthrough or response timing.

3.1.2 Buildup Tests

Epic Consulting Services Ltd. provided analyses of the E.T. O'Daniel Wells 38, 39, and 40 buildup tests using the FAST WellTest package. The buildup tests were taken prior to the SRIT. Both the single porosity and dual porosity model were used. The length of the buildup test and quality of data indicate that Well 39 is the most reliable analysis. The following results were obtained from the analyses:

Single Porosity Model

Parameter	**Well 38**	**Well 39**	**Well 40**
Permeability to oil, k (md)	0.014	0.014	0.033
Skin, s	-2.844	-3.305	-3.411
Storage coefficient, C_D	461.5	846.9	2167
Current average pressure (psi)	1318	1344	1024

Dual Porosity Model

Parameter	**Well 38**	**Well 39**	**Well 40**
Permeability to oil, k (md)	0.014	0.014	0.033

Skin, s	-3.57	-3.93	-4.24
Storage coefficient, C_D	620	1312	2892
Interporosity coefficient, λ	1.34E-4	4.6E-5	4.0E-5
Storativity ratio, ω	2.85E-6	3.9E-5	1.6E-5
Current average pressure (psi)	1090	1081	874

Wellbore storage is high and dominates the majority of the tests. The storage masks the early pressure transient flow in the fracture system, which causes the calculated permeability to be low and representative of the matrix rather than an effective permeability. The pressure determined from these tests are low and below the MMP necessary for the CO_2 flood. However, as the pulse test proceeds and more water is injected, the pressure is expected to increase. The transition to pseudo-steady-state (PSS) from radial flow apparently did not occur because the tests were not long enough (1000 hours for well 39). The dual porosity parameters of λ (interporosity flow coefficient) and ω (storativity ratio) are small. A small λ indicates the permeability is in the fractures and a small ω indicates most of the storage capacity is in the matrix. This seeming contradiction is due to the length of the test and the domination by wellbore storage.

3.1.3 Step Rate Testing (SRT)

Step rate injection tests to obtain formation parting pressures were conducted in the new injection wells O'Daniel 46 (**Figs. 3.1 and 3.2**) and 47. The conventional SRT analysis assumes a steady-state Darcy flow into the injection well and is based on the steady-state solution of the diffusivity equation[4] given by

$$\bar{p} - p_{wf} = 141.2\frac{qB\mu}{kh}\left[\ln\left(\frac{r_e}{r_w}\right)+s\right]$$

If a steady-state condition is achieved, then the external drainage radius, r_e, and average pressure at r_e will be constant and a linear relationship will exist between the p_{wf} and q at the end of each rate. Normally the rates are not long enough to reach steady-state conditions. However, the drainage radius or radius of influence of the rate change can be used if we assume that the $\ln\frac{r_d}{r_w}$ is insensitive to small changes in r_d. A plot of p vs q will yield a straight line prior to the formation parting. After formation parting pressure has been exceeded, the resulting fracture acts as an additional fluid conductor and causes a change in the slope. There is no theoretical basis for drawing a second straight line through the points above the parting pressure. However, conventional analysis suggests this and the intercept of the pre-parting straight line and post-parting straight line is assumed to be the parting pressure. Singh, Agarwal and Krase[4] showed that this may lead to erroneous parting or propagation pressure. To try to quantify the actual parting pressure and thus lend theoretical basis to the determination of the formation parting or fracture propagation pressure, the multirate superposition analysis technique introduced by Odeh and Jones[5] and suggested and extended by Singh and Agarwal[4] is used.

The Odeh and Jones method assumes transient radial flow into the reservoir during each constant rate period. **Figure 3.3** shows the radial Odeh and Jones plot for well 46. For data below parting pressure and in true radial flow, the Odeh and Jones method should provide a single straight line for all data below parting pressure. In addition the slope and intercept of this line provide a method to obtain formation flow capacity, *kh*, and wellbore skin, *s*, before fracturing (**Fig. 3.4**). The method breaks down after fracturing. **Figure 3.3** shows a downward shift for each rate after the first rate indicating fracture length is increasing. From the above it is apparent that radial type flow may not be completely valid. Therefore the data was analyzed using the Odeh and Jones superposition linear flow equation.[4,6] **Figure 3.5** shows the resulting plot for Well 46. Like the radial analysis, this shows a definite shift in the data for each subsequent step after the second step and possibly during the second step also. This indicates propagation pressure for fractured wells where linear flow is occurring. Note that the first and second curves in **Fig. 3.5** are fairly close, indicating that the fracture lengths may not have extended much during the second step. This can also be seen in the radial analysis in **Fig. 3.3.** In addition, Agarwal's equivalent time was employed to see if this would lend the possibility of using type curves to the analysis and if manipulation of the time function in this way would formulate any overlay of the data. The parting pressure or extension pressure is difficult to ascertain since no radial flow is seen therefore the end of the first step is conservatively estimated to be the parting pressure or 2215 bottomhole for the specific gravity of water obtained prior to the SRT of 0.452 psi/ft.

Using the equivalent wellbore radius concept determining the fracture length can be done for each step above FPP.[4] This type of calculation may not be possible if the fracture is still extending during the rate or the data is not in the bilinear flow regime and preferredly in pseudoradial flow. Similarly, using a simulation program, the fracture length was obtained for each step. The results are shown in **Table 1**.

Inconsistencies appear to exist in the above table in regards to the effective permeability and the fracture length. Calculated finite conductivity hydraulic fractures in a fissured formation have been shown to exhibit significantly smaller lengths than the real length.[7] As the fracture becomes longer and perhaps intersects more of the natural fracture system the total response of the system becomes that of the fissures. Because each step rate is not long enough to be outside of bilinear flow (and propagation may be continuing during each rate) and certainly has not attained pseudo-steady-state, the information is qualitative at best and any additional conclusions would be conjecture. The first few step rates exhibit early time behavior of a fissured system.

The MRT analysis of O'Daniel Well 47 is masked by significant afterflow (see **Figs. 3.6-3.10**). The first step is actually not part of the SRT design, but is an attempt to fill up the tubing prior to the SRT. As a result the first rate severely distorts the test and makes analysis difficult or impossible, thus the parting pressure is suggested to have been exceeded in the first step.

3.1.4 Conclusions

1. Except for Well 39, the buildup data is generally poor and dominated by wellbore storage because of the low permeability and flow rates. The storage masks early pressure transient flow in the fracture system, and hence the permeability calculated is very low and representative of the matrix rather than an effective permeability.
2. These same effects appear to limit the multirate analysis of the SRTs also.
3. The skin calculated from the buildup tests is negative and in the range of -2.8 to -3.4 for the singe porosity model and -3.5 to -4.2 for the dual porosity model.
4. The current average reservoir pressure is 1331 psi based on the single porosity model and 1100 psi based on dual porosity model. Both of these pressures are below the MMP for CO_2 but the average pressure is expected to continually increase during the interference/pulse test.
5. The transition to pseudo steady-state flow probably did not occur in either the buildup and SRT since the buildup tests and SRT rates were not long enough to get beyond domination of wellbore storage effects.

3.1.5 References

1. Schechter, D.S.: "Advanced Reservoir Characterization and Evaluation of CO_2 Gravity Drainage in the Naturally Fractured Spraberry Trend Area," quarterly technical progress report to DOE under contract No.: DE-FC22-95BC14942, U.S. DOE (October 5, 1998).
2. Schechter, D.S.: "Advanced Reservoir Characterization and Evaluation of CO_2 Gravity Drainage in the Naturally Fractured Spraberry Trend Area," quarterly technical progress report to DOE under contract No.: DE-FC22-95BC14942, U.S. DOE (January 13, 1999).
3. Schechter, D.S.: "Advanced Reservoir Characterization and Evaluation of CO_2 Gravity Drainage in the Naturally Fractured Spraberry Trend Area," third annual technical progress report to DOE under Contract No.: DE-FC22-95BC14942, U.S. DOE (December1998).
4. Singh, P.K., Agarqal, R.G., and Jrase, L.D.: "Systematic Design and Analysis of Step-Rate Tests To Determine Formation Parting Pressure," paper SPE 16798 presented at the 1987 Annual Technical Conference and Exhibition, Dallas, Tx., 27-30 September.
5. Odeh, A.S. and Jones, L.G.: "Pressure Drawdown Analysis, Variable Rate Case," *JPT* (Aug. 1965) 960.
6. Earlougher, R.C., Jr.: Advances in Well Test Analysis, Monograph Series Volume 5, Society of Petroleum Engineers, Dallas (1977)
7. Naceur, K.B. and Economides, M.J.: "Production From Naturally Fissured Reservoirs Intercepted by a Vertical Hydraulic Fracture," SPE 17425 *SPERE* (December 1989) 550.

Table 3.1—Fracture propagation

k_{eff} (md)	L_f (ft)
4.308	11.389
12.968	12.374
21.867	13.783
37.625	19.027
42.276	20.062
54.642	21.9
142.41	10.099
201.1	6.44
268.92	5.1217

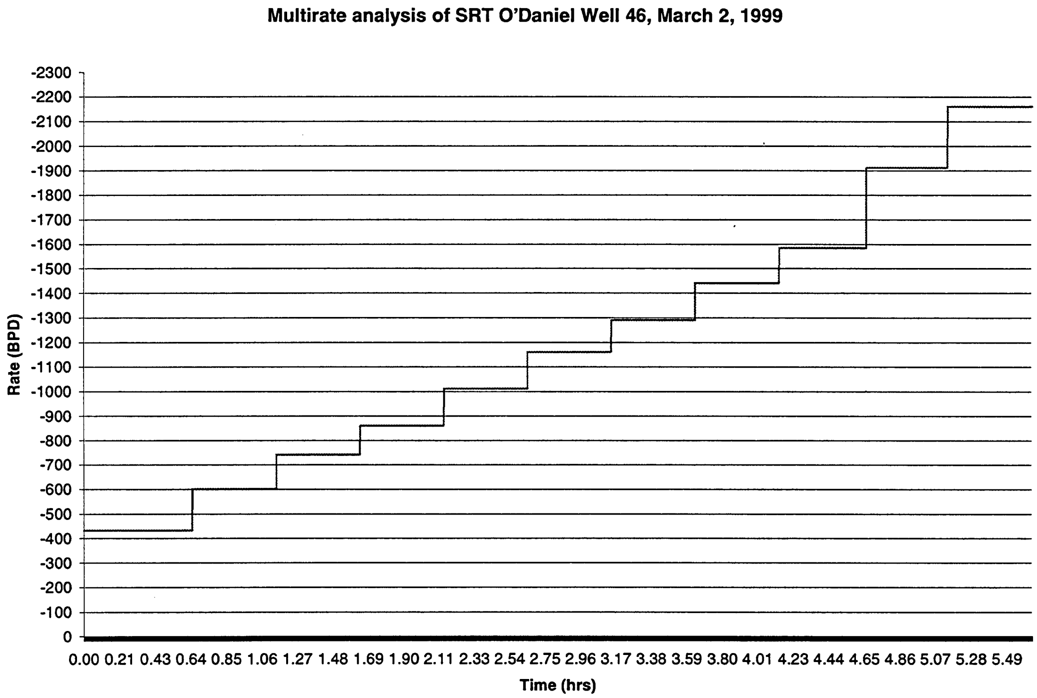
Multirate analysis of SRT O'Daniel Well 46, March 2, 1999

Fig. 3.1—Step rate test (SRT) design for O'Daniel injection Well 46.

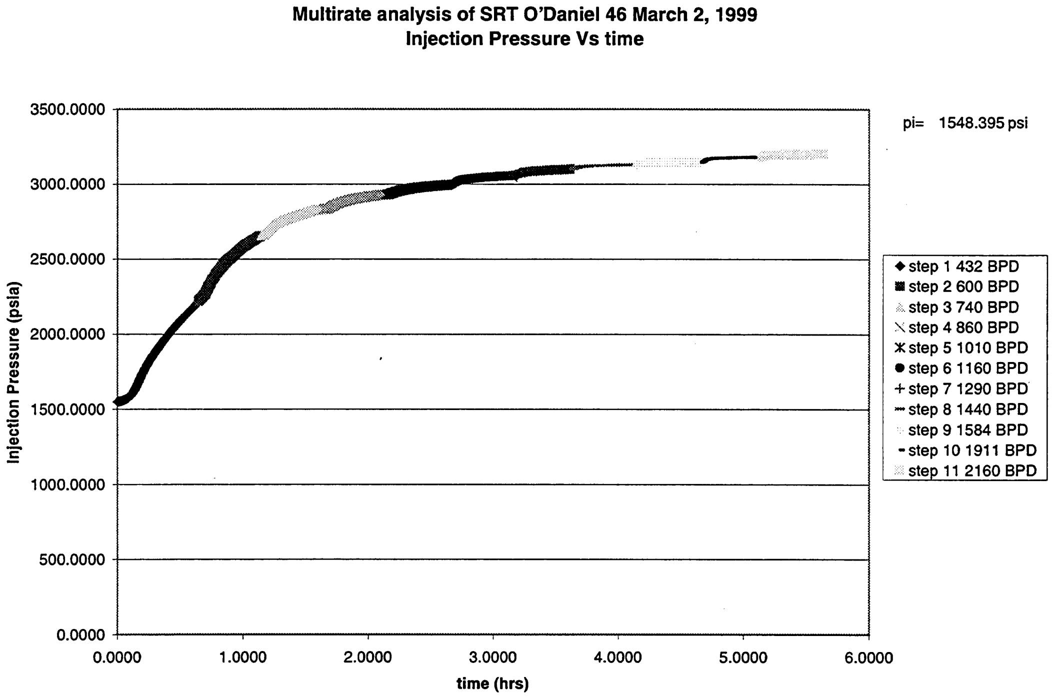

Fig. 3.2—Plot of injection pressure versus cumulative time O'Daniel Well 46.

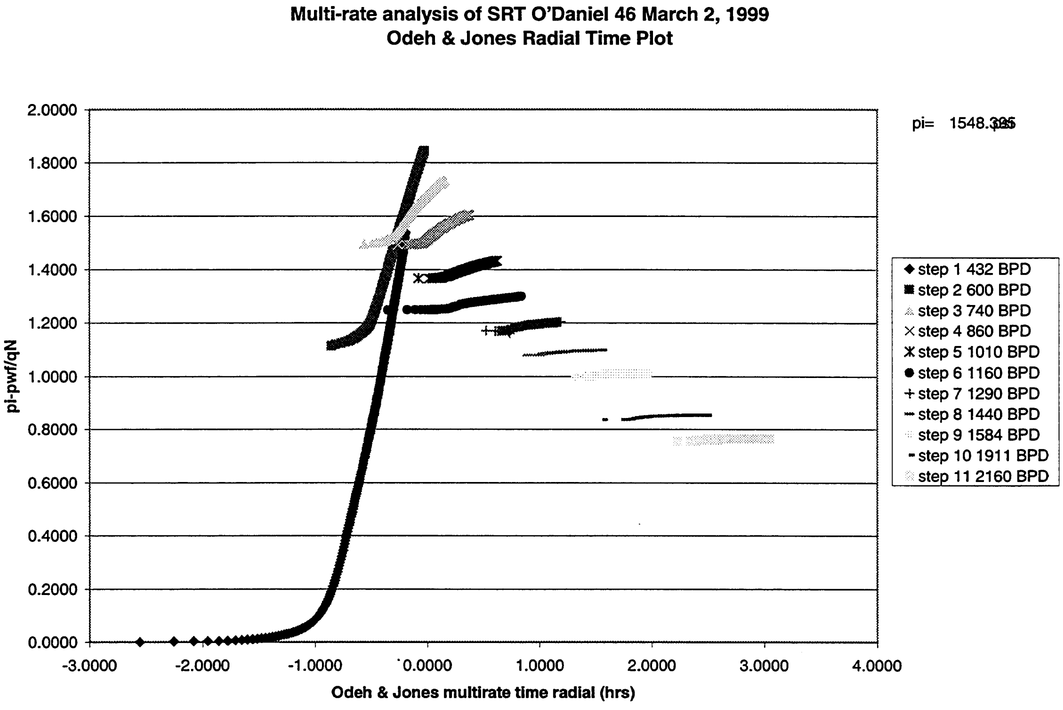

Fig. 3.3—Radial Odeh & Jones plot for Well 46.

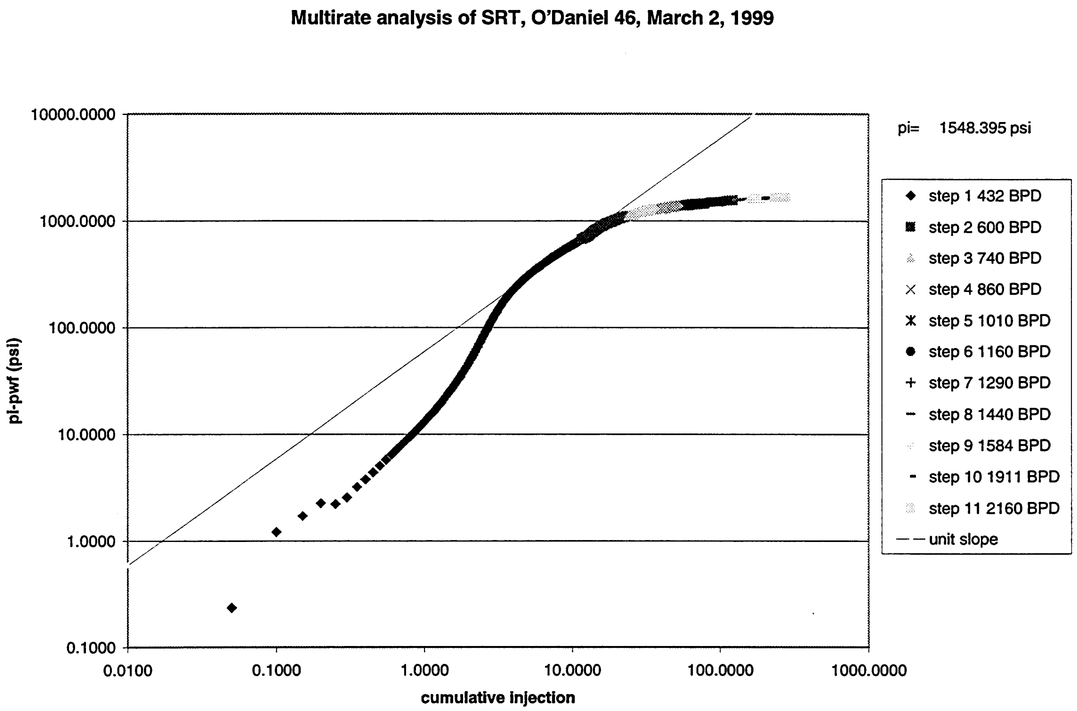

Fig. 3.4—Pressure vs. cumulative injection during SRT O'Daniel Well 46 with unit slope line to determine effects of wellbore storage on rates.

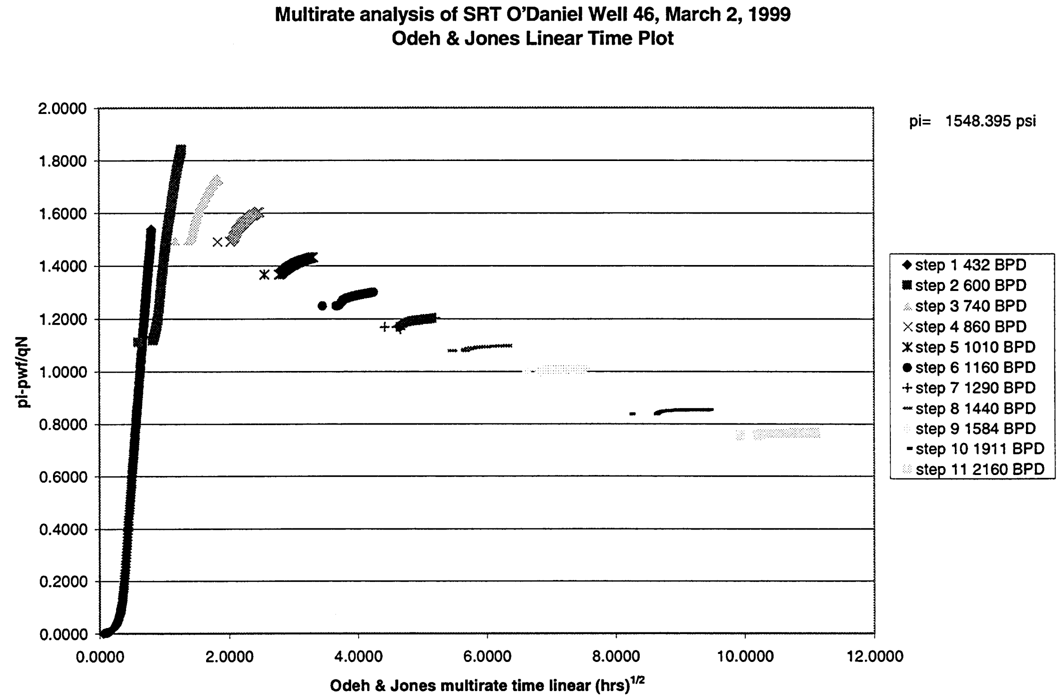

Fig. 3.5—Odeh & Jones linear time plot for O'Daniel Well 46.

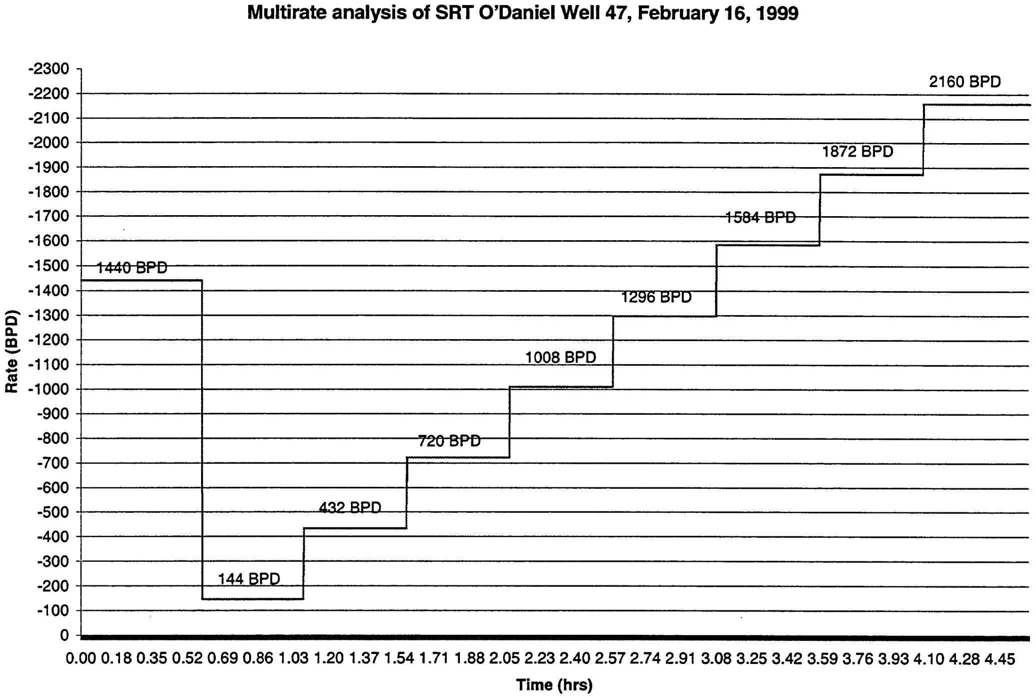

Fig. 3.6—Step rate test history of O'Daniel Well 47.

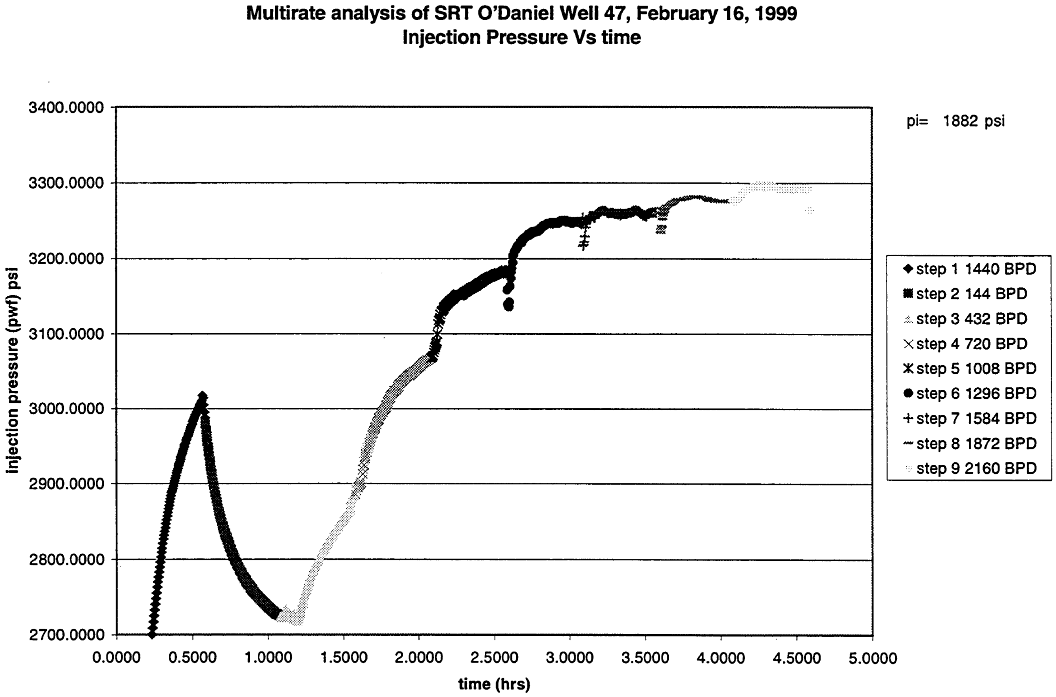

Fig. 3.7—Pressure/time history plot of O'Daniel Well 47.

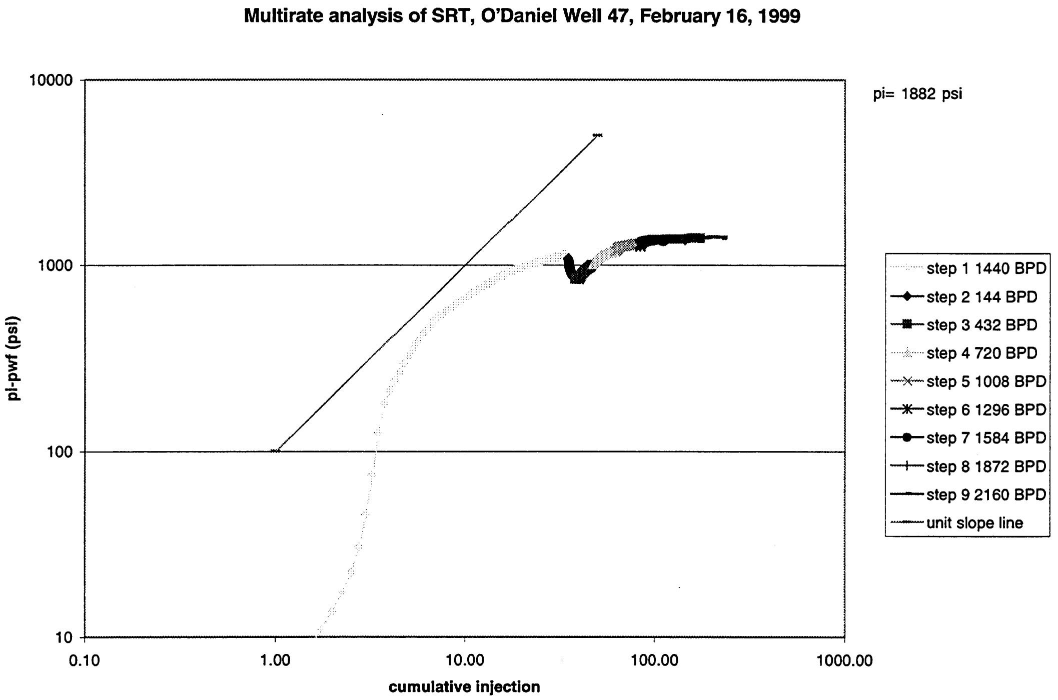

Fig. 3.8—Cumulative injection plot during SRT on O'Daniel Well 47.

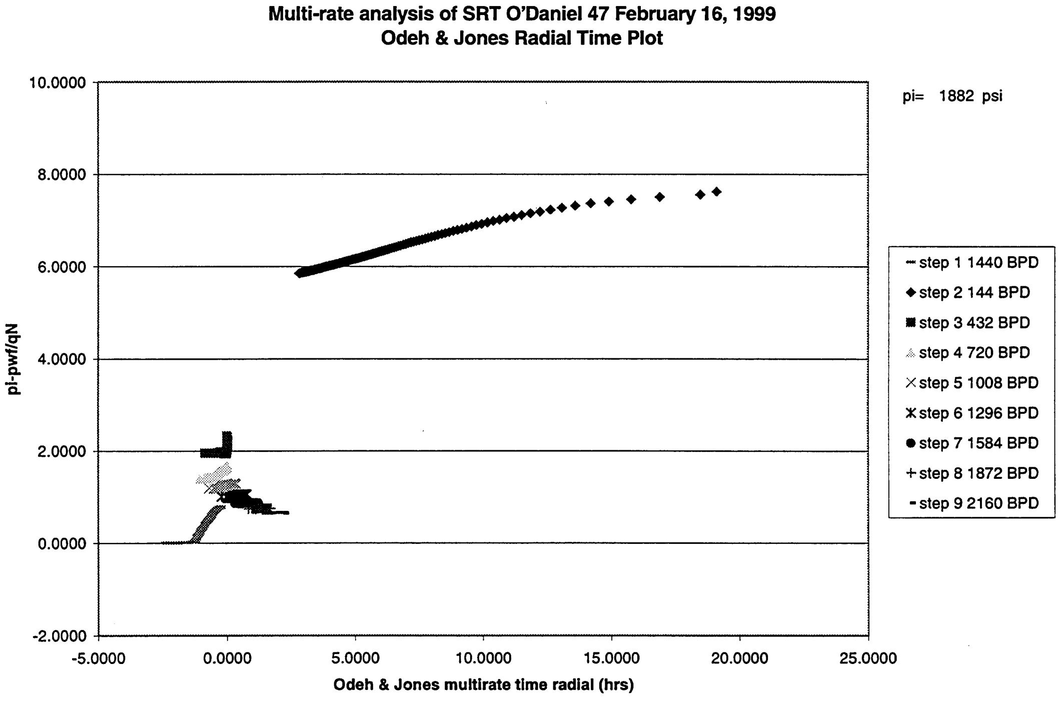

Fig. 3.9—Odeh & Jones multirate radial plot for O'Daniel Well 47.

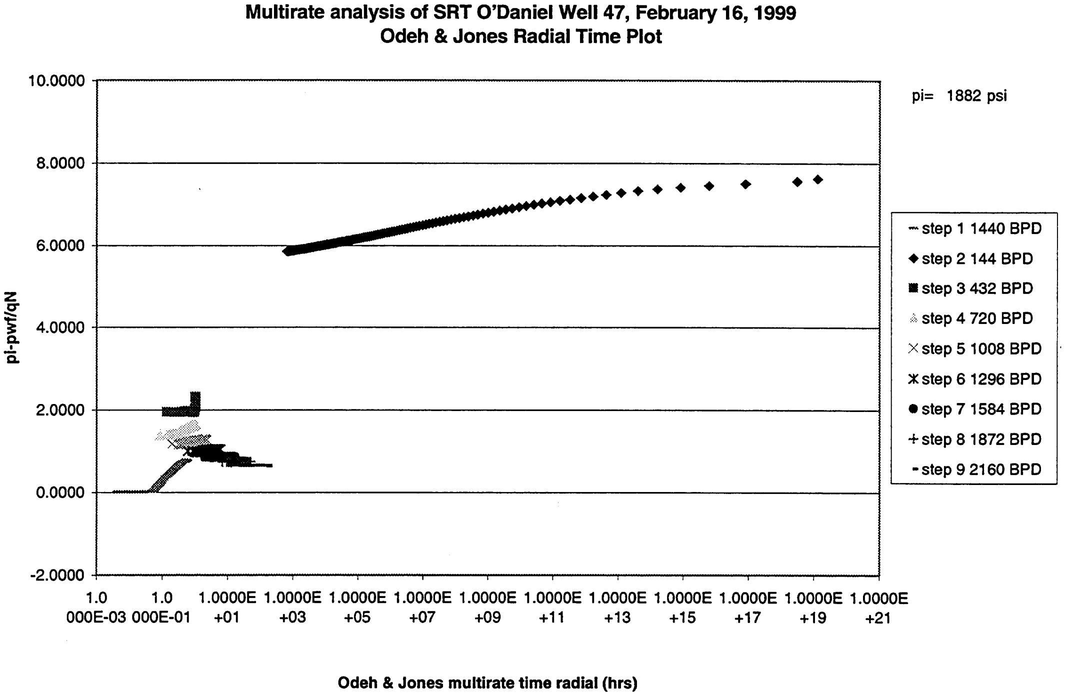

Fig. 3.10—Odeh & Jones multirate linear time plot for O'Daniel 47.

4. EXPERIMENTAL INVESTIGATIONS ON CO_2 GRAVITY DRAINAGE IN A FRACTURED SYSTEM

4.1 LABORATORY EXPERIMENTS OF CO_2 GRAVITY DRAINAGE

4.1.1 Introduction

During the first three years of this project, five experiments were performed on two 4 in. Berea cores, one 4 in. reservoir core, one 3.5 in. reservoir core and two 2.5 in. reservoir cores. The cores were taken from the Spraberry reservoir. The permeabilities to brine of 4 in. and 3.5 in. Spraberry cores are 0.01 md and 0.38 md, respectively. The absolute permeabilities of the two 4 in. Berea cores are 500 md and 50 md, respectively. The two 2.5 in. reservoir cores, which were stacked vertically during the experiment, have air permeabilities of 0.16 md and 0.13 md, respectively, while an average permeability to brine of 0.057 md was measured for the whole stack during the experiment. Table 4.1 summarizes the physical properties of those whole cores.

All five experiments were conducted to investigate the efficiency of CO_2 gravity drainage and the effect of initial water saturation during CO_2 gravity drainage experiments. The last experiment, which used a stack of two 2.5 in. Spraberry cores, was also performed to investigate the effects of core discontinuity and impermeable layers at the top and the bottom of the pay zone on the efficiency of the CO_2 gravity drainage. The partial results are also presented in Table 4.1.

Figure 4.1 summarizes the results (oil recovery curves) of all five experiments, which were given in the Third Annual Technical Progress Report. The results are redrawn in Figs. 4.2 and 4.3 as curves of oil recovery vs. rock permeability and oil recovery vs. initial water saturation. It is clearly seen from the figures that the efficiency of CO_2 injection decreases as permeability decreases and initial water saturation increases. It appears that core discontinuity and impermeable layers at the top and bottom of the pay zone affects the efficiency of the CO_2 gravity drainage, as can be seen by comparing the result of the last experiment (stacked core, K= 0.05 md and $Sw_I = 0.376$) with that of the third experiment (continuous core, K= 0.01 md and $Sw_I = 0.386$). The permeability and the water saturation of the cores are almost similar for that experiment but the recovery from stacked core (19% IOIP) is lower than the continuous core (31 % IOIP) as shown in Table 4.1. Figures. 4.2 and 4.3 show that the effect of initial water saturation on oil recovery is more pronounced than the effect of permeability.

In order to optimize the CO_2 pilot design in the E.T. O'Daniel Unit of the Spraberry Trend Area, the previous experimental results were scaled up to field scale using the mathematical model proposed by Schechter and Guo (1996). The modeling results indicate that significant amounts of oil can be recovered from the pilot area by CO_2 flooding in a relatively short time period, depending on matrix permeability, initial water saturation and fracture intensity.

During the fourth year of this project, another experiment was performed to model the actual field experience of first flooding and then CO_2 recovery in the naturally fractured Spraberry Trend Area. The objective of the experiment is to investigate the effect of water imbibition followed by CO_2 gravity drainage on oil recovery under reservoir conditions. The effects of temperature and cyclic CO_2 injection were also investigated during the experiment. The experiment was initially designed to use a Berea core and a reservoir core from the Spraberry Trend Area. As the experiment on the Spraberry core has not been completed at the time of this writing, only the results from the experiment of the Berea core are presented in this report.

4.1.2 Laboratory Experiment

4.1.2.1 Materials used in the experiment

Core Sample. A 4 in Berea core with dimension of 55.25 cm (21.75") in long and 10.16 cm in diameter was used in this experiment. The total bulk volume is 4476.62 cm^3 and the pore volume is 1004.0 cm^3. Thus the calculated porosity is 22.43%. The permeability of the Berea core was measured under room temperature (26°C) using synthetic Spraberry brine. Permeability to brine measured were 625.97, 619.78, 609.45, 600.50 and 593.68 md corresponding to the pressure drops of 3.2, 5.5, 7.4, 9.5 and 13.2 psia. Therefore, the average permeability of the core to brine is 610 md. The physical properties are given in Table 4.2.

Brine. Synthetic Spraberry brine was used in the experiment. Density and viscosity of the brine is 1.08 g/cm^3 and 1.21 cp, respectively, measured under room temperature (26°C) and ambient pressure (12.6 psia).

Oil. Spraberry dead oil was used in the experiment. The composition of the oil was obtained from GC analysis as shown in Table 4.3. The average molecular weight of the dead oil is 230.4, oil density is 0.865 g/cm^3 and oil viscosity is 2.956 cp measured under room conditions.

4.1.2.2 Core preparation

Cleaning. The core was put into a core holder and cleaned under room temperature by injecting methanol, toluene, THF and chloroform. Methanol was at first injected in order to remove potential salts in the core. Then the four solvents were alternatively injected. Finally, methanol was injected once again to remove all other solvents. The core was flushed with N_2 to remove methanol inside of the core and then with moist N_2 in order to recover its wettability. The core was then vacuum-pumped. After being cleaned, it was taken from the core holder and put into another oven under high temperature for drying.

Saturation. The core was put back into the core holder and air was removed from inside of core using a vacuum pump. Synthetic Spraberry brine was injected from the bottom of the core. A total of 1004 cm^3 brine was put into the core, so the porosity, ϕ, can be estimated at about 22.43 %. The synthetic brine then was flushed through the core. The permeability of the core was measured under room temperature (26°C) after the flow was stable. Permeabilities measured were 625.97, 619.78, 609.45, 600.50 and 593.68 md corresponding to the pressure drops of 3.2, 5.5, 7.4, 9.5 and 13.2 psia. Thus, the average permeability is about 610 md.

Spraberry dead oil was injected into the core from the top under reservoir temperature of 58.9°C (138°F). The oil flow rate was 0.0225 cm^3/s (81 cm^3/hr) at the pressure difference of 2.2 psi, and later increased to 0.0451 cm^3/s (162 cm^3/hr) at the pressure drop of 5.1 psi. Oil broke through when 525 cm^3 of brine was produced. The total amount of dead oil injected was 1169 cm^3 (1.16 PV). The water saturation, S_w, and the oil saturation, S_o, were 42.6% and 57.4%, respectively. After aging core for 10 days under reservoir temperature 58.9 °C (138 °F) with pressure above 1600 psia, the core was flushed by injecting1350 cm^3 (1.35 PV) dead oil. Another 5.3 cm^3 brine was produced. Therefore, the total volume of oil within the core increased to 581.3 cm^3 and the initial oil saturation, S_{oi}, was 57.9 %. The initial water saturation, S_{wi}, decreased to 42.1%.

4.1.2.3 Procedure and experimental results

Figure 4.4 schematically illustrates the set-up used in this experiment. Basically, it consists of a drainage cylinder, a visual cell, a BPR, a pump, two accumulators for storing CO_2 and brine, an oil-gas separator and some glassware for measuring oil, gas and brine produced. Reservoir temperature is 58.9°C (138°F). The experiment was conducted in a drainage cylinder.

Water imbibition. The injection rate was 20 cm^3/hr and the backpressure was set above 1650 psia. A total of 194.38 cm^3 oil was produced during the water imbibition, which decreased the oil saturation from the initial oil saturation, 57.9 % to 38.5 %. The oil recovery was 33.44 % OOIP. The water saturation increased to 61.5 %.

During water imbibition, a total of 138.9 cm^3 gas was produced, which is under the pressure of 12.6 psia. The gas volume is about 1.389 cm^3 under the pressure of 1600 psia and temperature of 58.9°C (138°F). If we assume a gas factor equal to 0.85, the gas volume is only 0.13% the pore volume. Therefore, the gas saturation effect can be ignored.

CO_2 gravity drainage/injection. CO_2 gravity drainage was performed at two stages, dynamic gravity drainage (opened system) and static gravity drainage (closed system). At both stages, the backpressure was set up at above 1700 psia and the temperature was set up at 58.9°C (138°F). The total time for conducting CO_2 imbibition was 858 hours.

At the first stage, CO_2 was pumped into the drainage cylinder from the top and the injection rate was set up between 20 ~ 30 cm^3/hr. About 50 cm^3 black oil was produced approximately 40 hours after CO_2 injection initiated. Light oil was produced but the oil rate decreased significantly. This stage lasted for about 330 hours and after injecting CO_2 about 7105 cm^3 (7.08 PV).

At the second stage, the outlet was closed and CO_2 injection was stopped. The core, the CO_2 and the visual cell formed a closed system. The visual cell was connected to the bottom of the drainage cell to collect oil and water produced from the core. This stage was run for 528 hours. Not much CO_2 was used in this stage because the CO_2 remains in the cell (closed system).

Thirteen oil samples were taken from the oil produced during CO_2 gravity drainage for a GC analysis. The colors of the oil samples change from black to yellow and back to black.

A total of 93.2 cm^3 oil and 228.3 cm^3 water were produced during CO_2 gravity drainage. The oil recovery increased 16.03% OOIP, which made the total oil recovery increase to 49.4 % OOIP. The oil saturation within the core decreased down to 29.3 %. The water saturation dropped to 39.0%. Assuming that only water and oil exist in the core before CO_2 drainage begins, CO_2 saturation within the core was 31.7 %.

Temperature effect. To investigate the effect of temperature on the process of CO_2 drainage, temperature was increased gradually to 180°F in two days. The pressure in the drainage cell increased to above 2300 psia. This process lasted 167 hours. Only 0.5 cm^3 of oil and 1.0 cm^3 of water were produced.

Cyclic CO_2 injection. The last step was cyclic CO_2 injection, where the CO_2 was injected at elevated pressure, and after a certain period of time, the injection was stopped, with CO_2 being released to a lower pressure. During the pressure decrease stage, CO_2 injection was stopped and CO_2 was slowly released from the drainage cylinder until the pressure went down to 1450 psia. Then, the outlet was closed and CO_2 was injected into the cylinder with the pressure kept above 1750 psi. Then the pressure decrease stage was run again. One cycle took about one day. Oil and water were collected during the pressure decrease stage. A total of five cycles were run.

The volume of oil produced in this process was 13.1 cm^3, which increased the oil recovery from 49.5 to 51.8% OOIP. The residual oil saturation dropped from 29.2 to 28.0%. The volume of water produced was 23.5 cm^3, which decreased the water saturation to 36.5%.

Table 4.4 summarizes the experimental results. The oil and water producing histories are also plotted in Fig. 4.5. Figures 4.6 and 4.7 present the oil recovery and oil/water saturations vs. time, while Fig. 4.8 shows oil recovery and amount of CO_2 used during CO_2 injection/gravity drainage.

4.1.3 Analysis and Discussion

Our objective is to investigate effects of CO_2 gravity drainage after water imbibition on oil recovery under reservoir conditions. Thus, the discussion and analysis are concentrated on results obtained from CO_2 gravity drainage.

Nine of the 13 oil samples were analyzed using gas chromatography (GC). These oil samples were taken at different times. Table 4.5 shows the mole fraction and weight percent of different component groups in the oil samples. For convenient analysis, we divided the components of the oil samples into four groups – C1 ~ C10, C11 ~ C20, C21 ~ C30 and C31$^+$. The results are shown in Fig. 4.11 and 4.12. For more details, see Table 4.7 and 4.8. The results are also presented in Fig. 4.9 and 4.10.

The CO_2 extracted most of the middle components, C11 ~ C20, from the oil during CO_2 gravity drainage. The oil samples from this component group were about 85 % by mole fraction and about 80 % by weight percent (Figs. 4.11 and 4.12). The mole fraction of heavy components increased at the end of CO_2 injection/gravity drainage while more mole fraction of light components were extracted at the beginning of the experiment.

Densities of the oil samples were also measured at room temperature and ambient pressure. The average molecular weights of the samples obtained from gas chromatographic analysis are presented in Table 4.6 and plotted in Fig. 4.13. The oil sample at time 0 was Spraberry dead oil. Both density and average molecular weight increased with time except at the beginning of the experiment. At that point, heavier components were flooded by CO_2 and then CO_2 extracted the light component about 40 hours later, which indicated that CO_2 drainage initiated.

Temperature seemed to have no significant effect on CO_2 drainage process in this experiment (Fig. 4.5), because CO_2 may have a more pronounced effect than temperature on increasing the mobility of oil and decreasing the interfacial tension (IFT).

Cyclic CO_2 injection may be effective in improving the oil recovery during CO_2 gravity drainage, as displayed in Fig. 4.5. A cyclic injection scheme in this experiment enhanced the oil recovery up to 2.3% OOIP. Considering that cyclic CO_2 injection was performed at low oil saturation (29.2%), the oil increment may be considered significant.

Figure 4.8 shows the volume of CO_2 used during CO_2 injection/drainage. A lot of CO_2 was used in this experiment. It should be noted also that the rate of pumping CO_2 into the drainage cell did not significantly affect the final oil recovery from the core, but only increased the amount of CO_2 usage as shown in Fig. 4.8. The oil production rate did not decrease when CO_2 injection was stopped. The only significant effect of the CO_2 injection rate may be on the oil production rate at the beginning of the CO_2 process. However, CO_2 injectivity studies need to be performed to clarify this issue.

Figure 4.14 shows that water imbibition followed by CO_2 injection may achieve higher oil recovery than using CO_2 injection alone. That comparison was made between Core No. 1 (k = 500 md) and this experiment (k = 500 md) (see Table 4.1) because of almost similar rock properties.

4.1.4 Conclusions

From the results obtained in this experiment, the following conclusions can be drawn:

1. CO_2 gravity drainage could significantly increase oil recovery after waterflooding in the naturally fractured Spraberry Trend Area.
2. Water imbibition followed by CO_2 injection may be more efficient than injecting CO_2 alone.
3. The efficiency of CO_2 injection decreases as permeability decreases and initial water saturation increases.
4. The effect of initial water saturation may have more effect on oil recovery than permeability.
5. Cyclic CO_2 injection may enhance oil recovery during a CO_2 gravity drainage process.
6. Temperature does not have a significant effect on the CO_2 gravity drainage process because CO_2 has more pronounced effect on increasing the mobility of oil and decreasing the interfacial tension (IFT).

4.1.5 References

1. Schechter, D.S.: "Advanced Reservoir Characterization and Evaluation of CO_2 Gravity Drainage in the Naturally Fractured Spraberry Trend Area," Third Annual Technical Progress Report, Contract No. DE-FC22-95BC14942, U.S. DOE, (Dec 1998).

2. Schechter, D.S. and Guo, B.: "Mathematical Modeling of Gravity Drainage after Gas Injection into Fractured Reservoirs," paper SPE 35170 presented at the 1996 SPE Improved Oil Recovery Symposium Tulsa, April 22-24, 1996.

Table 4.1—Physical properties of the core samples used in previous experiments and partial results obtained.

Core No.	1	2	3	4	5
Core Type	Berea	Berea	Spraberry	Spraberry	Spraberry
Configuration	continuous	continuous	continuous	continuous	stacked
Length, cm	55.52	55.25	55.0	55.245	24.77 25.08
Diameter, cm	10.16	10.16	10.16	8.89	6.53 6.58
Porosity, %	18.7	13.0	10.0	11.1	10.7
Brine Permeability, md	500	50	0.01	0.38	0.057
Water Saturation, %	35.0	29.3	38.6	45.0	37.6
Residual Oil Saturation, %	37.5	32.5	42.5	41.8	50.5
OOIP, cc	544.5	411.1	273.8	209.3	111.0
OWIP, cc	293.2	171.2	172.1	171.3	67.0
Oil Recovery, %	42.0	54.0	30.8	24.0	19.1
Time of Experiment, (day)	6	220	190	167	331

Table 4.2—Physical properties of the core sample used in this experiment.

Properties of the Berea Core	Value
Length, cm	55.25
Diameter, cm	10.16
Bulk Volume, cm^3	4476.62
Pore Volume, cm^3	1004.0
Porosity, %	22.43
Brine Permeability, md	610.0
OOIP, %	581.3
OWIP, %	422.7
Initial Water Saturation, %	42.1
Initial Oil Saturation, %	57.9

Table 4.3—GC results of the Spraberry dead oil used in the experiment.

Carbon No.	Molec. wt.	Weight %	Moles	Mole fract.	Molec. wt. %
1	16.04303	0	0	0	0
2	30.07012	0	0	0	0
3	44.09721	0	0	0	0
4	58.12430	0	0	0	0
5	72.15139	0.084064563	0.001165114	0.002683957	0.193651205
6	86.17848	0.761713828	0.008838794	0.020361054	1.754684680
7	100.20557	4.299808405	0.042909874	0.098847226	9.905042626
8	114.23266	5.136605594	0.044966173	0.103584119	11.832689410
9	128.25975	4.251297195	0.033145996	0.076355148	9.793292159
10	142.28684	5.343655162	0.037555512	0.086512913	12.309648980
11	156.31393	3.725624838	0.023834247	0.054904594	8.582352830
12	170.34102	3.498245901	0.020536720	0.047308408	8.058562498
13	184.36811	3.682212712	0.019972070	0.046007678	8.482348616
14	198.39520	3.928306014	0.019800409	0.045612239	9.049249375
15	212.42229	3.053448865	0.014374428	0.033112945	7.033927635
16	226.44938	2.829626878	0.012495627	0.028784937	6.518331098
17	240.47647	3.067010969	0.012753892	0.029379878	7.065169311
18	254.50356	2.735307623	0.010747620	0.024758228	6.301057176
19	268.53065	1.868650564	0.006958798	0.016030294	4.304625171
20	282.55774	2.671345541	0.009454158	0.021778607	6.153714065
21	296.58483	2.231717507	0.007524719	0.01733395	5.140986518
22	310.61192	2.097276207	0.006752079	0.015554095	4.831287414
23	324.63901	1.886004976	0.005809545	0.013382874	4.344602811
24	338.66610	1.820107843	0.005374343	0.012380342	4.192802113
25	352.69319	4.814449489	0.013650531	0.031445377	11.09057030
26	366.72028	1.758789839	0.004795998	0.011048066	4.051549904
27	380.74737	1.765568922	0.004637114	0.010682060	4.067166205
28	394.77446	1.273149915	0.003225006	0.007429126	2.932829323
29	408.80155	1.844834162	0.004512787	0.010395659	4.249761686
30	422.82864	1.735618455	0.004104780	0.009455775	3.998172280
31	436.85573	3.053084504	0.006988771	0.016099339	7.033088293
32	450.88282	1.873150914	0.004154407	0.009570097	4.314992181
33	464.90991	2.543647873	0.005471270	0.012603624	5.859549596
34	478.93700	1.597259782	0.003335010	0.007682533	3.679449114
35	492.96409	1.604971432	0.003255757	0.007499966	3.697213677
36	506.99118	2.651509536	0.005229893	0.012047586	6.108019825
C37+	563.09954	14.51193399	0.025771525	0.059367309	33.429704590
Total/Average		100	0.434102968	1	230.3600927

Table 4.4—Experimental results during different stages.

	Water Imbibition	CO_2 Drainage	Temperature Increase	Cyclic CO_2 Injection
Initial Oil Saturation, %	57.9	33.5	29.3	29.2
Final Oil Saturation, %	33.5	29.3	29.2	28.0
Initial Water Saturation, %	42.1	66.5	39.0	38.9
Final Water Saturation, %	66.5	39.0	38.9	36.5
Gas/CO_2 Saturation, %	0.1	31.7	31.7	35.5
Oil Recovery, %	33.44	49.4	49.5	51.8
Time of Experiment, day	22	36	7	5

Table 4.5—GC results of different group components of oil samples obtained from CO_2 gravity drainage/injection.

Time (hr)	*C1 ~ C10*		*C11 ~ C20*		*C20 ~ C30*		*C31+*	
	Mole frac.	**(Weight %)**	**Mole frac.**	**(Weight %)**	**Mole frac.**	**(Weight %)**	**Mole frac.**	**(Weight %)**
0	0.388344	19.87714	0.347678	31.05978	0.139107	21.22752	0.124870	27.83556
10	0.266333	16.76627	0.600432	58.15009	0.094344	15.58787	0.038891	9.495767
37	0.438436	29.86307	0.475120	51.93866	0.060512	11.19651	0.025932	7.001758
42.5	0.055843	3.423766	0.854845	83.13537	0.088145	13.17068	0.001167	0.270184
50.5	0.049993	3.011592	0.847875	81.78595	0.099050	14.51070	0.003082	0.691760
89	0.072391	4.696062	0.857835	84.41236	0.068740	10.64875	0.001034	0.242836
209.5	0.085529	5.485306	0.801255	77.32346	0.111675	16.83614	0.001541	0.355099
301	0.012867	0.709839	0.875925	83.48775	0.109502	15.46458	0.001705	0.337837
330	0.017890	1.042006	0.836478	75.82748	0.109121	15.46735	0.036511	7.663163
359.5	0.106067	4.144405	0.346742	23.13898	0.280836	30.83610	0.266355	41.88052

Table 4.6—Properties of oil samples obtained from CO_2 gravity drainage/injection.

Time, hr	0	10	37	42.5	50.5	89	209.5	301	330	359.5
Ave. Molec. Weight	230.4	206.3	181.0	217.6	221.7	208.5	210.5	233.6	235.4	322.4
Density	0.865	0.864	0.852	0.823	0.844	0.833	0.832	0.848	0.870	0.901

Table 4.7—Mole fraction of oil samples obtained from CO_2 gravity drainage/injection

Sample Carbon#	Dead oil	sample #1	sample #2	sample #3	sample #4	Sample #5	sample #6	sample #7	sample #8	sample #9
1	0	0	0	0	0	0	0	0	0	0
2	0	0	0	0	0	0	0	0	0	0
3	0	0	0	0	0	0	0	0	0	0
4	0	0	0	0	0	0	0	0	0	0
5	0.00268	0.00035	0.00042	0.00020	0.00008	0.00008	0.00006	0.00014	0.00048	0.00015
6	0.02036	0.00182	0.00871	0.00024	0.00017	0.00026	0.00023	0.00009	0.00002	0.00135
7	0.09885	0.01982	0.07283	0.00288	0.00237	0.00042	0.00302	0.00114	0.00009	0.01425
8	0.10358	0.04912	0.11511	0.00694	0.00620	0.00875	0.00853	0.0025	0.00080	0.02440
9	0.07636	0.06911	0.10832	0.01098	0.01049	0.01598	0.01714	0.00279	0.00226	0.02563
10	0.08651	0.12612	0.13305	0.03460	0.03069	0.04690	0.05654	0.00619	0.01424	0.04030
11	0.05491	0.09859	0.08972	0.05517	0.04488	0.07254	0.07913	0.01046	0.03824	0.03361
12	0.04731	0.09426	0.07957	0.09314	0.07964	0.10944	0.11267	0.02908	0.07255	0.03436
13	0.04601	0.09301	0.07277	0.11257	0.12060	0.14581	0.14459	0.07278	0.11012	0.04649
14	0.04561	0.09138	0.06381	0.11886	0.11265	0.16095	0.14222	0.16015	0.15203	0.03780
15	0.03311	0.05536	0.04199	0.15125	0.14637	0.10333	0.08909	0.14729	0.13196	0.03719
16	0.02879	0.04670	0.03544	0.09859	0.09721	0.08595	0.07213	0.14002	0.09595	0.03495
17	0.02938	0.04856	0.03695	0.08987	0.09316	0.07572	0.06834	0.13411	0.10036	0.03868
18	0.02476	0.03627	0.02705	0.05721	0.07329	0.04658	0.04525	0.09675	0.06479	0.03498
19	0.01603	0.02027	0.01581	0.04884	0.04328	0.03596	0.02917	0.05222	0.04226	0.02473
20	0.02178	0.01603	0.01201	0.02936	0.03680	0.02158	0.01867	0.03308	0.02823	0.02396
21	0.01733	0.01684	0.01564	0.02717	0.02752	0.02196	0.01971	0.02465	0.02986	0.03582
22	0.01555	0.01280	0.00847	0.01612	0.02323	0.01466	0.06393	0.02396	0.01816	0.03686
23	0.01338	0.00731	0.00620	0.01025	0.01238	0.00849	0.00727	0.01041	0.01285	0.02739
24	0.01238	0.00494	0.00353	0.00681	0.00827	0.00595	0.00488	0.00688	0.00958	0.02740
25	0.03145	0.03647	0.01744	0.02204	0.01975	0.01271	0.01165	0.03466	0.01572	0.03173
26	0.01105	0.00376	0.00238	0.00283	0.00354	0.00241	0.00195	0.00351	0.00593	0.02604
27	0.01068	0.00382	0.00154	0.00165	0.00218	0.00135	0.00117	0.00205	0.00519	0.02562
28	0.00743	0.00237	0.00149	0.00068	0.00095	0.00055	0.00046	0.00113	0.00329	0.01875
29	0.01040	0.00302	0.00191	0.00045	0.00089	0.00066	0.00056	0.00216	0.0077	0.02707
30	0.00946	0.00302	0.00192	0.00014	0.00035	0.00000	0.00010	0.00009	0.00086	0.02416
31	0.01610	0.00177	0.0039	0.00022	0.00026	0.00012	0.00030	0.00052	0.00613	0.04041
32	0.00957	0.00160	0.00335	0.00003	0.00008	0.00006	0.00009	0.00029	0.00192	0.02395
33	0.01260	0.00149	0.00179	0.00009	0.00005	0.00003	0.00005	0.00030	0.00558	0.01168
34	0.00768	0.00423	0.00270	0.00002	0.00064	0.00004	0.00006	0.00020	0.00386	0.04292
35	0.0075	0.01136	0.00622	0.00006	0.00047	0.00039	0.00054	0.00031	0.00422	0.02009
36	0.01205	0.01087	0.00396	0.00041	0.00122	0.00034	0.00046	0.00008	0.00642	0.01773
C37+	0.05937	0.00759	0.00401	0.00034	0.00037	0.00004	0.00006	0.00001	0.00837	0.10957

Table 4.8—Weight percent of oil samples obtained from CO_2 gravity drainage/injection.

Sample Carbon#	Dead oil	sample #1	sample #2	sample #3	sample #4	sample #5	sample #6	sample #7	sample #8	sample #9
1	0	0	0	0	0	0	0	0	0	0
2	0	0	0	0	0	0	0	0	0	0
3	0	0	0	0	0	0	0	0	0	0
4	0	0	0	0	0	0	0	0	0	0
5	0.08407	0.01216	0.01675	0.00673	0.00247	0.00287	0.00222	0.00444	0.01473	0.00327
6	0.76171	0.07585	0.41457	0.00937	0.00654	0.01073	0.00944	0.00345	0.00057	0.03595
7	4.29981	0.96277	4.03216	0.13275	0.10711	0.02030	0.14357	0.04907	0.00384	0.44291
8	5.13661	2.71991	7.26451	0.36444	0.31964	0.47932	0.46298	0.12226	0.03883	0.86451
9	4.25130	4.29653	7.67572	0.64724	0.60674	0.98283	1.04470	0.15344	0.12309	1.01941
10	5.34366	8.69903	10.4594	2.26324	1.96909	3.20002	3.82240	0.37719	0.86095	1.77836
11	3.72563	7.47039	7.74821	3.96434	3.16355	5.43733	5.87671	0.69977	2.53889	1.62927
12	3.49825	7.78327	7.48817	7.29323	6.11800	8.93982	9.11862	2.12040	5.24956	1.81537
13	3.68221	8.31264	7.41246	9.54002	10.0280	12.8916	12.6647	5.74429	8.62417	2.65816
14	3.92831	8.78818	6.99383	10.8393	10.0795	15.3126	13.4050	13.6026	12.8124	2.32592
15	3.05345	5.70065	4.92830	14.7685	14.0220	10.5257	8.99132	13.3942	11.9075	2.45002
16	2.82963	5.12607	4.43446	10.2621	9.92809	9.33387	7.75970	13.5738	9.22973	2.45478
17	3.06701	5.66027	4.90898	9.93368	10.1037	8.73180	7.80800	13.8070	10.2522	2.88520
18	2.73531	4.47492	3.80324	6.69294	8.4122	5.68459	5.47126	10.5409	7.00441	2.76140
19	1.86865	2.63826	2.34560	6.02793	5.24131	4.63128	3.72143	6.00357	4.82074	2.05921
20	2.67135	2.19545	1.87542	3.81336	4.68968	2.92379	2.50668	4.00121	3.38793	2.09967
21	2.23172	2.42092	2.56221	3.70379	3.68095	3.12359	2.77740	3.13000	3.76143	3.29470
22	2.09728	1.92768	1.45368	2.30184	3.25395	2.18332	9.43365	3.18612	2.39594	3.55070
23	1.88601	1.15016	1.11231	1.52891	1.81258	1.32244	1.12068	1.44671	1.77158	2.75749
24	1.82011	0.81124	0.66065	1.06033	1.26245	0.96598	0.78458	0.99729	1.37755	2.87761
25	4.81445	6.23558	3.39843	3.57371	3.14109	2.14898	1.95245	5.23260	2.35507	3.47088
26	1.75879	0.66769	0.48276	0.47751	0.58559	0.42432	0.33983	0.55094	0.92360	2.96196
27	1.76557	0.70482	0.32340	0.28952	0.37409	0.24591	0.21212	0.33435	0.83997	3.02536
28	1.27315	0.45331	0.32402	0.12309	0.16967	0.10420	0.08706	0.19171	0.55115	2.29597
29	1.84483	0.59749	0.43134	0.08423	0.16386	0.12918	0.10844	0.37818	1.33719	3.43259
30	1.73562	0.61899	0.44773	0.02775	0.06647	0.00084	0.01994	0.01670	0.15388	3.16885
31	3.05309	0.37378	0.94125	0.04500	0.05143	0.02524	0.06187	0.09774	1.13757	5.47525
32	1.87315	0.34855	0.83466	0.00647	0.01627	0.01376	0.01854	0.05651	0.36835	3.34928
33	2.54365	0.33505	0.45840	0.01954	0.01053	0.00768	0.01035	0.06003	1.10272	1.68472
34	1.59726	0.98137	0.71374	0.00340	0.13761	0.00978	0.01318	0.04057	0.78533	6.37557
35	1.60497	2.71556	1.69478	0.01277	0.10382	0.09320	0.12560	0.06440	0.88457	3.07171
36	2.65151	2.67109	1.11019	0.09621	0.27864	0.08236	0.11099	0.01735	1.38304	2.78763
C37+	14.5119	2.07037	1.24874	0.08680	0.09347	0.01083	0.01460	0.00124	2.00158	19.1364

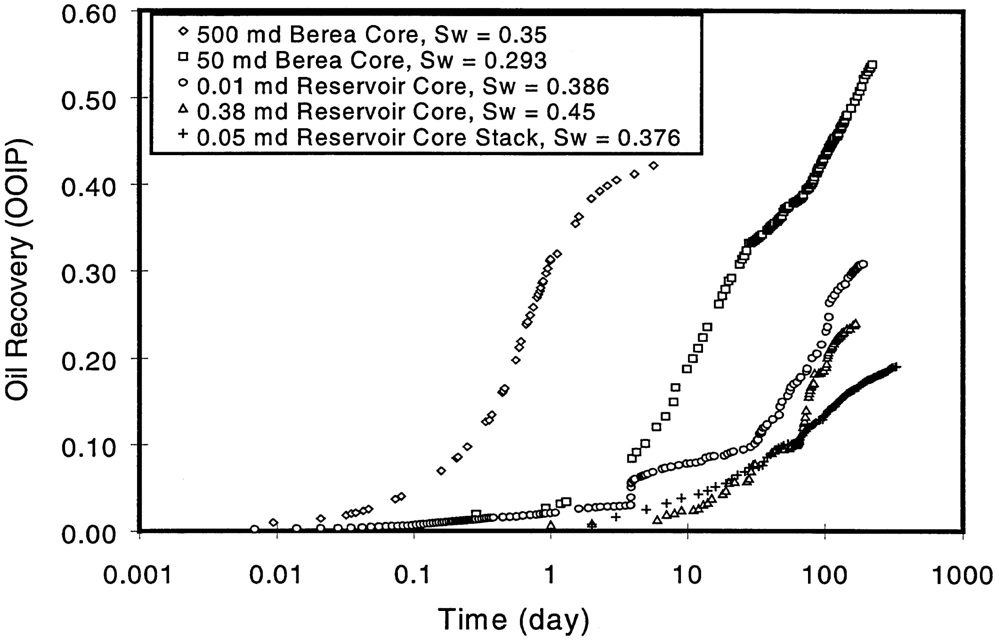

Fig. 4.1—Oil recovery curves obtained from the five experiments with different permeabilities and initial water saturations.

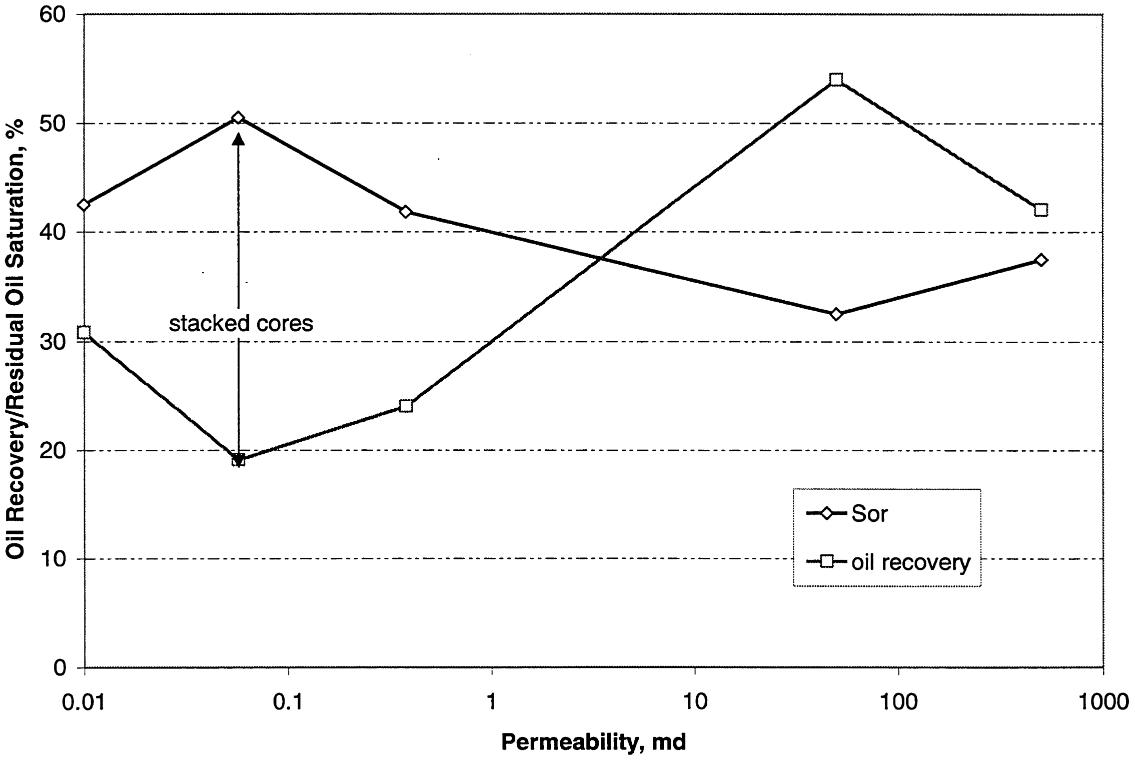

Fig. 4.2—Effect of permeability on oil recovery of CO_2 injection.

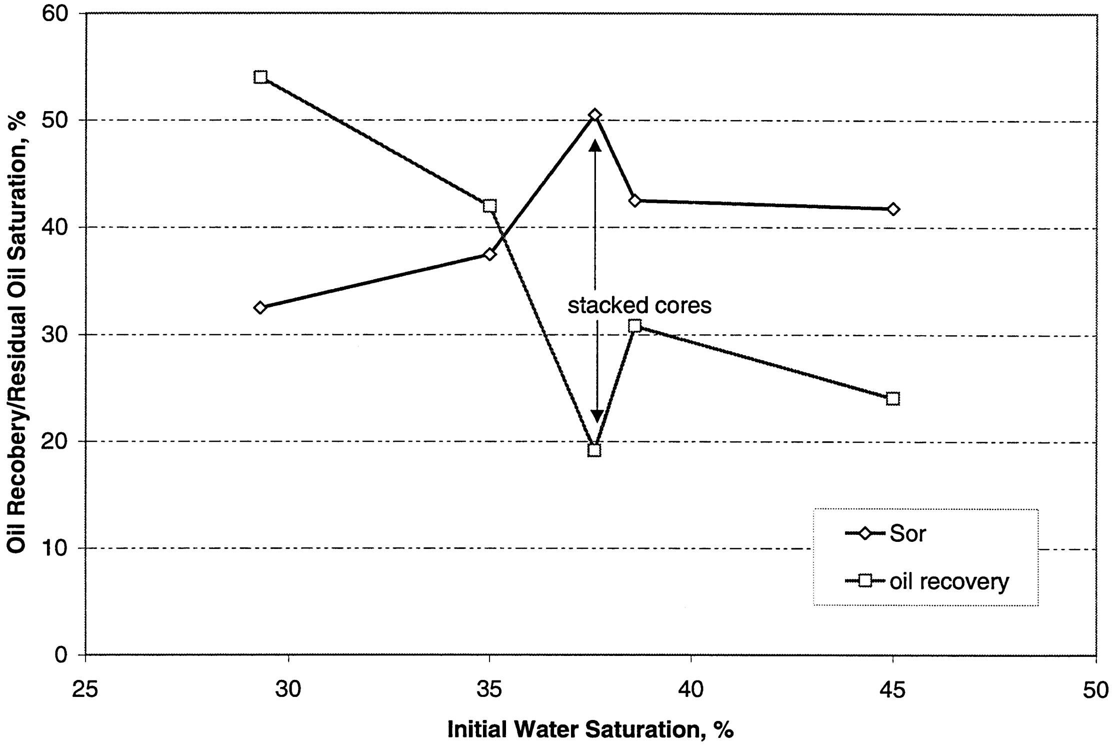

Fig. 4.3—Effect of initial water saturation on oil recovery of CO_2 injection.

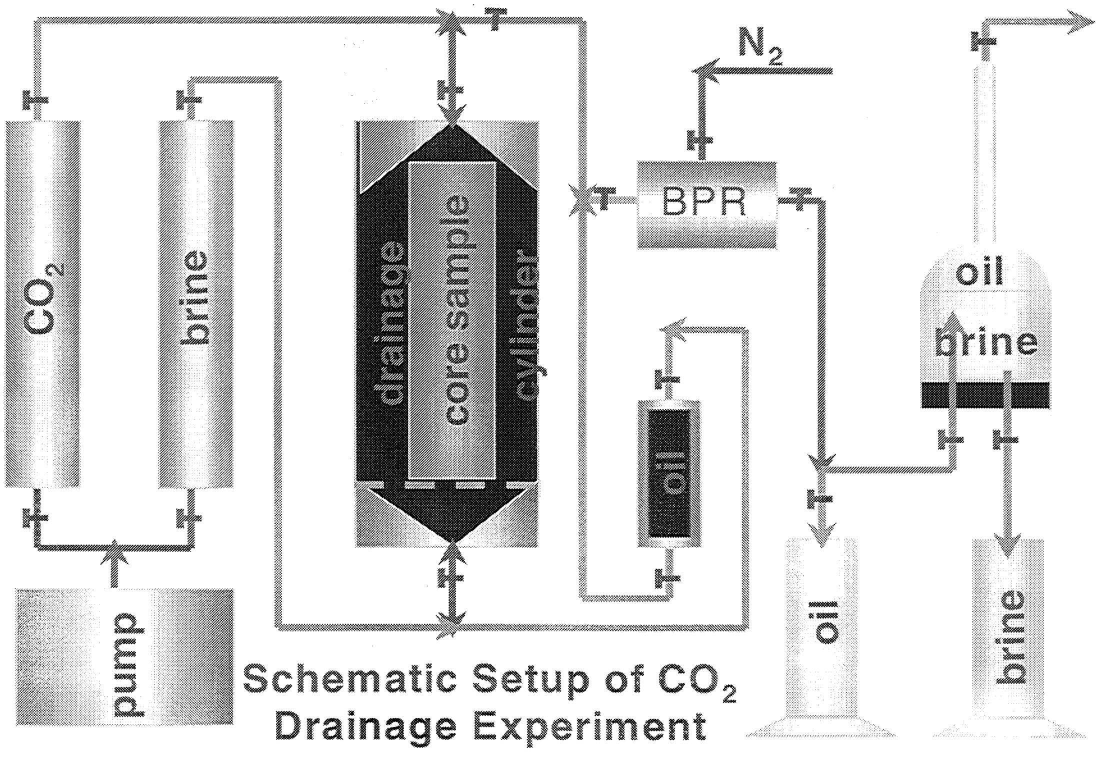

N_2
BPR
CO_2
brine
drainage
core sample
cylinder
oil
oil
brine
oil
brine
pump
Schematic Setup of CO_2
Drainage Experiment

Fig. 4.4—Set-up for water and CO_2 gravity drainage experiment.

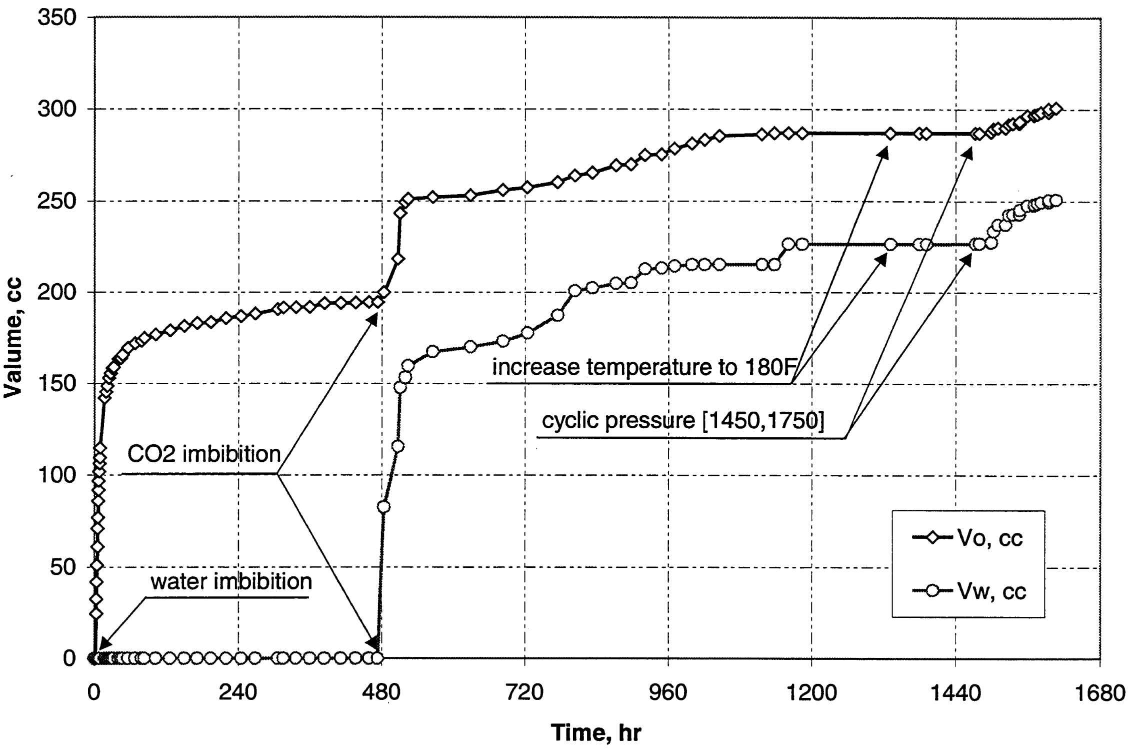

Fig. 4.5—Oil and water producing history during the experiment.

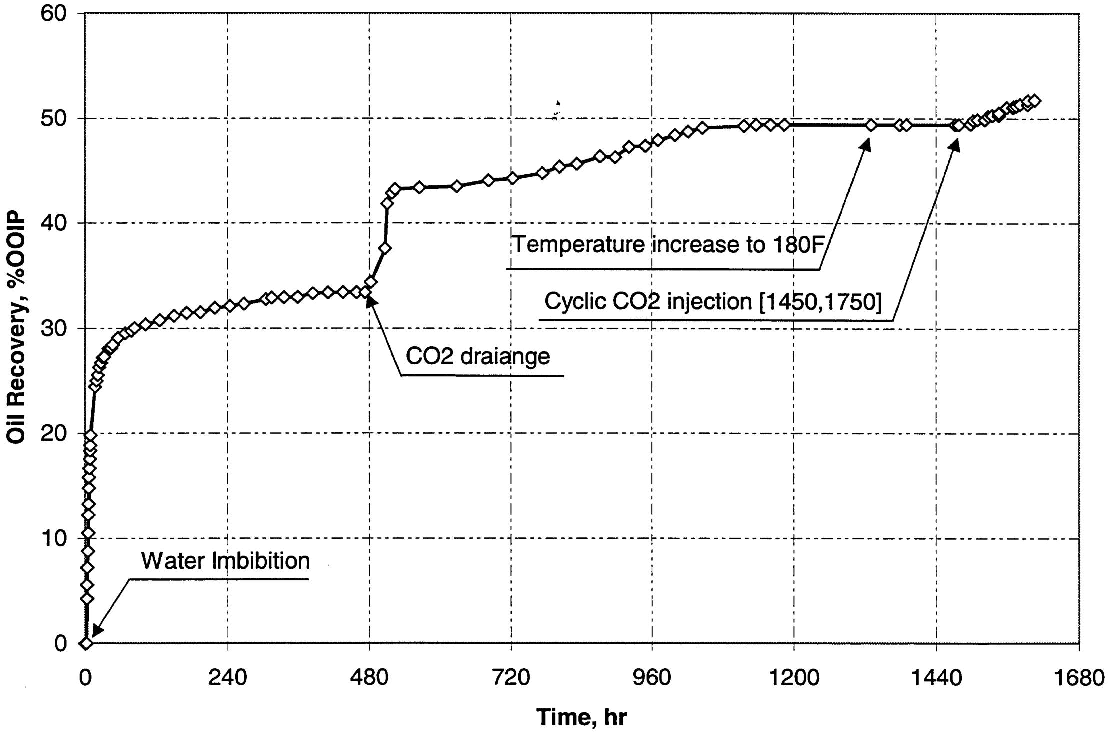

Fig. 4.6—Oil recovery curve for the whole experiment.

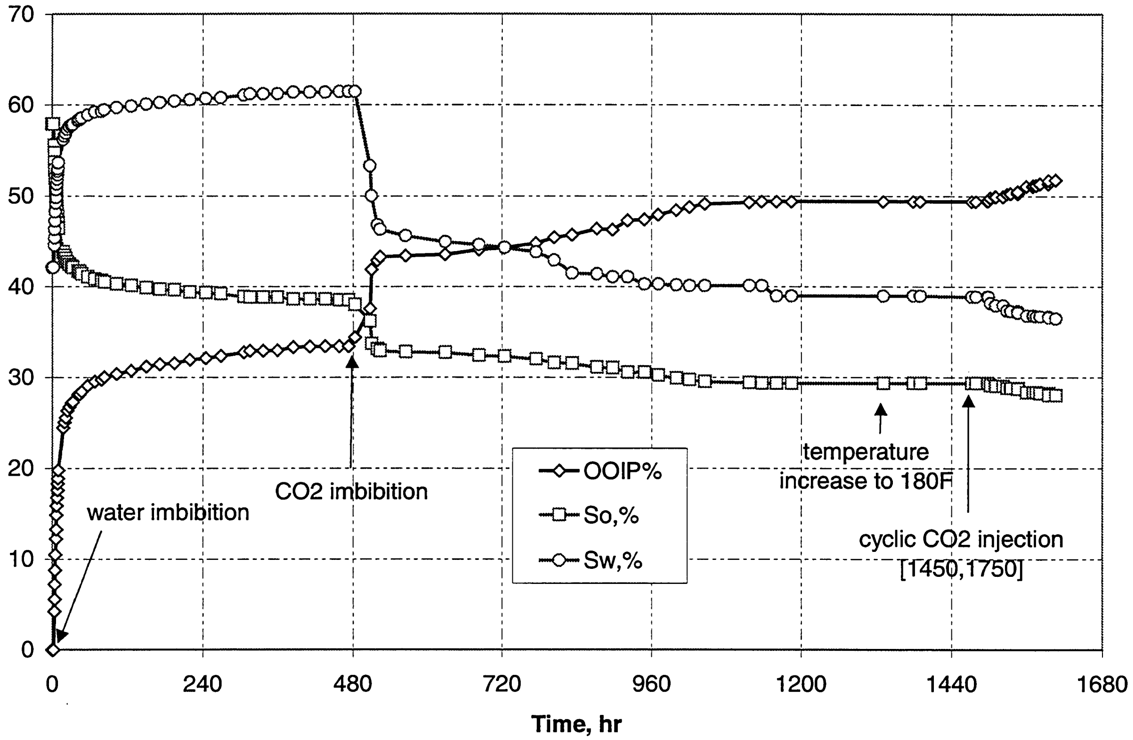

Fig. 4.7—Oil and water saturation history and oil recovery curve.

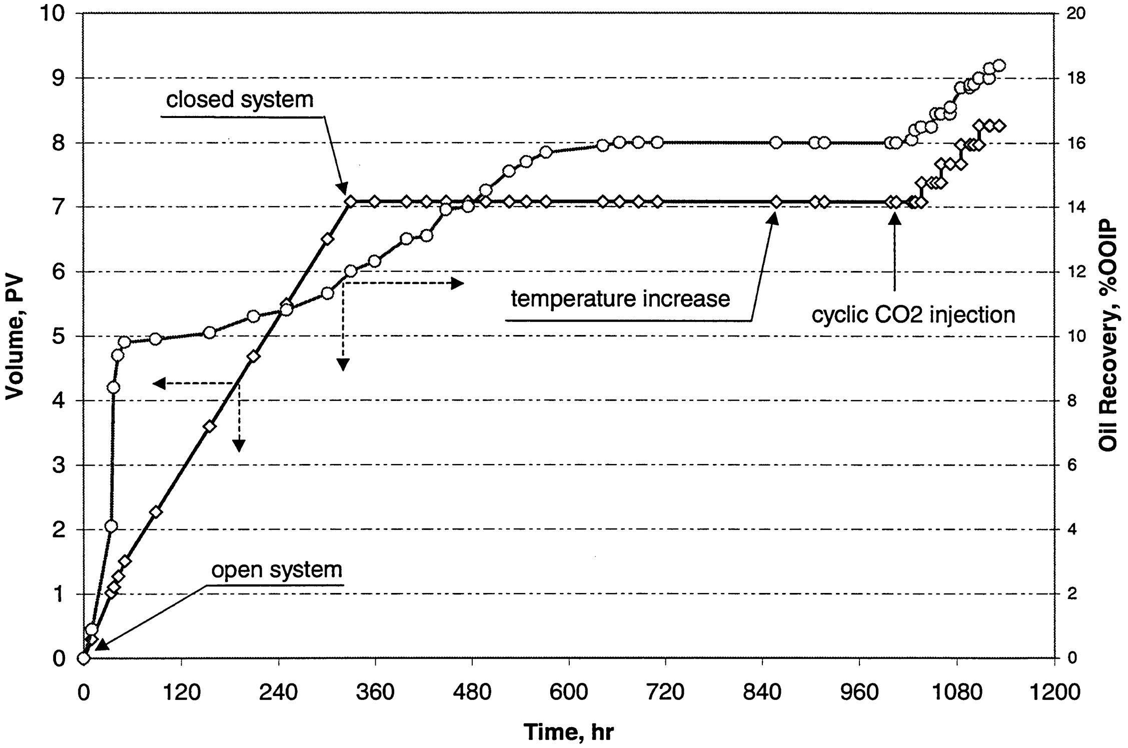

Fig. 4.8—Oil recovery and volume of CO_2 used during CO_2 drainage.

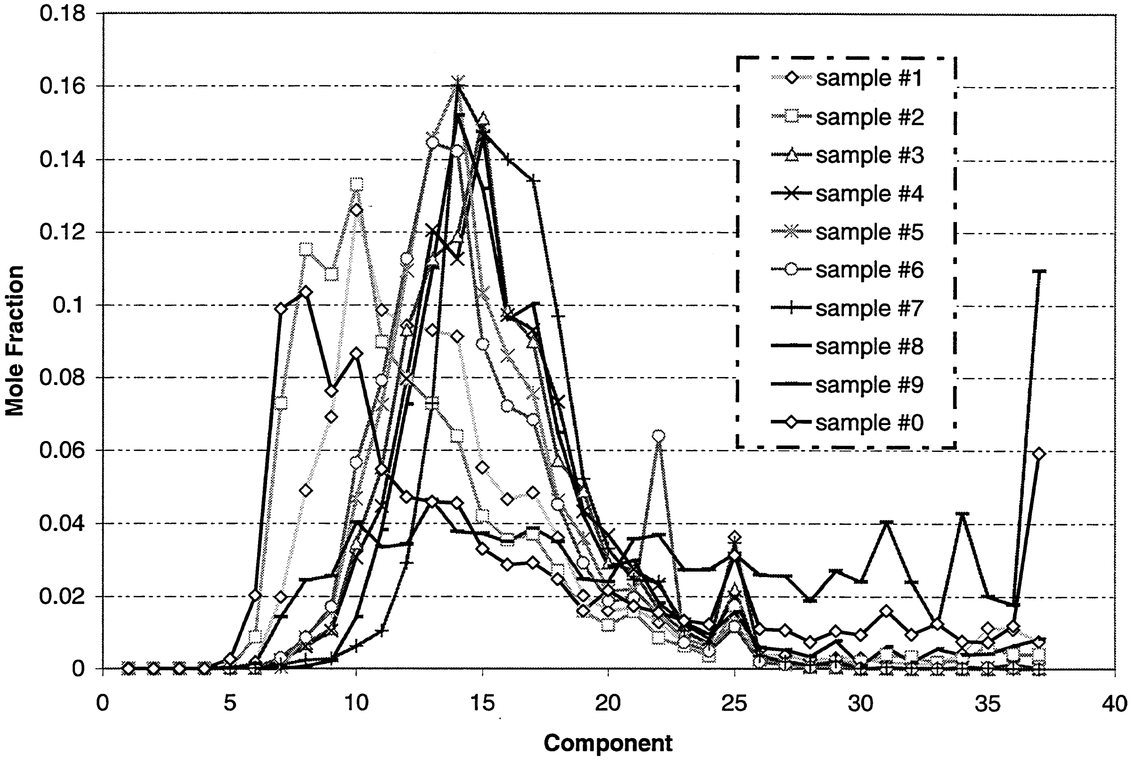

Fig. 4.9—Mole fraction of oil samples from CO_2 gravity drainage.

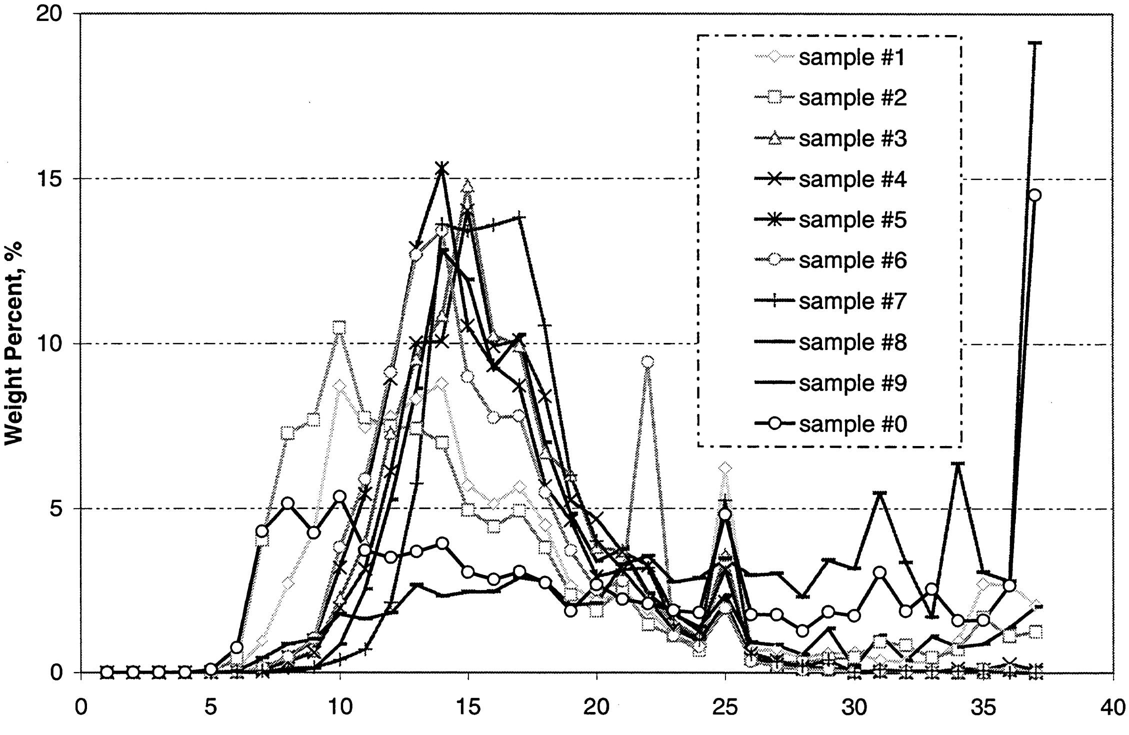

Fig. 4.10—Weight percent of components of oil samples from CO_2 drainage.

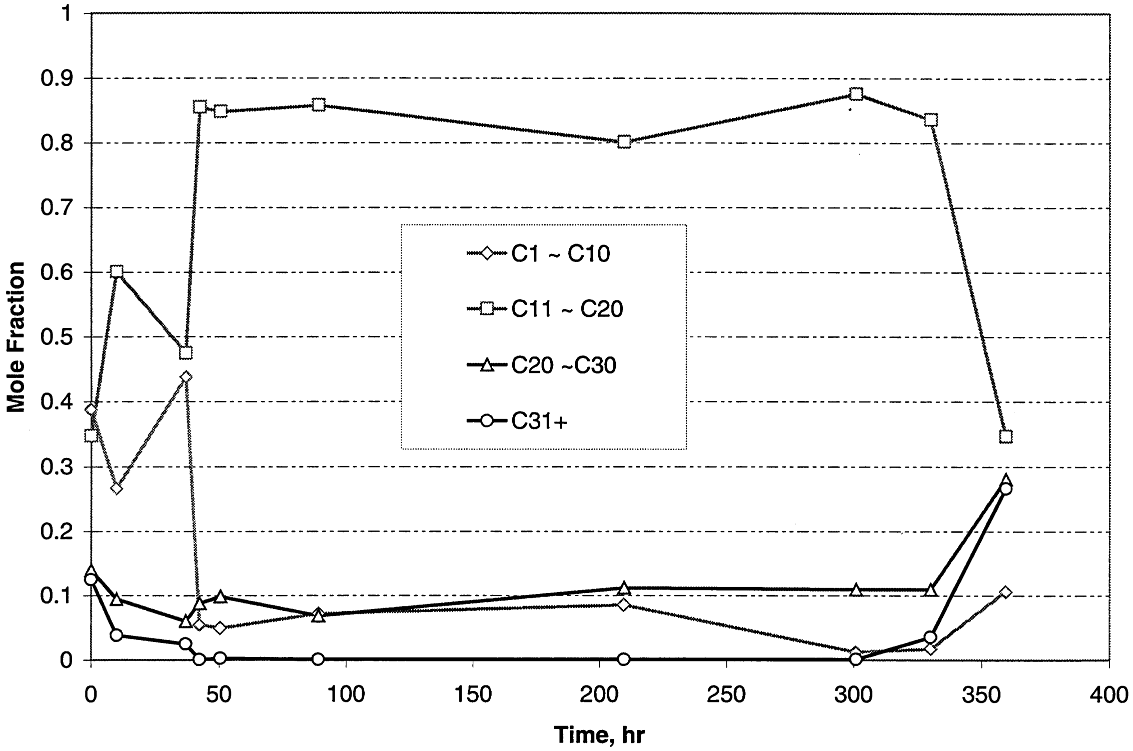

Fig. 4.11—Mole fraction of component groups of oil samples during CO_2 drainage.

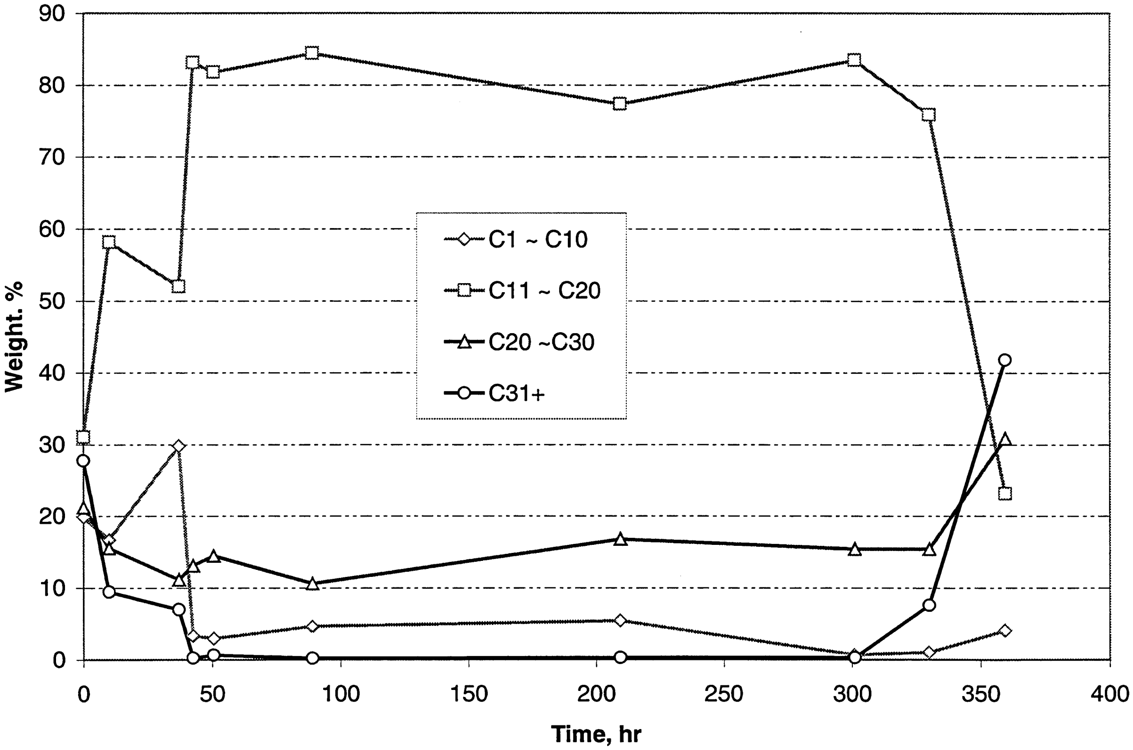

Fig. 4.12—Weight percent of component group of oil samples during CO_2 drainage.

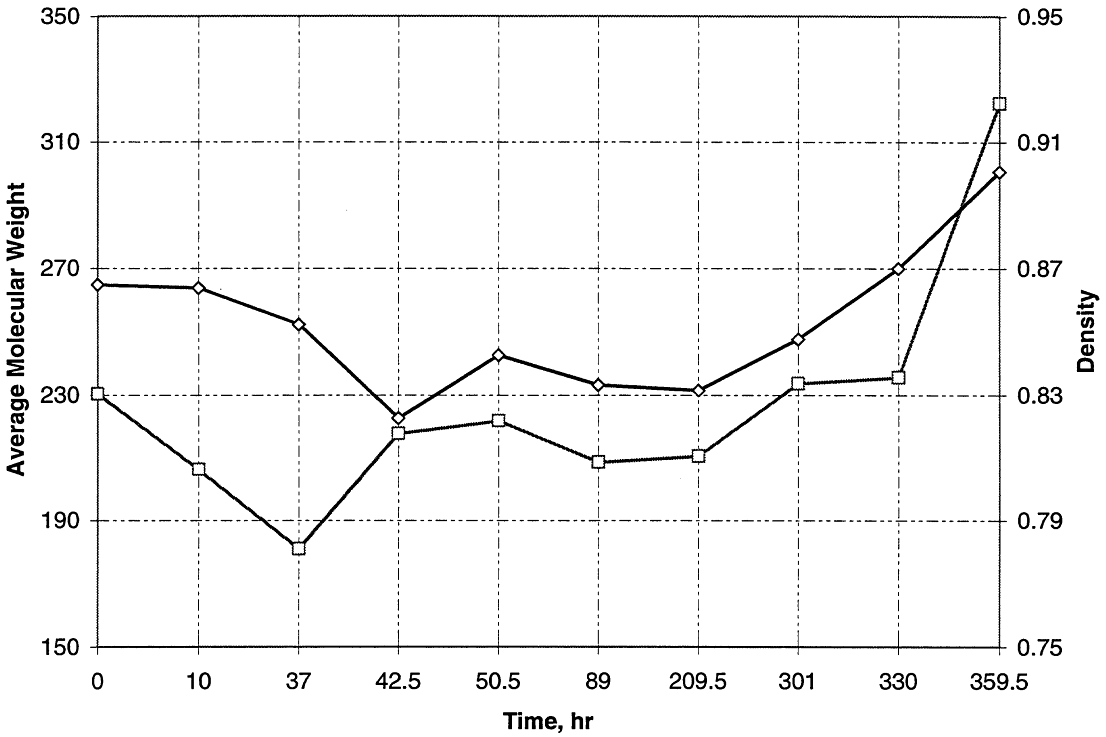

Fig. 4.13—Average molecular weight and density of oil samples from CO_2 drainage.

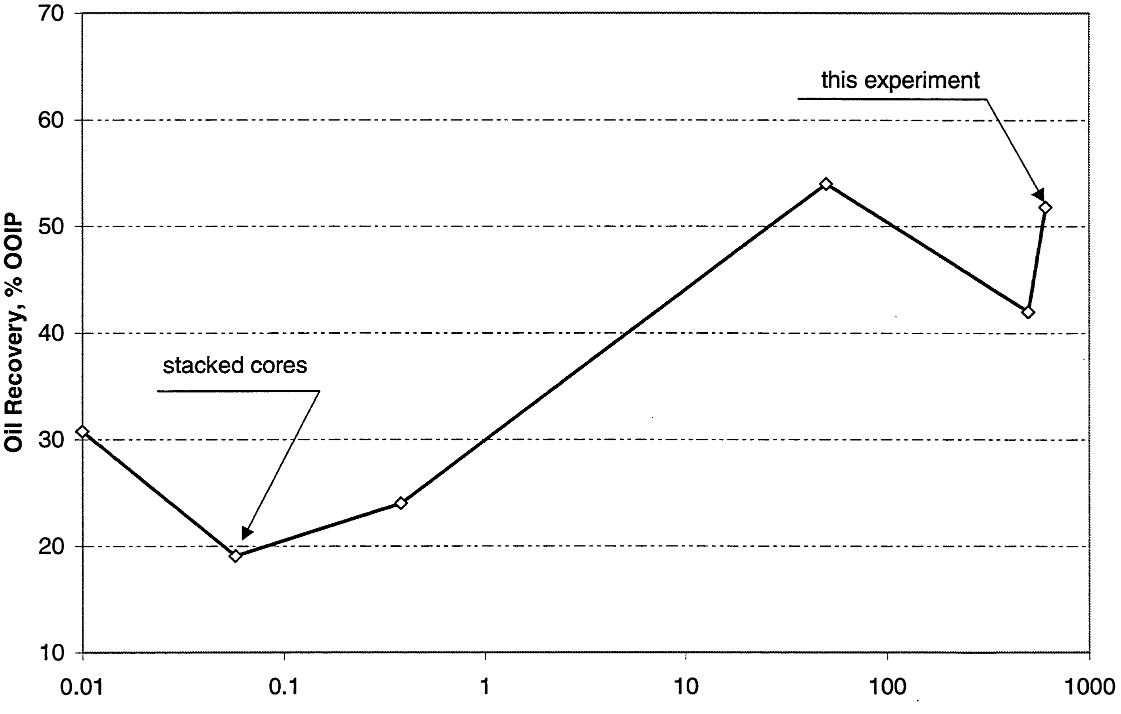

Fig. 4.14—Oil recovery curves vs. rock permeability of the six experiments.